EFFECT OF GRAVITY DRAINAGE, MISCIBILITY, AND RELATIVE PERMEABILITY ON TIGHT MATRIX RESERVOIR WITH LOW-QUALITY NATURAL FRACTURES ON CARBON-DIOXIDE INJECTION

A THESIS SUBMITTED TO
THE GRADUATE SCHOOL OF NATURAL AND APPLIED SCIENCES
OF
MIDDLE EAST TECHNICAL UNIVERSITY

BY

MURAT CAN ÜLKER

IN PARTIAL FULFILLMENT OF THE REQUIREMENTS
FOR
THE DEGREE OF MASTER OF SCIENCE
IN
PETROLEUM AND NATURAL GAS ENGINEERING

SEPTEMBER 2024

Approval of the thesis:

EFFECT OF GRAVITY DRAINAGE, MISCIBILITY, AND RELATIVE PERMEABILITY ON TIGHT MATRIX RESERVOIR WITH LOW-QUALITY NATURAL FRACTURES ON CARBON-DIOXIDE INJECTION

submitted by **MURAT CAN ÜLKER** in partial fulfillment of the requirements for the degree of **Master of Science** i**n Petroleum and Natural Gas Engineering, Middle East Technical University** by,

Prof. Dr. Naci Emre Altun
Dean, **Graduate School of Natural and Applied Sciences** _____

Assoc. Prof. Dr. İsmail Durgut
Head of the Department, **Petroleum and Natural Gas Eng.** _____

Assist. Prof. Dr. Mehmet Onur Doğan
Supervisor, **Petroleum and Natural Gas Engineering** _____

Examining Committee Members:

Assoc. Prof. Dr. Çağlar Sınayuç
Petroleum and Natural Gas Eng., METU _____

Assist. Prof. Dr. Mehmet Onur Doğan
Petroleum and Natural Gas Eng., METU _____

Assist. Prof. Dr. Selçuk Erol
Energy Systems Eng. İYTE _____

Date: 04.09.2024

I hereby declare that all information in this document has been obtained and presented in accordance with academic rules and ethical conduct. I also declare that, as required by these rules and conduct, I have fully cited and referenced all material and results that are not original to this work.

Name Last name : Murat Can Ülker

Signature :

ABSTRACT

EFFECT OF GRAVITY DRAINAGE, MISCIBILITY, AND RELATIVE PERMEABILITY ON TIGHT MATRIX RESERVOIR WITH LOW-QUALITY NATURAL FRACTURES ON CARBON-DIOXIDE INJECTION

Ülker, Murat Can
Master of Science, Petroleum and Natural Gas Engineering
Supervisor: Assist. Prof. Dr. Mehmet Onur Doğan

September 2024, 126 pages

Oil production in primary production phase declines continuously in the world. It is believed that there are very few fields that is not been discovered yet. The brown fields of the world are either abandoned with low recovery factors or they produce at low production rates due to reservoir pressure or water cut problems. Since the twentieth century, EOR techniques have been studied and applied in several fields. It has been observed that the oil production rate and the recovery factor can be increased and one way to do it is the injection of carbon-dioxide into the light-oil reservoir. Miscible carbon-dioxide injection in light-oil reservoirs is a way to enhance oil recovery and has gained attention since the 1970s from the industry. The advantage of carbon-dioxide injection to the light-oil reservoirs is the low viscosity levels of light oil. Oil interacts with low viscous carbon-dioxide resulting in moderate mobility and, thus, may prevent viscous fingering. Other advantages that carbon-dioxide injection brings are increasing reservoir pressure, trapping in the oil molecules, and sweeping them, thus oil production increases. It also helps matrix to drain oil to the fractures due to gravity drainage effect. Gravity drainage effect occurs

due to the density difference between the fluids in the matrix and the fractures. In this thesis carbon-dioxide injection to the reservoir was studied in several aspects. The result indicates that the carbon-dioxide injection is feasible if some conditions are matched. This can be a turning point of Turkey's petroleum production since there are a small number of fields that have been applied carbon-dioxide injection as a recovery method. In this study, the effects of gravity drainage, relative permeability and miscibility to the recovery factor of one of the Turkey's tight matrix tight fracture oil reservoir are investigated. While miscible injection of carbon-dioxide increases the recovery factor significantly, the effect of relative permeability is very low using two different relative permeability models. The effect of the gravity drainage term in the dual-porosity formula is found lower than two other terms which are viscous displacement and imbibition term. However, it is proved that the effect of the gravity drainage can be increased if the injected carbon-dioxide is let to imbibe the matrix with shut-in periods.

Keywords: Carbon-dioxide, Injection, Gravity, Miscibility

ÖZ

KESİF MATRİKS VE DÜŞÜK KALİTELİ DOĞAL ÇATLAKLI REZERVUARLARDA KARBONDİOKSİT BASIMI ESNASINDA YERÇEKİMİ DRENAJI, KARIŞABİLİRLİK VE GÖRELİ GEÇİRGENLİK ETKİLERİ

Ülker, Murat Can
Yüksek Lisans, Petrol ve Doğal gaz Mühendisliği
Tez Yöneticisi: Dr. Öğr. Üyesi Mehmet Onur Doğan

Eylül 2024, 126 sayfa

Dünyada birincil yöntemlerle petrol üretimi sürekli azalıyor. Henüz keşfedilmemiş çok az petrol veya gaz sahasının kaldığına inanılmaktadır. Dünyanın kahverengi sahaları ya geri kazanım faktörlerinin düşük olması nedeniyle terk ediliyor ya da rezervuar basıncı ya da su üretimi sorunları nedeniyle düşük üretim oranlarında üretim yapılıyor. Yirminci yüzyıldan beri EOR teknikleri çeşitli alanlarda çalışılmış ve uygulanmıştır. Petrol üretim hızının ve geri kazanım faktörünün artırılabileceği ve bunu yapmanın bir yolunun da hafif petrol rezervlerine karbondioksit enjeksiyonu olduğu gözlemlenmiştir. Karışabilen karbondioksit enjeksiyonu, hafif petrol rezervuarlarında petrol üretimini artırmak için 1970'lerin sonunda petrol sektörünün dikkatini çekmeye başlamış bir kurtarma yoludur. Hafif petrol rezevuarlarına karbondioksit enjekte etmenin avantajı, hafif petrolün düşük viskozite değerlerine sahip olmasıdır. Petrolün düşük viskoziteli karbondioksit ile etkileşime girmesi, orta derecede mobiliteye neden olur, bu nedenle viskoz parmaklanmayı önleyebilir. Karbondioksit enjeksiyonunun getirdiği diğer avantajlar olarak rezervuar basıncını artırması, petrol molekülleri içinde kapana kısılıp molekülleri süpürmesi ve bu

sayede petrol kurtarımının artmasını sağlaması sıralanabilir. Ayrıca, karbondioksit enjeksiyonu yerçekimi drenajı etkisi sayesinde matriksteki petrolün çatlaklara akışı hususunda yardımcı olur. Yerçekimi drenajı etkisi matriks ve çatlaklarda bulunan akışkanların arasındaki yoğunluk farkından dolayı gerçekleşir. Bu tez çalışmasında karbondioksit enjeksiyonun farklı versiyonları çalışılmıştır. Çalışmanın fizibilitesi bazı şartlar uygulandığında olumlu olarak sonuç verdiği görülmüştür. Türkiye rezervuarlarında çok az uygulanan karbondioksit enjeksiyonu projelerinin kârlı olduğunu göstermek için yapılan bu çalışma, gelecek projeler için önemli bir dönüm noktası olabilir. Bu çalışmada, yerçekimi drenajı, göreli geçirgenlik ve karışabilirliğin Türkiye'deki kesif matriks ve kesif çatlaklı petrol rezervuarının kurtarım faktörüne etkisi araştırılmıştır. Karbondioksitin karışabilir enjeksiyonu kurtarım faktörünü önemli ölçüde artırırken, iki farklı göreli geçirgenlik modeli kullanıldığında göreli geçirgenliğin etkisinin çok düşük olduğu gözlemlenmiştir. Çift gözeneklilik formülündeki yerçekimi drenajı teriminin etkisi, diğer iki terim olan viskoz yer değiştirme ve emme teriminden daha düşük bulunmuştur. Bununla birlikte, enjekte edilen karbondioksitin üretimin kapalı olduğu dönemlerle matrise emilmesine izin verilirse yerçekimi drenajının etkisinin artırılabileceği kanıtlanmıştır.

Anahtar Kelimeler: Karbondioksit, Enjeksiyon, Yerçekimi, Karışabilirlik

To the Aegean, the Mediterranean, the Steppe..

ACKNOWLEDGMENTS

The author wishes to express his deepest gratitude to Gül Altınbay, Veli Volkan Üstün, Gülcan Türkarslan, and Melike Özkaya Türkmen for their guidance, advice, criticism, encouragement and insight not only throughout the research but also the time he started his career. Their support and trust in the author are the key to this study and career.

The author would also like to thank Ayşe Figan Ülker, Fuat Emre Ülker, Eylem Ülker Çanakçı, Onur Ülker, Çağrı Çanakçı, Duru Çanakçı and Doruk İlhan Çanakçı for being such a family that always protects and always loves. From birth to this moment, the author always felt their hands on his shoulders.

The author would also like to thank METU Music Societies for their friendship in their hearts and every moment, every challenges that they made it through. We gon' make it through (Fred Again.., 2020).

Finally, the author thanks Hasan Can Turunç, Gençay Merey, Demirhan Demir, Atahan Altay, and Alkım Sarıkaş, those who helped in the department and in life, in every moment.

TABLE OF CONTENTS

LIST OF TABLES

TABLES

LIST OF FIGURES

FIGURES

LIST OF ABBREVIATIONS

ABBREVIATIONS

NFA	No Further Action
MMP	Minimum Miscibility Pressure
DST	Drill Stem Test
EOR	Enhanced Oil Recovery
GOR	Gas-Oil Ratio
MICP	Mercury Injected Capillary Pressure
TVDSS	True Vertical Depth Sub Sea
M	Matrix
F	Fracture
DST	Drill Stem Test
SCF	Standard Cubic Feet
STB	Stock Tank Barrel
BBL	Barrel
SM3	Standard Cubic Meters
T	Temperature, ^{o}F
P	Pressure, psi

LIST OF SYMBOLS

SYMBOLS

M_{C5+} C5+ Molecular Weight of crude oil g/mol

M_{C7+} C7+ Molecular Weight of crude oil g/mol

x_{vol} Volatile components mole fraction (C1+N2) in the crude oil, percent

x_{med} Intermediate components mole fraction (C2-C6) in the crude oil, percent

P_{MMP} Minimum Miscibility Pressure

x_1 Reservoir Temperature, ^oC

x_2 Volatile components mole fraction (C1+N2) in the crude oil, percent

x_3 Intermediate components mole fraction (C2-C6) in the crude oil, percent

x_4 C5+ Molecular Weight of crude oil g/mol

x_5 Mole fraction of C1 in the injected gas, percent

x_6 Mole fraction of intermediate components in the injected gas, percent

x_7 Mole fraction of N2 in the injected gas, percent

x_8 Mole fraction of H2S in the injected gas, percent

x_{C1+N2} Volatile components mole fraction (C1+N2) in the crude oil, percent

x_{C2-C6} Intermediate components mole fraction (C2-C6) in the crude oil, percent

X_i Mole fraction in liquid phase

Y_i Mole fraction in vapor phase

Z_i Mixture mole fraction

F_i Hoffman factor

T_{bi} Normal boiling point, ^oK

T_{ci} Critical temperature, ^oK

T_{sp} Test temperature, ^oK

T_{sc} Standard temperature, ^oK

K K value

P_b Bubble point pressure, psia

P_{ci} Critical pressure, psia

P_{sat} Saturation pressure, psia

P_{sc} Standard condition pressure, psia

k_{ro} Oil relative permeability

k_{rg} Gas relative permeability

k_{rw} Water relative permeability

S_{wirr} Irreducible water saturation

S_{or} Residual oil saturation

S_{gc} Critical gas saturation

S_{wc} Critical water saturation

S_g Gas saturation

S_o Oil saturation

S_w Water saturation

λ_w Matrix/fracture transmissibility, STB/d/psi

p_{om} Density of oil in matrix, lb/ft^3

p_{of} Density of oil in fracture, lb/ft^3

p_{cf} Capillary pressure in fracture, psi

p_{cm} Capillary pressure in matrix, psi

h_{wm} Height potential of water in matrix, psi

h_{wf} Height potential of water in fracture, psi

V_{bm} Bulk volume in matrix, rm^3

B_w Water formation volume factor, rm^3/STB

L_z Height of grid block in z-dir, m

Φ Porosity

c_a Mass fraction of component a

p_a Density of the component a

S_a Saturation of phase a

v_a Phase velocity of phase a

J_a Flux due to diffusion of the component in phase a

q_a Source term

CHAPTER 1

INTRODUCTION

In dual porosity systems, carbon-dioxide injection has an advantage named as gravity drainage effect. The gravity drainage effect occurs due to the density difference between two fluids in the reservoir. In G-Field case, it is desired to replace low density gas in fractures with the higher dense oil in the matrix. Therefore, the matrix recovery of the field can increase significantly. Research on gravity drainage in dual-porosity reservoirs was initiated by McLennan and Fancher (1980) who provided an important theoretical framework based on combining Darcy's law with the gravity-driven flow equations to describe fluid migration between matrix and fractures, giving rise to subsequent works in this subject area (McLennan & Fancher, 1980). This pioneering work was taken a step further by Ho and Haaland (1985) by employing advanced mathematical models to describe gravity drainage mechanisms in fractured reservoirs, with an added focus on fluid flow dynamics due to the presence of fractures (Ho and Haaland, 1985). Watson and McLaughlin (1990) built on these developments, providing a detailed survey of theoretical, numerical and experimental work on gravity drainage, synthesizing our understanding to that point and highlighting areas where the literature was incomplete (Watson & McLaughlin, 1990). Hartman and Stevens (1995) furthered the field with numerical simulation techniques specifically designed for dual-porosity reservoirs, integrating dual porosity and permeability concepts to improve performance predictions (Hartman & Stevens, 1995). Liu and Zhang (2000) contributed empirical data from laboratory models to validate theoretical models and observe gravity drainage behavior in fractured reservoirs (Liu & Zhang, 2000). Smith and Johnson (2005) explored various gravity-assisted recovery methods and provided practical recommendations

for enhancing oil recovery through gravity drainage based on theoretical and field data (Smith & Johnson, 2005). In their studies, Zobeidi, Shafie and Ghazvini (2021) found out that the effect of gravity drainage to the recovery in a highly fractured reservoir is 13% which is the half of the total recovery.

Regarding relative permeability models for oil and gas reservoirs, the research appears to have progressed in dealing with the challenges posed by fluid flow in porous media. The earliest relevant attempts by Corey (1977) laid down the principles of relative permeability and introduced data driven approaches to model multi-phase flow regimes focused on oil, gas and water movement (Corey, 1977). However, such orientations of the developments have been progressively challenged by Stone (1979) in his Stone 1 and 2 models whereby the hysteresis and capillary pressure effects were incorporated to allow accurate relative permeability characterization of multi-phase systems (Stone, 1979). Brooks and Corey (1980) attempted to revise these models with elements such as dimensionless empirical and parametric relationships which correlate to varying degrees of fluid saturations and other interactions (Brooks & Corey, 1980). In the 1990s, more advanced such as Van Genuchten's models dating back to 1991 enhanced relative permeability modeling accuracy by providing methods to account for saturation history and capillary pressure effects on the relative permeability than the models that came before them (Van Genuchten, 1991). Morrow and Buckley (2006), who have contributed new ideas and models, offered greater details coalescing laboratory inputs and numerical simulations wherein more accurate relative permeability models was developed able to take into account heterogeneity, non-equilibrium effects, and other complexities (Morrow & Buckley, 2006). Finally, Zhang et al. (2012) presented a more comprehensive model-of-relativity-on-permeability that integrates several modeling methods to study relative permeability trends in a wider range of pervading conditions (Zhang, Li, & Wang, 2012).

The carbon-dioxide injection is an EOR technique that is been used in industry for decades. In Turkey, carbon-dioxide injection in Batı-Raman Field still continues and its efficiency is described in the published papers. The injection of carbon-dioxide

can be divided into two, namely a miscible and immiscible injection. The controlling mechanism of the miscible injection is the minimum miscibility pressure of the oil and the reservoir pressure of the field. The minimum miscibility pressure can be measured with slim-tube experiments, slim-tube simulation or correlations published in the literature. Miscibility between oil and carbon-dioxide has been an area of research that has developed quite a lot over the years. Hsu and Morrison (1974), for example, attempted to offer earlier investigations as to the fundamental concepts of an interaction existing between carbon-dioxide and oil and made first attempts to formulate criteria for determination of the miscibility conditions related to pressure and temperature (Hsu & Morrison, 1974). Doughty and Hsu (1990) continued this research and improved the models making them more applicable by including detailed analysis of phase behavior and the mechanisms of miscibility and pointed how difficult it will be and how it can be improved by subsurface injection of carbon-dioxide to improve its miscibility and therefore how much of oil recoverable (Doughty & Hsu, 1990). However, in the mid,' 90s Zhang and Wichterle (1995) carried out research to check whether the theoretical concepts were correct and presented data on temperatures and pressures necessary for dissolution of various crudes with CO2 (Zhang & Wichterle, 1995). Following up on this, Johnson and Tham, (2001) proposed a more complex model which was to test the applicability of oil composition and CO2 concentration on the miscibility aspects by giving carbon-dioxide enhanced oil recovery application (Johnson & Tham, 2001). Alvarado and Manrique (2002) later discussed results of a number of field trials and design studies on various techniques and operational strategies for carbon-dioxide flooding with respect to achieving miscibility and various factors and issues which needed to be taken into account and how these might be used in the field (Alvarado & Manrique, 2002).

In this thesis, the numerical simulation of the G-Field has been done. PVT sample was analyzed in the laboratory. The results were quality-checked with various methods. The compositional fluid model is built with the FluidModeler software by Slb. The minimum miscibility pressure of the fluid is simulated with the simulation

software Eclipse300 by Slb. The capillary pressure and porosity permeability data were measured in the laboratory. Relative permeability data is derived from the capillary pressure data. Since the relative permeability is not measured with the laboratory tests, the sensitivity analysis has been done with two different relative permeability models. Observed data, bottom hole pressure, water cut, and oil rate, were used as input to the history match. In order to find bottom hole pressure, a MatLAB code is developed. The field is simulated with the Intersect Compositional software by Slb. Different daily injection rate, different relative permeabilities, miscible and immiscible displacement, huf and puf method and gravity drainage effect cases were run to understand the different aspects of carbon-dioxide injection.

CHAPTER 2

LITERATURE REVIEW

2.1 PVT Quality Check

The reservoir fluid properties that flow through the porous media are important parameters for reservoir simulation. Reservoir fluid properties can be obtained by the laboratory measurements. In the laboratory, the Constant Composition Test is done to find bubble point pressure, the Ø-Flash Separation Test is done to measure formation volume factor, density, and gas-oil ratio, and the viscosity test is done to measure the viscosity of the reservoir fluid. The composition of the fluid is determined with the gas emerging during the Ø-Flash Separation test. However, the PVT analysis quality should be checked with the various techniques. In a field development plan, any inconsistency in the fluid properties may lead wrong results. In their article, Hashemi et al. (2020) gathered the consistency check procedures together.

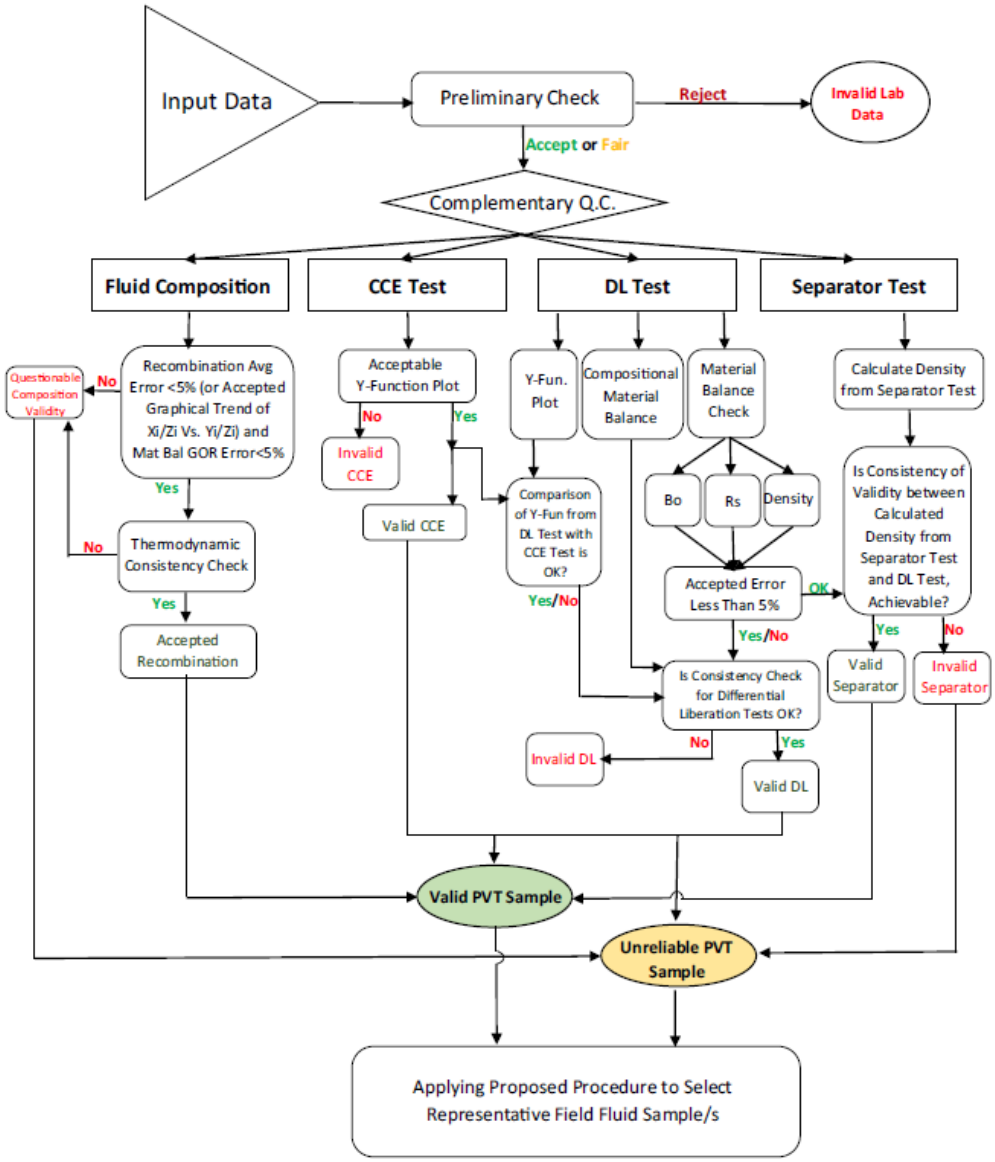

Figure 2.1. The flowchart for the selection of fluid samples represent the reservoir (Hashemi et al., 2020)

The procedures they proposed includes the Vasquez-Beggs Plot, Hoffman Plot, and Material Balance Check for the PVT Quality Check. The validation of viscosity test in the laboratory can be done with the Vasquez-Beggs plot. The yielding straight line

of the plot μ_o/μ_{ob} vs P/P_b can be thought to be a consistency check for the viscosity of the fluid.

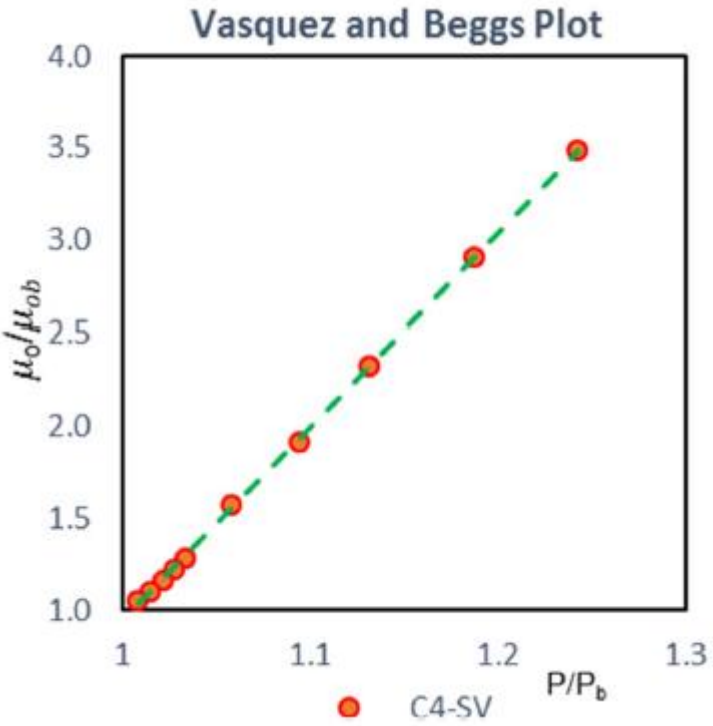

Figure 2.2. Consistent behavior of viscosity checked with Vasquez-Beggz Plot (Hashemi et al., 2020)

The compositional analysis can be checked with two different methods. Recombination and Material Balance check is developed to analyze the liquid and vapor phase molar fraction consistency.

$$\frac{Y_i}{Z_i}=\left(-\frac{L}{V}\right)\left(\frac{X_i}{Z_i}\right)+\frac{F}{V} \tag{2.1}$$

$$z_i=F_g\gamma_i+(1-F_g)*x_i \tag{2.2}$$

$$F_g=\frac{1}{1+136.986*\left(\frac{\gamma_o}{Mw_oR_s}\right)} \tag{2.3}$$

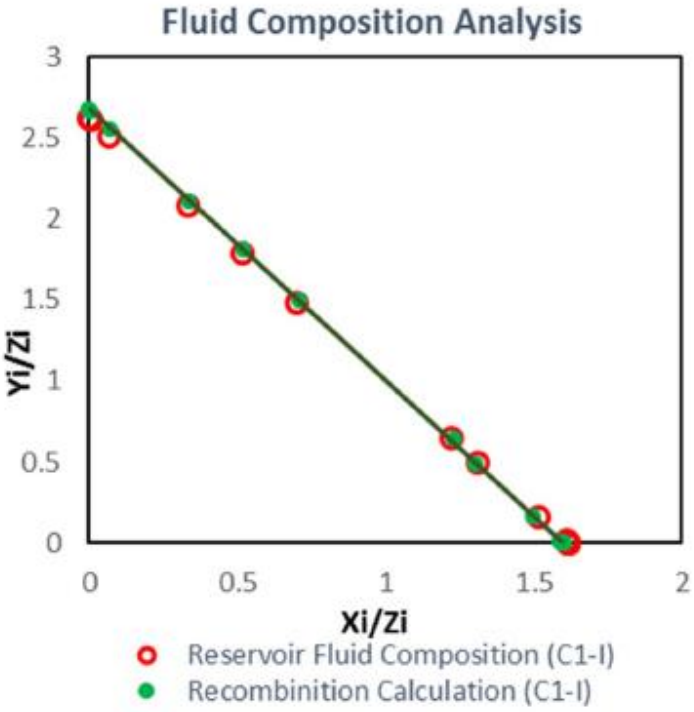

Figure 2.3. Material Balance Check Plot for Fluid Composition Consistency (Hashemi et al., 2020)

Another composition analysis consistency check is described based on the thermodynamic equilibrium. Hofmann Plot developed by Hoffman et al. (1953) is a technique to check the compositional analysis. It uses the K value denoting the vapor phase molar composition of a component divided by the liquid phase of a mixture reached the equilibrium.

$$K_i = \frac{\gamma_i}{x_i} \tag{2.4}$$

Hoffman Factor, F_i, is introduced by Hoffman et al. to create the Hoffman Plot and check the consistency of the compositional analysis.

$$F_i = \frac{\log\left(\frac{P_{ci}}{P_{sc}}\right)}{\frac{1}{T_{bi}} - \frac{1}{T_{ci}}} * \left(\frac{1}{T_{bi}} - \frac{1}{T_{sp}}\right) \tag{2.5}$$

The intermediate (C1-C6) components log(K_i) vs F_i plot should yield a straight trend based on the Hoffman et al.

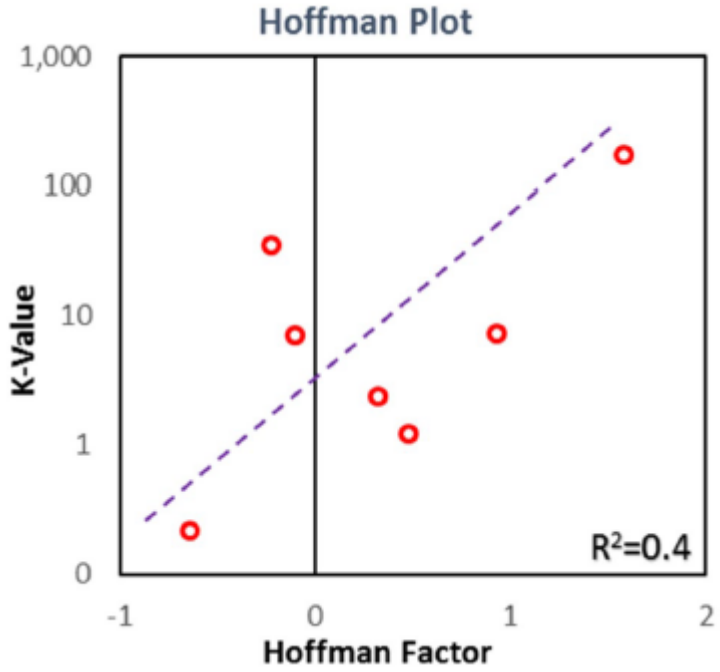

Figure 2.4. Hoffman Plot for the thermodynamic consistency check of the compositional analysis (Hashemi et al., 2020)

2.2 Minimum Miscibility Pressure

Minimum Miscibility Pressure (MMP) is the lowest pressure value required for petroleum to mix with another fluid (usually another hydrocarbon or fluid). This concept is critical in secondary and tertiary recovery methods. Secondary recovery methods can be named as water injection or carbon-dioxide injection to pressurize the field. On the other hand, tertiary production methods generally alters the rock or fluid properties. During the production, the reservoir pressure decreases, therefore the viscosity of oil increases due to its fluid properties. This causes lower production rates in the field. In secondary or tertiary recovery methods, oil viscosity may be reduced due to the pressure increase in the pores or miscibility. The factors affecting the MMP are oil composition, reservoir temperature, or dissolved gas ratio in the oil.

As the reservoir temperature increases, the MMP value of the oil decreases, or as the dissolved gas ratio increases, MMP decreases. There are several techniques to measure or calculate the MMP value of an oil. Slim-tube experiments, slim-tube simulations, or correlations can yield minimum miscibility pressure of the oil. (Li et al., 2012b)

The slim Tube experiment depends on a setup where a tube with a thin diameter is loaded with sand packages to create a porous media. The porous media is saturated with the tested oil. The desired fluid that is tested, whether it is miscible or immiscible with the crude oil then flooded into the tube. The oil recovery from the tube is recorded with the different pressure inlets. After some point, the acceleration of recovery of the oil will decrease due to the miscibility. The pressure point where the 90% oil recovery is accepted to be Minimum Miscibility Pressure. (Ameri et al., 2013)

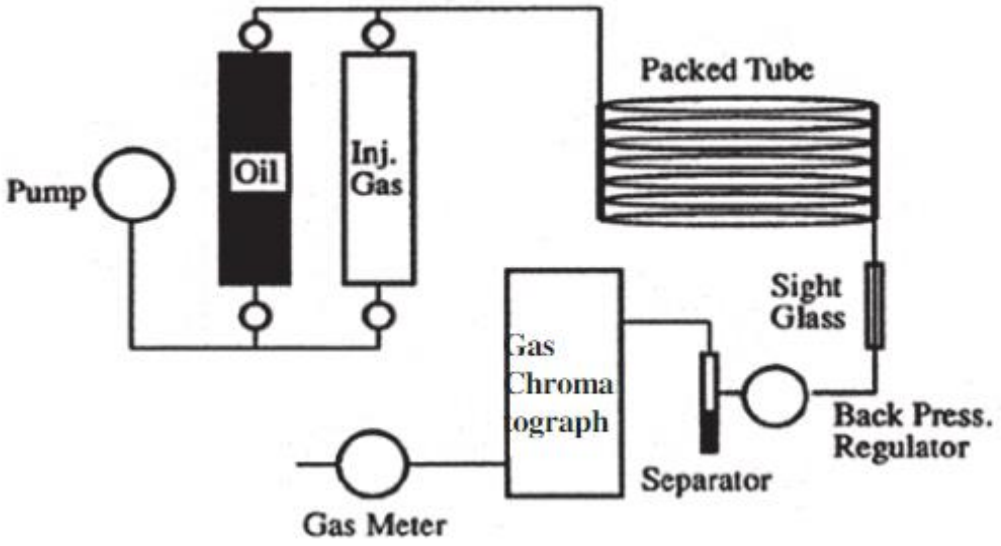

Figure 2.5. Slim-tube experiment setup (Ameri et al., 2013)

The minimum miscibility pressure also can be calculated with the correlations. In their article, Zhang et al., (2015), gathered 8 different correlations from 8 different authors. They also mentioned the limitations of those correlations where reservoir temperature, oil gravity, MMP range, etc. taken into account.

$$P_{MM,\,pure}=0.11027*(1.8T+32)^{0.744206+0.0011038M_{C5}+0.0015279x_{vol}} \quad (2.6)$$

$$P_{MM,\,pure}=7.3924*10^{2.772-\left[\frac{1519}{492+1.8T}\right]} \quad (2.7)$$

$$P_{MM,\,pure}=12.6472+0.01553(1.8T+32)+1.24192*10^{-4}(1.8T+32)^2-\left(\frac{716.9427}{1.8T+32}\right) \quad (2.8)$$

$$P_{MM,\,pure}=0.101386*\exp\left[10.91-\left(\frac{2105}{255.372+0.5556(1.8T+32)}\right)\right] \quad (2.9)$$

$$P_{MM,\,pure}=5.58657-2.3477*10^{-2}M_{C7+}+1.1725*10^{-11}M_{C7+}^{3.73}*\exp^{786.8M_{C7+}^{-1.058}}(1.8T+32) \quad (2.10)$$

$$P_{MM,\,pure}=6.0536*10^{-6}(1.8T+32)^{1.06}(M_{C5+})^{1.78}\left(\frac{x_{vol}}{x_{med}}\right)^{0.136} \quad (2.11)$$

$$P_{MM,\,pure}=5.0093*10^{-5}(1.8T+32)^{1.164}(M_{C5+})^{1.2785}\left(\frac{x_{vol}}{x_{med}}\right)^{0.11} \quad (2.12)$$

$$P_{MM,\,pure}=3.9673*10^{-2}T^{0.8293}*(M_{C7+})^{0.5382}(x_{C1+N2})^{0.1018}(x_{C2-C6})^{-0.2316} \quad (2.13)$$

Equation 2.6 introduced by Cronquist (1977) has limitations of oil API between 23.7 and 44.8, reservoir temperature between 21.67 to 120.8 ^{o}C, and MMP value between 7.4 to 34.5 MPa.

Equation 2.7 introduced by Lee (1979) accepts if the calculated MMP value is lower than bubble point pressure, MMP is taken as bubble point pressure.

Equation 2.8 developed by Yelling & Metcalfe (1980) considers the reservoir temperature between 35.8 and 88.9 ^{o}C.

Equation 2.9 published by Orr & Jensen (1984) described their correlation is suitable for the reservoirs with low reservoir temperature, $T_{res} < 49$ ^{o}C.

Equation 2.10 introduced by Glaso (1985) only considers whether the molar fraction of intermediate components, C2-C6, is higher than 0.18 or not.

Equation 2.11 developed by Alston et al. (1985) has no limitations, however, it uses bubble point pressure as MMP if the calculated MMP is lower than bubble point pressure.

Equation 2.12 published by Emera & Sarma (2005) has limitations of reservoir temperature, MMP and M_{C5+} value. Reservoir temperature should be in between 40.8 and 112.2 ^{o}C, MMP value calculated from this equation should be in between 8.28 and 30.2 MPa and M_{C5+} value should be in between 166.2 and 267.5 g/mol.

Equation 2.13 published by Chen et al. (2013) has limitations of reservoir temperature, MMP and M_{C5+} value. Reservoir temperature should be in between 32.2 and 118.3 ^{o}C, MMP value calculated from this equation should be in between 6.9 and 28.17 MPa and M_{C5+} value should be in between 185 and 249 g/mol.

2.3 Relative Permeability Models

Relative permeability is the key parameter of the multiphase porous media flow. It determines the flow capacity of a fluid in the system where other fluids in place. It can be described as the ratio of the effective permeability of a fluid divided by the absolute permeability of the medium. The relative permeability of a rock can be measured with the laboratory measurements, as well as with correlations and models created by various authors. Corey (1954) introduced his empirical model in his article derived from the capillary pressures. Afterwards, Brooks & Corey (1964) extended the model.

$$k_{ro}=\left(\frac{S_o-S_{or}}{1-S_{or}}\right)^{\frac{2+\lambda}{\lambda}} \quad (2.14)$$

$$k_{rw}=\left(\frac{S_w-S_{wirr}}{1-S_{wirr}}\right)^{\frac{2+\lambda}{\lambda}} \quad (2.15)$$

$$k_{rg}=\left(\frac{1-S_g}{1-S_{gc}}\right)^{2} * \left[1-\left(\frac{S_g-S_{gc}}{1-S_{gc}}\right)^{\frac{2+\lambda}{\lambda}}\right] \quad (2.16)$$

Equation 2.14, 2.15, and 2.16 can be applied only to the porous media initially saturated with oil. Those equations do not let the critical gas saturation to be zero value. Those equations are Brook & Corey equations, however, they can be reduced to the Corey equation if the λ value equals to two. λ value describes the pore throat size distribution. If the distribution of the pore sizes are narrow, λ value is greater than 2. On the other hand, for the wide distributions, it is lower than 2.

There are also modified Brooks & Corey models for the corresponding phase described as Power Law.

$$k_{ro}= k_{ro,max}\left(\frac{S_o- S_{or}}{1- S_{or}-S_{wc}- S_{gc}}\right)^{n_o} \quad (2.17)$$

$$k_{rw}= k_{rw,max}\left(\frac{S_w- S_{wc}}{1- S_{or}-S_{wc}- S_{gc}}\right)^{n_w} \quad (2.18)$$

$$k_{rg}= k_{rg,max}\left(\frac{S_g- S_{gc}}{1- S_{or}-S_{wc}- S_{gc}}\right)^{n_g} \quad (2.19)$$

The n_o, n_w, and n_g exponents are ranging from one to six.

2.4 Gravity Drainage

The phenomenon of gravity drainage in petroleum reservoirs arises due to variations in the densities of the reservoir fluids. This process can be demonstrated by placing crude oil and water in a container, then agitating the mixture. Upon allowing the container to settle, the denser fluid will gravitate to the bottom, while the less dense fluid will float above the denser fluid. This separation is a direct result of the gravitational forces exerted on the fluids.

In petroleum reservoirs, the effects of gravity result in a stratified arrangement of fluids: gas is located at the uppermost layer, oil is found beneath the gas, and water resides at the bottom. This stratification is a consequence of prolonged petroleum accumulation and migration processes, which generally lead to an equilibrium state among the reservoir fluids. Under equilibrium conditions, the interfaces between gas and oil, as well as between oil and water, are expected to be nearly horizontal. Although precise determination of the fluid contacts can be challenging, existing data suggest that these contacts are predominantly horizontal in most reservoirs. Gravity segregation of fluids is likely present to varying degrees in all petroleum reservoirs, with its significance in oil production potentially being substantial depending on the angle of the reservoir dip. (Ahmed, 2006)

In their laboratory studies, Zobeidi and Fassihi (2018) concluded that gas infiltration into the matrix block is more effective when the block height is higher. The oil recovery from the matrix blocks is a function of block number. Miscible injection to the system is better understood with the assumption of effective mixing of solvent and the oil in the fractures.

In their study, Zobeidi, Shafie and Ghazvini (2021) showed the gravity drainage effect on a highly fractured reservoir. They simulated both cases where the gravity drainage option is open and closed and briefly explained the difference between two cases. They find out that in a highly fractured reservoir, the gravity drainage contributes to the recovery factor about 50%.

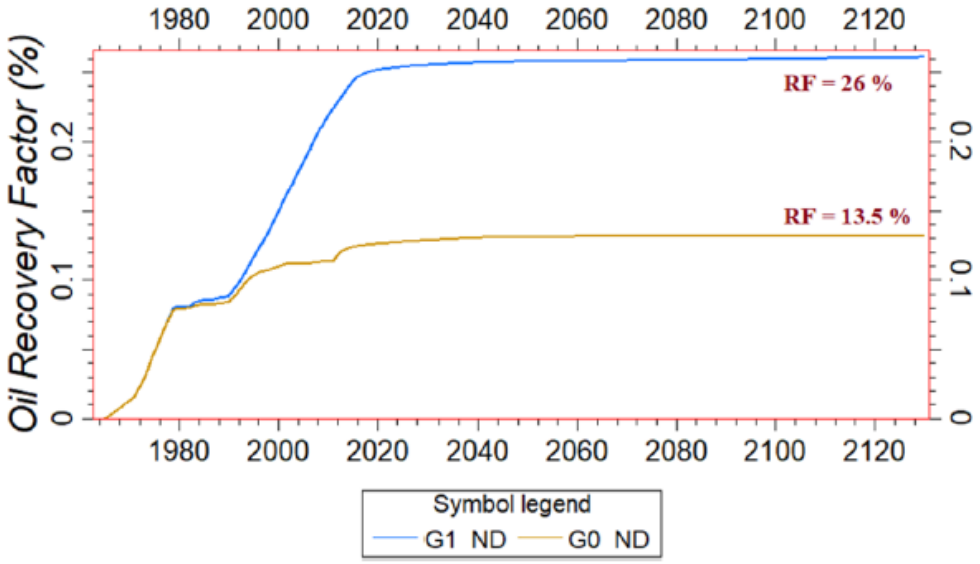

Figure 2.6. Comparison of cases with gravity drainage and no gravity drainage (Zobeidi et al., 2021)

Thomas et. al. (1983), characterized the flow in dual porosity systems with below formula.

$$-\lambda_w\left(p_{om}-p_{of}+\left(p_{cf}-p_{cm}\right)+C\Delta p_{gravity}\right)=\left(\frac{V_{bm}}{\Delta t}\right)\delta\left(\frac{\emptyset S_w}{B_w}\right)_m \tag{2.20}$$

Later, Sonier et. al. (1988), changed the gravity term to the dynamic gravity term.

$$-\lambda_w\left(p_{om}-p_{of}+\left(p_{cf}-p_{cm}\right)+\gamma_w(h_{wm}-h_{wf})\right)=\left(\frac{V_{bm}}{\Delta t}\right)\delta\left(\frac{\emptyset S_w}{B_w}\right)_m \tag{2.21}$$

$$h_w=\left(\frac{S_w-S_{wc}}{1-S_{wc}-S_{or}}\right)*L_z$$

The gravity drainage term is decribed as the head difference between the fluids in the fracture and matrix. The eliminated gravity drainage means the neglection of the gravity term from the dual porosity three phase flow equation.

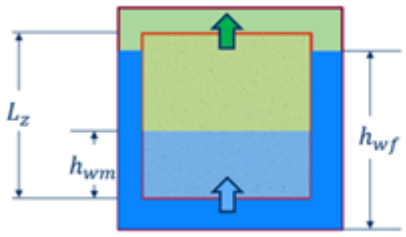

Figure 2.7. Graphical explanation of the fracture-matrix imbibition by the gravity drainage

2.5 Miscible Injection

In their study, Abdullah and Hasan (2021) stated that carbon-dioxide injection represents a well-established enhanced oil recovery method widely employed within the oil and gas sector for several decades. This technique is typically applied subsequent to primary recovery, which extracts 10% to 20% of the original oil in place, and secondary recovery, which yields an additional 10% to 20%. The primary role of carbon-dioxide injection is to act as a solvent, facilitating the extraction of residual oil. Under reservoir conditions, carbon-dioxide can dissolve in the oil, achieving a miscible state. This miscibility reduces the oil's viscosity and causes it to swell, thereby enhancing its flow through the reservoir. Most carbon-dioxide EOR projects operate under conditions of miscibility; however, carbon-dioxide can also be used under immiscible conditions for oil extraction (Cooney et al., 2018; Steinsbo et al., 2014; Tadesse, 2018; Whittaker and Perkins, 2013; Kalra et al., 2017).

Nonetheless, not all reservoirs are available for CO2 injection. Factors such as the reservoir depth, composition of the oil, temperature, and other relevant characteristics must be considered. The concept of minimum miscibility pressure (MMP) is crucial in this context. MMP refers to the lowest pressure at a constant temperature at which CO2 becomes miscible with the oil, resulting in a single-phase system that enhances fluid flow efficiency. Accurate estimation of MMP is essential for optimizing CO2 flooding and can significantly improve recovery outcomes (Al-

netaifi, 2008; Liu, 2013; Rezaei et al., 2013). Typically, effective CO2 injection occurs at depths exceeding 2500 feet, with oils possessing greater than 22 degrees API gravity and viscosities below 10 cP. Additionally, the oil saturation should be greater than 20% of the pore volume (Ansarizadeh et al., 2015; Aroher and Archer, 2010; Meyer, 2007). Globally, CO2 injection has facilitated the recovery of approximately 450 billion barrels of oil (Bergmo and Anthonsen, 2014; Cook, 2012; US Chambers, 2021; Tian and Zhao, 2008).

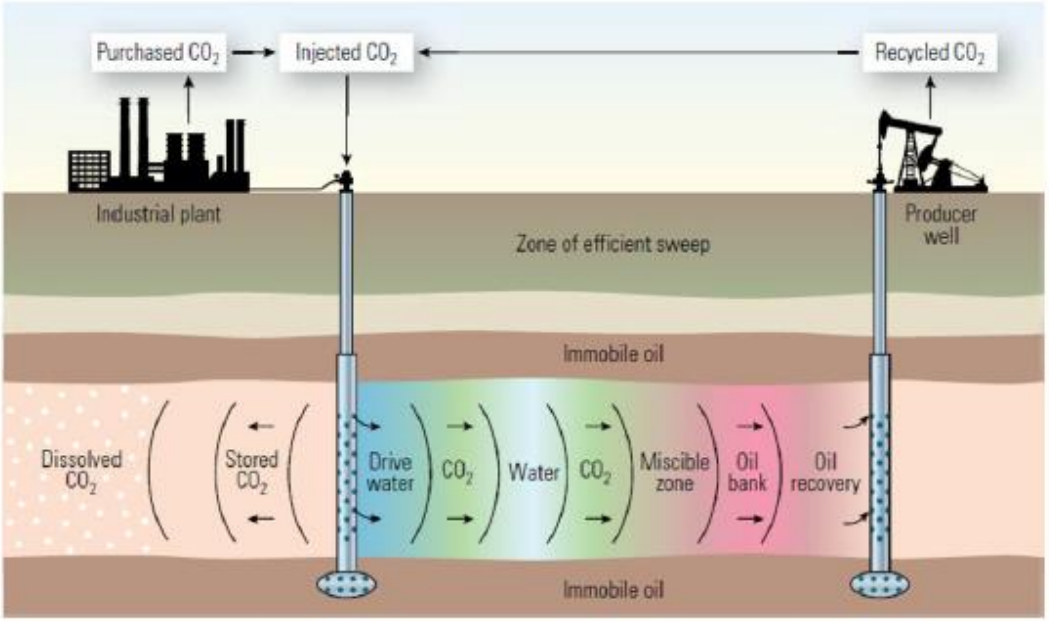

Figure 2.8. Illustration of miscible CO2 injection (Aroher and Archer, 2010)

2.5.1 Single Contact Miscibility

Single-contact miscibility refers to the phenomenon where CO_2 and oil achieve a homogeneous, single-phase mixture in a single interaction or exposure. This condition is typically assessed in laboratory experiments where a sample of oil is brought into contact with CO_2 under controlled temperature and pressure conditions. The critical pressure and temperature at which CO_2 and oil become fully miscible in one step indicate single-contact miscibility. This type of miscibility is characterized by the formation of a single-phase fluid where the CO_2 is dissolved in the oil, reducing its viscosity and improving its flow characteristics, which facilitates enhanced oil recovery (Srivastava et al., 2017; Alvarado and Manrique, 2010).

2.5.2 Multiple-Contact Miscibility

Multiple-contact miscibility involves the process where CO_2 and oil undergo several stages of interaction before achieving a single-phase mixture. This process typically simulates real-world conditions where CO_2 interacts with oil through successive stages or cycles, each contributing to the overall miscibility. In this scenario, miscibility is achieved not in a single contact but through a series of interactions that gradually reduce the interfacial tension and enhance the solubility of CO_2 in the oil (Rojas et al., 2015; Liu et al., 2018). This approach is particularly relevant in practical applications where CO_2 injection might occur in multiple phases or stages.

2.6 Component Based Material Balance

In many situations, a phase can contain multiple chemical species that are mixed at the molecular level, typically sharing the same velocity and temperature. This contrasts with immiscible flows, as dispersion and Brownian motion lead to the redistribution of components when there are significant gradients in mass fractions.

In multicomponent, multiphase flow scenarios, it is optional to conserve mass either for individual components or for entire fluid phases. If it is desired to conserve mass for fluid phases, source terms should be included in simulation equations to account for the transfer of components between phases. For a system with N fluid phases and M chemical species, the mass conservation equation for each component i, where i=1,...,M, is given by;

$$\frac{\partial}{\partial t}\left(\emptyset \sum_{\alpha} c_{\alpha}^{l}\rho_{\alpha}s_{\alpha}\right) + \nabla \cdot \left(\sum_{\alpha} c_{\alpha}^{l}\rho_{\alpha}\overrightarrow{v_{\alpha}} + \overrightarrow{J_{\alpha}^{l}}\right) = \sum_{\alpha} c_{\alpha}^{l}\rho_{\alpha}q_{\alpha} \qquad (2.22)$$

Here, v_a represents the superficial phase velocity, and q_a is the source term. This system is closed similarly to single-component phases, but it should be ensured that the sum of mass fractions equals zero. This equation can also be applied to miscible displacements, where the composition of the fluid phases changes due to variations in pressure and saturation within the porous medium, requiring consideration of components present. (Lie, 2019, p. 246)

CHAPTER 3

STATEMENT OF PROBLEM

Naturally fractured reservoirs are heterogeneous environments. The permeability tensor of a fracture depends on the azimuth and the strike angle of the fracture. The injection direction of a fluid can easily bypass the matrix and sweep only the fracture. In this study, the injection directions are determined with respect to the fracture azimuth and strike angles to gain the most efficient petroleum recovery.

Injection of a fluid into the reservoir sweeps the reservoir fluid with a specific sweep efficiency. Sweep efficiency can be affected by the mobility ratio of the fluids. The mobility ratio depends on the relative permeability and viscosity of the fluids. Relative permeability is a rock property whereas viscosity is a fluid property. In this study, the sweeping efficiency of the injection is investigated with changing fluid and rock properties.

G-Field is a naturally fractured carbonate reservoir where the both matrix and fracture quality are not in a desirable level. The production from the field continues from 4 different reservoir units with 4 production wells. However, the performance of the wells decreases as the production continues due to a rapid decline in the reservoir pressure due to the closed environment of the reservoir and low aquifer support.

It has been observed that the field itself will not produce effective oil since the oil transported from matrix to fracture while producing is not sufficient. There is a lack of porosity and permeability in the reservoir sections. The recovery factor of the field will be very low if the field is not intervened. There are secondary or tertiary production techniques that can be applied to increase the oil recovery. However, the field must provide rock and fluid properties to be successful in those techniques. For example, water flooding requires water-wet rock or good matrix properties such as

porosity and permeability. G-Field is an oil-wet carbonate reservoir, thus the water flooding can not be applied. Miscible or immiscible carbon-dioxide injection can be applied to the G-Field. The gravity drainage mechanism can exchange the gas in the fractures and the oil in the matrix due to the density difference, thus increasing the matrix recovery. The pressure support provided by the injected gas can increase cumulative oil production.

CHAPTER 4

G-FIELD OVERVIEW

G Field, located in Adıyaman District of Turkey, is an oil field discovered in August 2020 with the exploration well G-1. The field is operated by the Turkish Petroleum Corporation (TPAO). There are five wells drilled, where four of them produce oil and one is abandoned due to geological reasons. G Field is a relatively small field where the reservoir area is 1.74 km^2. The field is bounded by 2 faults, the Adıyaman Fault and G Fault, and by the Oil Water Contact. The first producing well, G-1, tested three possible hydrocarbon-bearing formations, K-C, KRG and SYD. The second producing well, G-4, tested a possible hydrocarbon-bearing formation which is DRD, but the reservoir fluid was water. However, the G-4 well tested another possible hydrocarbon-bearing formation, K-B, where the G-1 well did not test. Therefore, it is understood that there are four formations bearing oil in the G Field.

The petroleum system of the G field consists of three elements as usual. Shaly limestone K-A formation and cherty limestone KRG formations are the source rocks of the field. Naturally fractured K-B, K-C, KRG and SYD formations are the reservoirs, but based on the Nelson Classification of Fractured Reservoirs (Nelson, 2001), those formations should be separated due to their porosity and fracture behaviors. In the field, limestone K-B and cherty limestone KRG formations have no significant porosity, thus should be considered as Type II reservoir based on the Nelson Classification of Fractured Reservoirs. The main reservoir of the field is naturally fractured limestone K-C formation. It has the main porosity system and the fractures open to flow, therefore most of the oil is stored in the K-C formation. The formation has an average of 5% porosity and matrix permeability of 0.1 to 5 mD. The main flow mechanism is the fractures in the formation, where the system permeability has been measured as 0.1 to 100 mD. Although it has a matrix porosity, the matrix does not contribute to the production as the fractures contribute, so the K-

C formation should be grouped as Type III reservoir. The cap rock of the field is SYD formation which is naturally fractured shaly limestone. Due to the lack of porosity, SYD formation can contribute to the system as cap rock. However, due to tectonic activity in the region after the deposition, the secondary porosity, natural fractures, occurred in the SYD formation where the oil can migrate into them. The fractures are the only flow and storage mechanism in the SYD formation so that SYD formation can be grouped as Type I reservoir also.

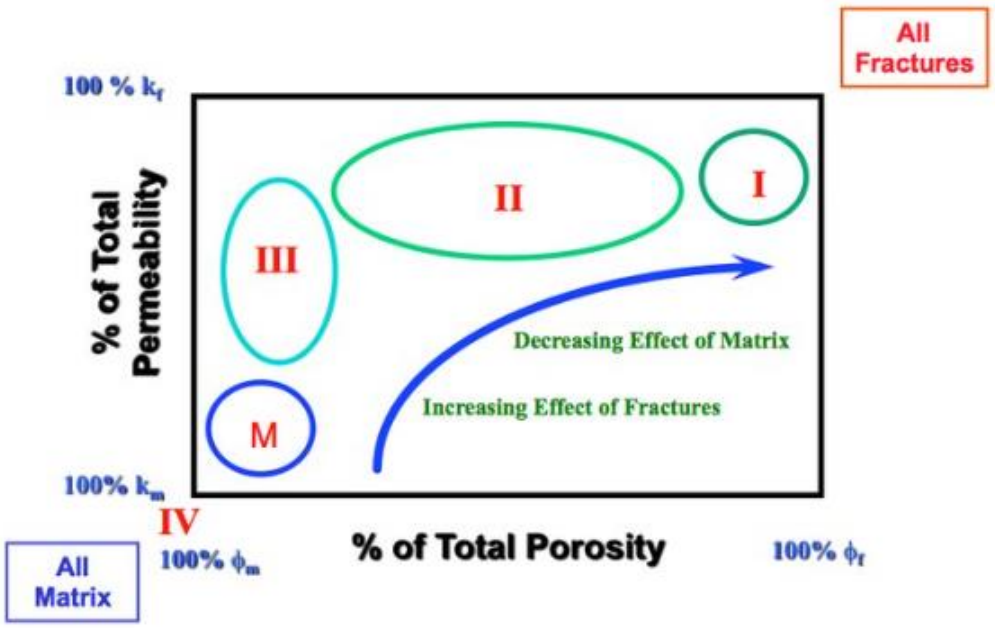

Figure 4.1. Nelson Classification of Naturally Fractured Reservoir, Nelson (2001)

The exploration well G-1 put on production on the 28th of August, 2020 with three perforations. During the drilling of the well, there have been two DST operations, one comprises SYD and KRG formations while other one is done in the K-C formation. Workover operations started after the drilling, where three perforations tested with the swab operations. Perforations belong to the K-C, KRG

and SYD formations, respectively. The K-C formation perforation is also tested with Cased Hole DST. After the workover operations, a PVT sample taken from the bottom hole of the well to be analyzed in the laboratory. The original reservoir pressure of the field has been determined by the Amerada operation done before the PVT sampling which is 3030 psi at the -1750 TVDSS.

The drilling and workover activities of the appraisal well G-4 was done and the well put on the 9th of April, 2022. It was the first well to test the productivity of K-B formation. A core sample from the K-C formation taken from the well to be analyzed on the laboratory. The G-4 well also tested DRD formation for its oil production possibility in the region, however, the only reservoir fluid was water. This gave an idea about the Oil Water Contact of the field.

The production wells, G-3 and G-5 started producing oil on the 21st of June 2022 and 5th of January 2023, respectively. G-3 well has only one perforation at the K-C formation while G-5 well has 4 perforations, one in the K-C formation, one in the KRG formation, and 2 in the SYD formation.

Workover operations continued after the production started. After the oil exploration in the K-B formation with the G-4 well, G-1 well was stopped to do workover operation on the 21st of May, 2022. Already drilled K-B formation was perforated in G-1 well in this operation. After the perforation, stimulation operation as acidizing has been done. The oil production rate increased by 325 STB/d. Another workover operation was also carried out in the G-4 well. Due to the low oil rate, K-C formation was perforated and acidized with the K-B formation perforation. Oil rate increased by 50 STB/d in this well also. G-5 well is another well subjected to workover operation after the production started. Due to the low bottom hole pressure in the well, acidizing job carried out in the well. After the acidizing, the bottom hole pressure of the well increased by 1000 psi.

4.1 Fluid Properties

The PVT sample taken from the G-1 well was analyzed on the TPAO Research and Development Center Reservoir Technologies Directorate laboratory. The sample taken from 2100 meters MD bottom of the well. The live oil PVT sample subjected to Constant Composition Expansion (CCE) test, Ø-Flash Separation test, Viscosity test and Composition analysis. All of the tests done at the reservoir temperature which is 205 ^{o}F. (Türkmenoğlu & Arslan, 2020)

$$Oil\ Gravity = 32\ API$$

$$Bubble\ Point\ Pressure = 350\ psig$$

$$Thermal\ Expansion\ Constant = 4.5 * 10^{-4} cc/\frac{cc}{^{o}F}$$

Table 4.1 Compositional Analysis from the Lab of G-Field Oil

Component	Seperator Gas Mol %	Seperator Oil Mol %	Reservoir Oil Mol %	MW (g/mol)
N2	26.59	0	0.59	28.014
CO2	37.09	0	0.83	44.01
C1	15.78	0	0.35	16.043
C2	5.14	0	0.11	30.07
C3	6.54	0.74	0.87	44.097
i-C4	1.38	1.99	1.98	58.124
n-C4	4.03	0	0.09	58.124
i-C5	1.51	0	0.03	72.151
n-C5	1.65	0.18	0.21	72.151
n-C6	0.09	0.71	0.7	86.178
n-C7	0.13	3.3	3.23	96
C8	0.06	14.64	14.32	107
C9	0	11.13	10.88	121
C10	0	13.49	13.19	134
C11	0	7.86	7.68	147
C12	0	8.32	8.14	161
C13	0	5.2	5.09	175
C14	0	6.54	6.39	190
C15+	0	25.89	25.31	310.136

Table 4.2 CCE Test Results, Oil Compressibility

Pressure (psig)	Oil Compressibility (cc/cc/psig*10-6)
2000	8.0713
1500	8.6982
1000	9.4897
750	10.052
500	10.6833
400	26.7264

Table 4.3 CCE Test Results, Relative Volume

Pressure (psig)	Relative Volume (Vi/Vk)
3000	0.9746
2000	0.9824
1500	0.9865
1000	0.991
750	0.9936
500	0.996
400	0.9973
350	1
250	1.2656
125	2.149

Table 4.4 Ø-Flash Separation Test Results

Pressure (psig)	Oil FVF (bbl/STB)	GOR (SCF/STB)	Oil Density (g/cc)
3000	1.1038	88.4	0.806
2000	1.1126	88.4	0.7996
1500	1.1173	88.4	0.7963
1000	1.1224	88.4	0.7927
750	1.1253	88.4	0.7907
500	1.128	88.4	0.7887
400	1.1295	88.4	0.7877
350	1.1326	88.4	0.7856
0	1.0666	0	0.8114

Table 4.5 Viscosity Test Results

Pressure (psig)	Oil Viscosity (cP)
3000	2.089
2500	2.013
2000	1.927
1500	1.845
1000	1.771
750	1.679
500	1.67
350	2.118

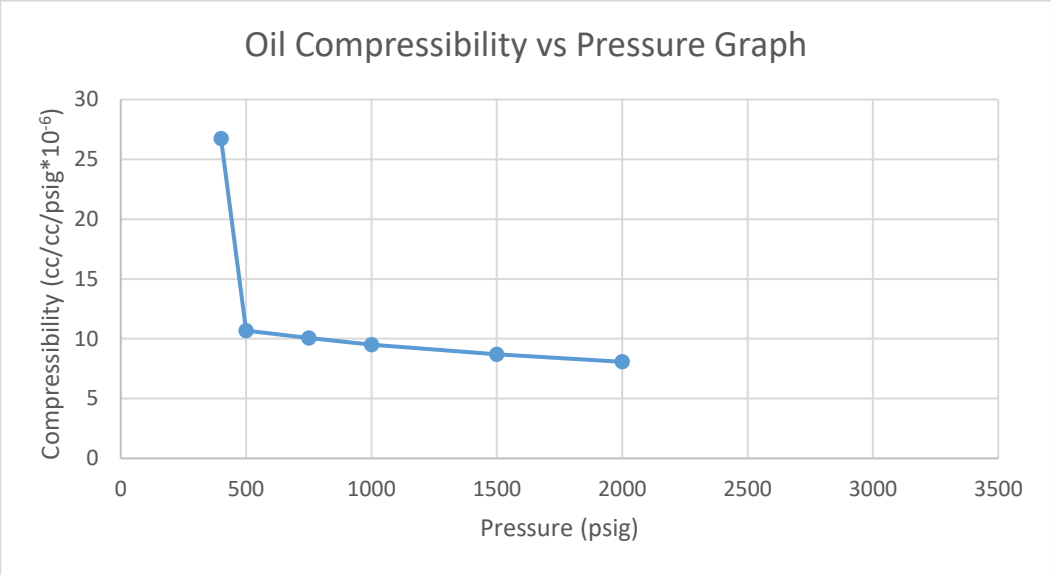

Figure 4.2. Oil Compressibility vs Pressure Graph

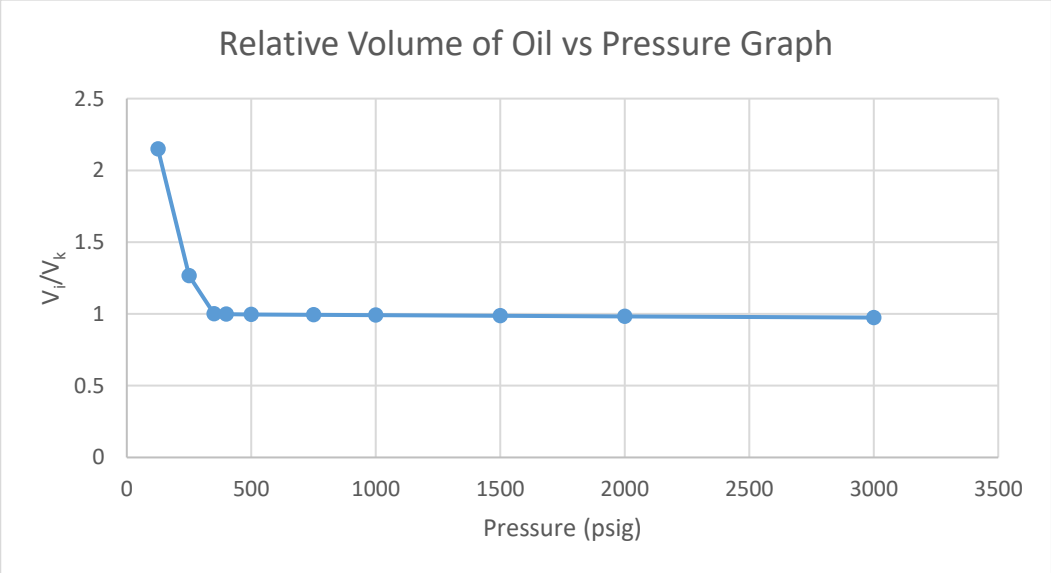

Figure 4.3. Relative Volume vs Pressure Graph

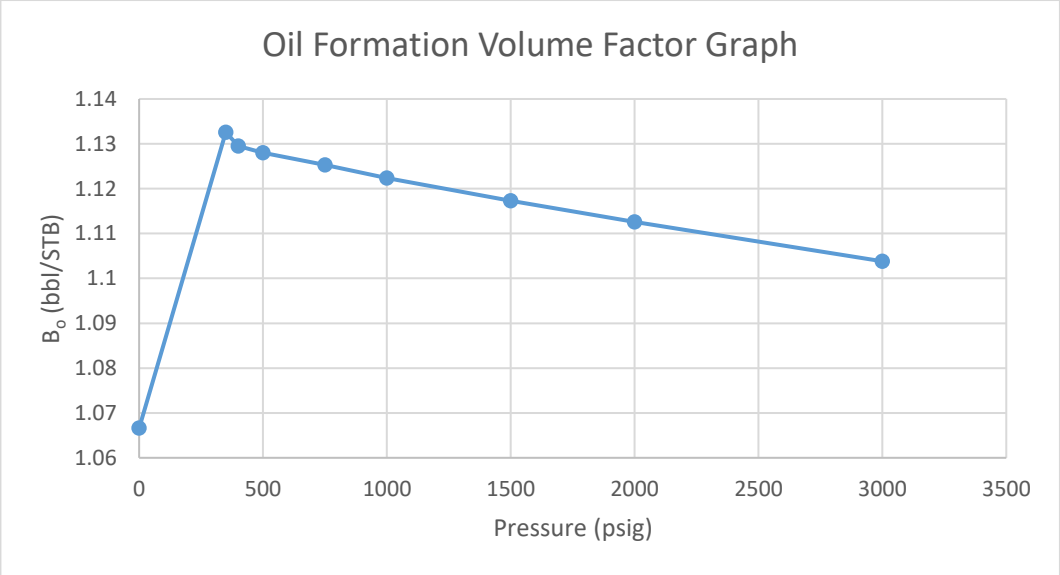

Figure 4.4. Oil FVF Graph

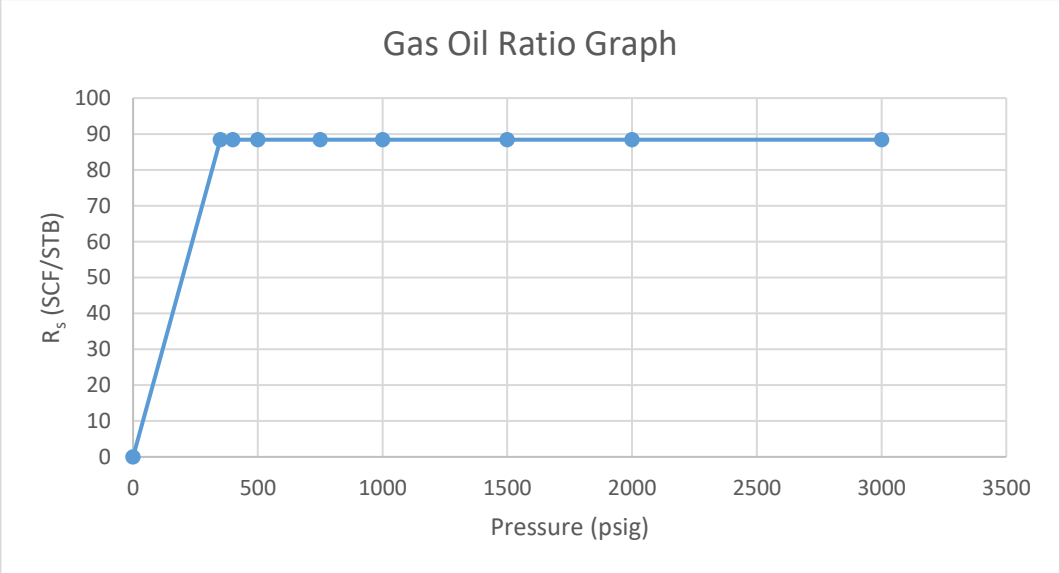

Figure 4.5. GOR vs Pressure Graph

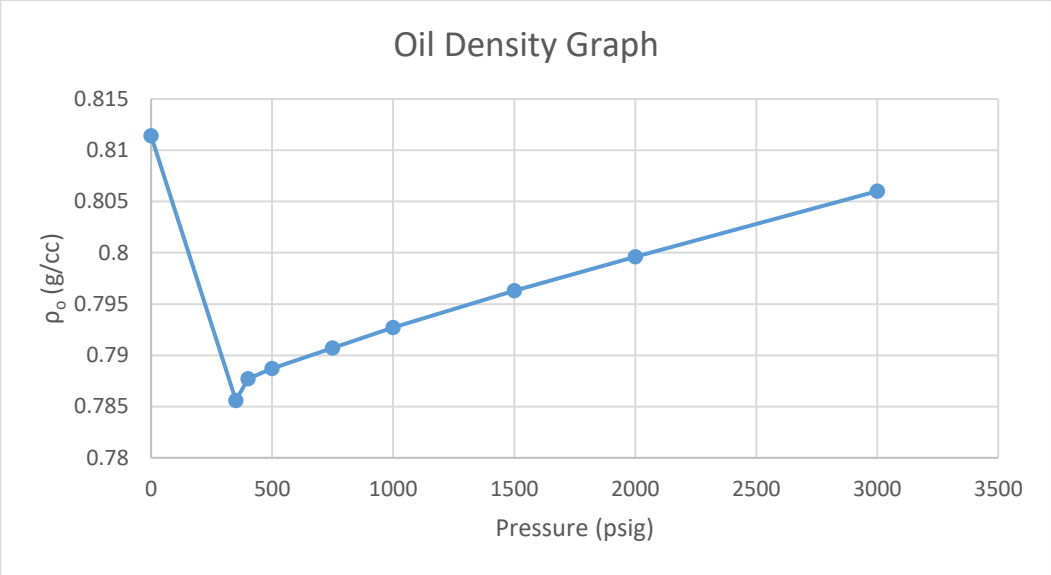

Figure 4.6. Oil Density vs Pressure Graph

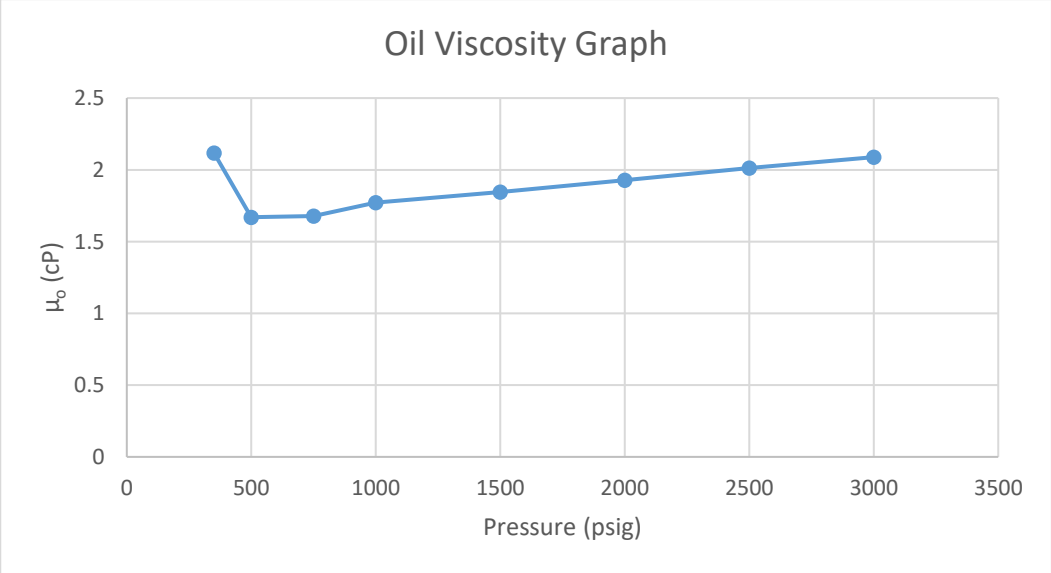

Figure 4.7. Viscosity vs Pressure Graph

4.1.1 PVT Quality Check

In order to validate the results and do quality check, Vasquez-Beggz, Hoffman Plot and Material Balance techniques for the PVT tests have been done.

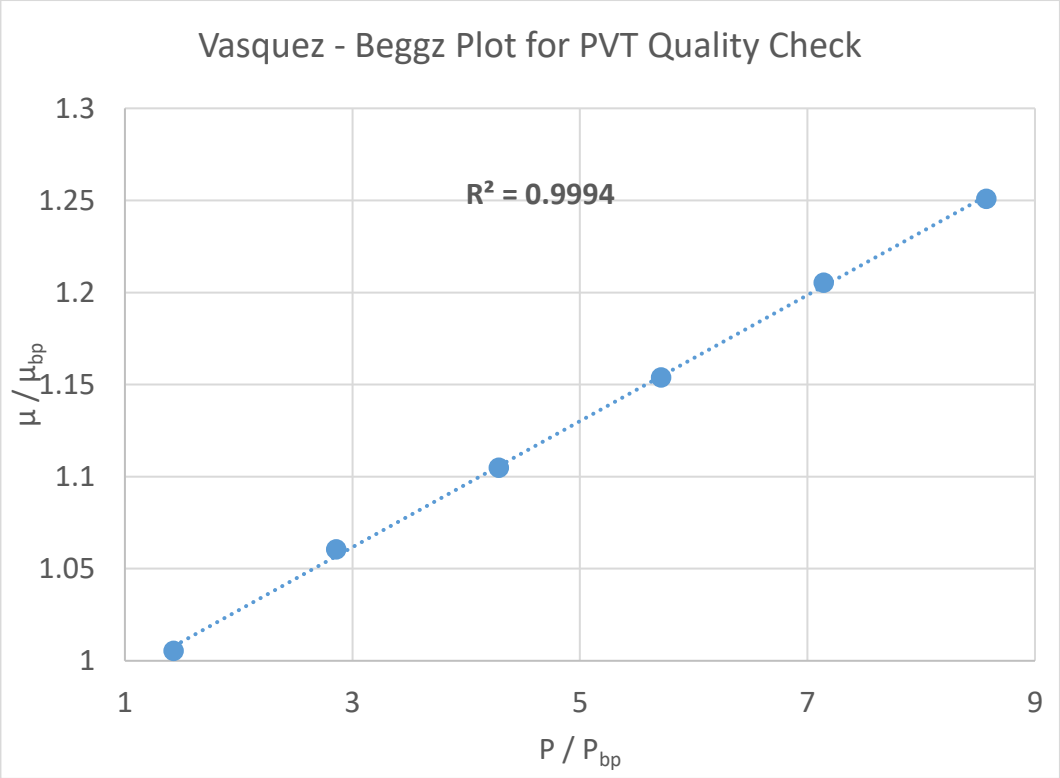

Figure 4.8. Vasquez-Beggz Plot for PVT QC

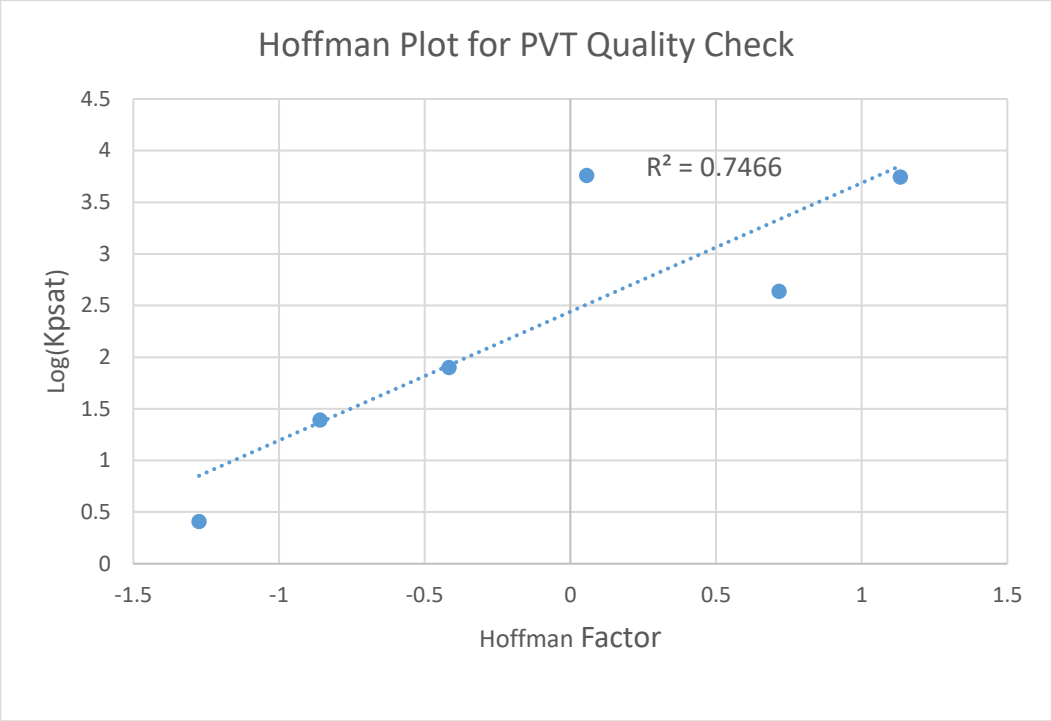

Figure 4.9. Hoffman Plot for PVT QC

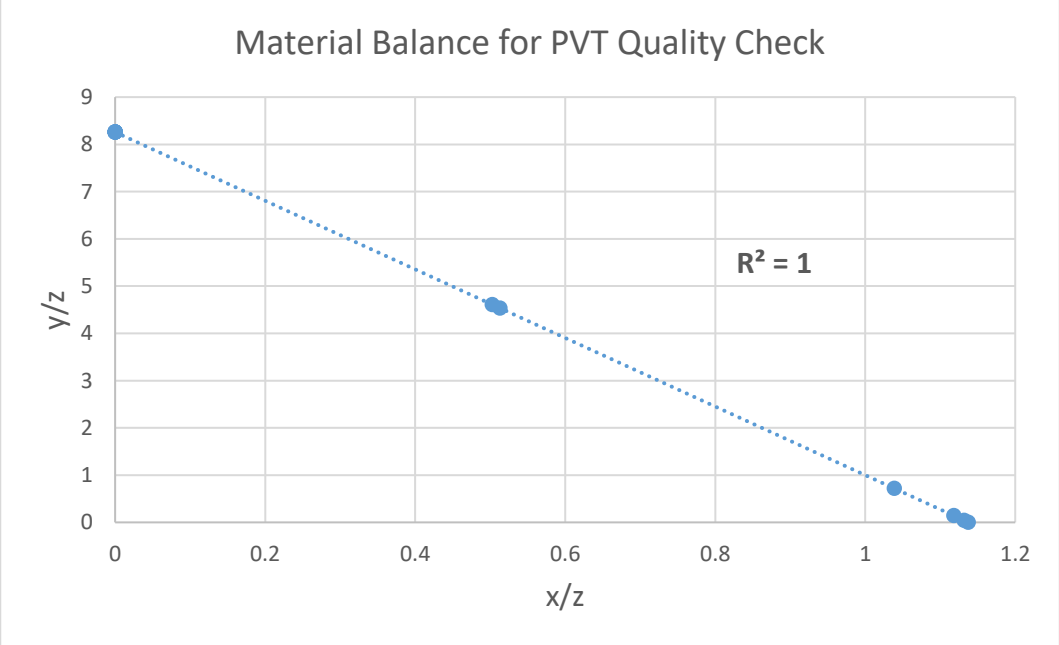

Figure 4.10. Material Balance Technique for PVT QC

4.2 PVT Simulation

The simulation program requires a compositional fluid model to run while CO2 is present for an EOR technique. It compositionally calculates the miscibility of oil and CO2 in a grid block with their saturation, temperature, and pressure. The compositional fluid model is created using FluidModeler software by Slb. The equation of states and viscosity model is used in the software. The compositional analysis done by the laboratory gives compositions up to C15+, however, to clarify the uncertainties, the C7+ section of the compositions is divided into four pseudo components. The property match has been done by the arranging the critical temperature and critical pressure of the pseudo components since those parameters change with the lumping process of C7 to C15+. The fluid model derived in the FluidModeler is compostional model and it uses the Peng-Robinson (1976) Two Variables equation of state. From Figure 4.10 to 4.14, the laboratory measurements and simulation results are compared. Table 4.6 describes the merged components properties. Table 4.7 to 4.9 describes the error percentage in the simulation.

Table 4.6 The component properties of the oil created by the FluidModeler

	Mole Fraction	Molecular Weight	$T_{critical}$, bar	$P_{critical}$, bar	$V_{critical}$, bar
N2-C1	0.00940	23.56	150.18	38.45	0.09
CO2	0.00830	44.01	304.70	73.87	0.09
C2	0.00110	30.07	305.43	48.84	0.15
C3	0.00870	44.10	369.80	42.46	0.20
i-C4-n-C4	0.02070	58.12	408.84	36.54	0.26
i-C5-n-C5	0.00240	72.15	468.45	33.72	0.31
C6	0.00700	84.00	506.86	32.37	0.36
C7+	0.94239	183.81	544.59	20.12	0.74

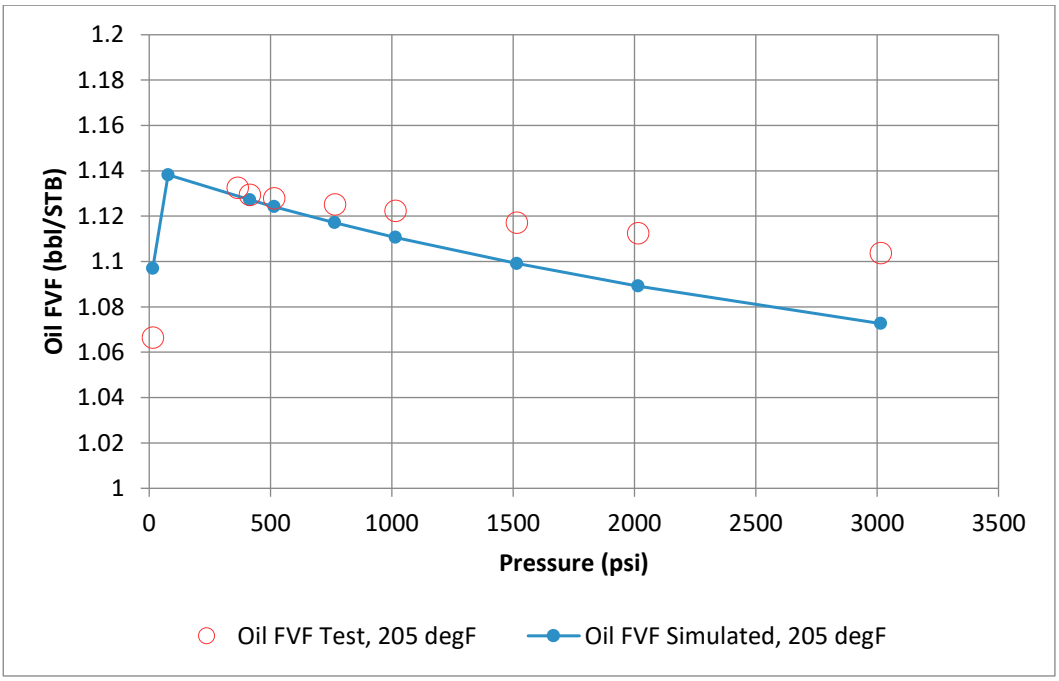

Figure 4.11. Simulation Result vs Laboratory Results for Oil FVF

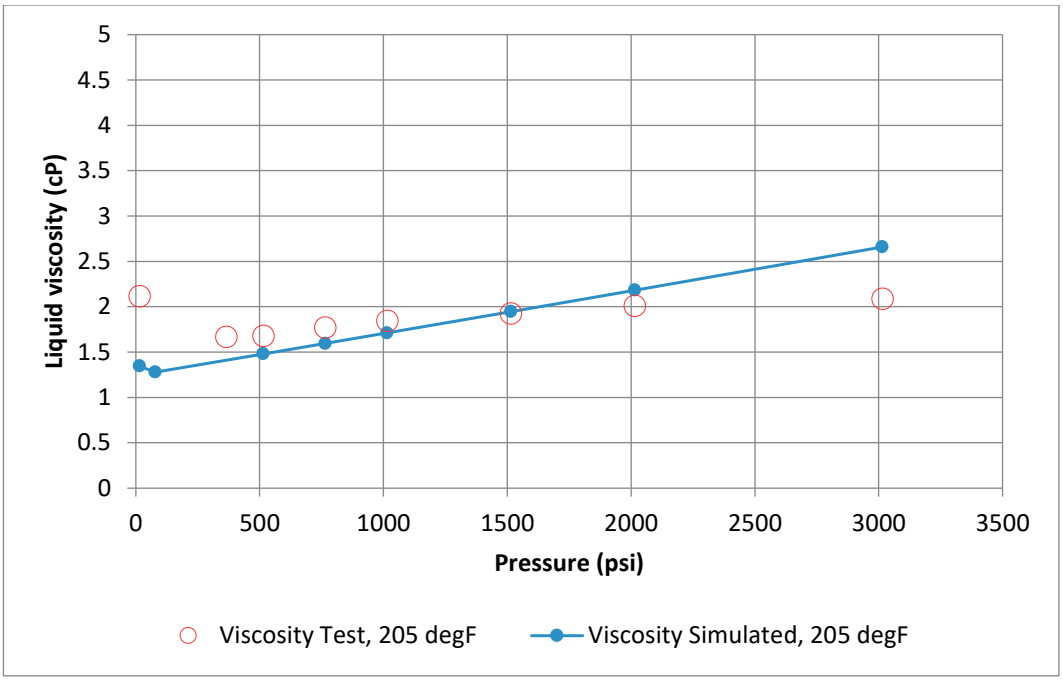

Figure 4.12. Simulation Result vs Laboratory Results for Oil Viscosity

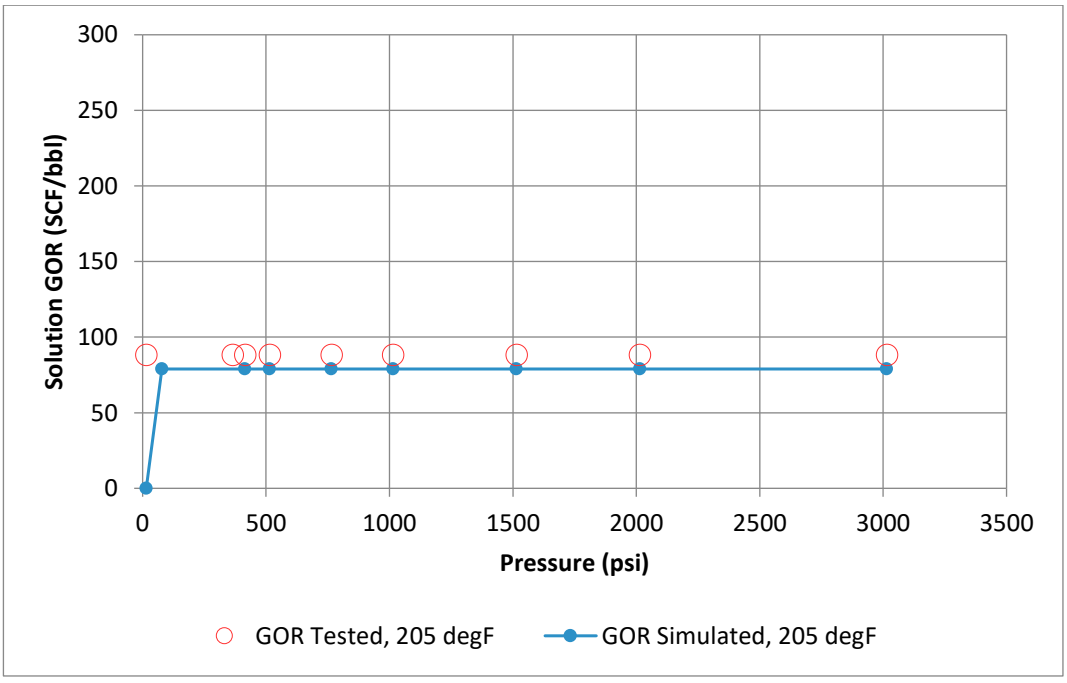

Figure 4.13. Simulation Result vs Laboratory Results for GOR

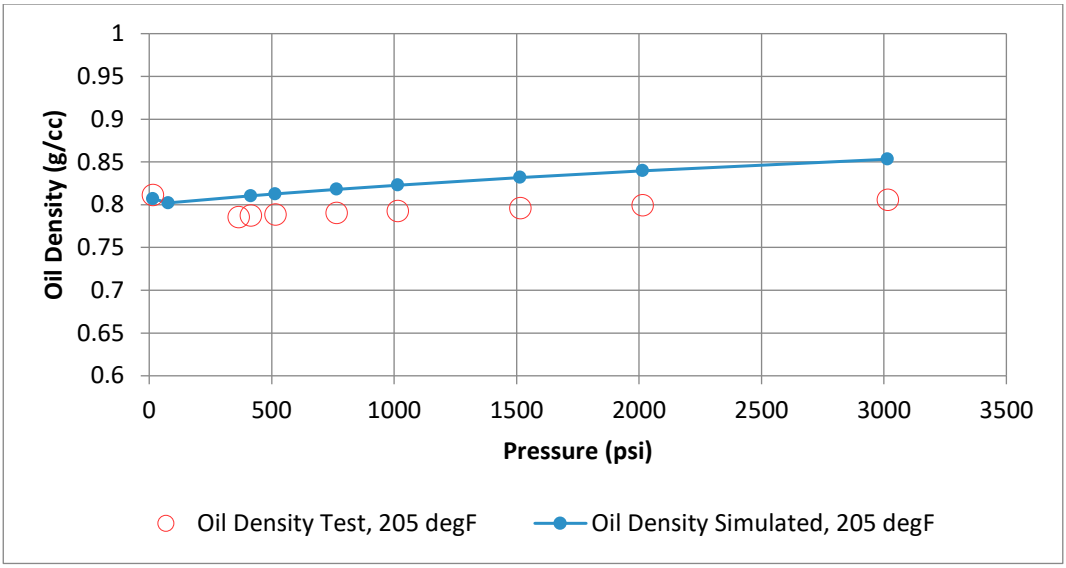

Figure 4.14. Simulation Result vs Laboratory Results for Oil Density

Table 4.7 Oil FVF Comparison, Tested vs Simulated

Oil FVF	**Tested, 205 degF**	**Simulated, 205 degF**	**Error**
Pressure, psi	Oil FVF, bbl/STB	Oil FVF, bbl/STB	%
3014.696	1.104	1.073	2.823
2014.696	1.113	1.089	2.106
1514.696	1.117	1.099	1.626
1014.696	1.122	1.111	1.047
764.696	1.125	1.117	0.726
514.696	1.128	1.124	0.338
414.696	1.130	1.127	0.204
364.696	1.133	1.138	0.497
14.696	1.067	1.097	2.848

Table 4.8 Viscosity Comparison, Tested vs Simulated

Oil Viscosity	**Tested, 205 degF**	**Simulated, 205 degF**	**Error**
Pressure, psi	Oil Viscosity, cP	Oil Viscosity, cP	%
3014.696	2.089	2.659	27.300
2014.696	2.013	2.183	8.456
1514.696	1.927	1.947	1.019
1014.696	1.845	1.712	7.219
764.696	1.771	1.595	9.924
514.696	1.679	1.479	11.890
364.696	1.670	1.279	23.412
14.696	2.118	1.347	36.425

Table 4.9 GOR Comparison, Tested vs Simulated

GOR	**Tested, 205 degF**	**Simulated, 205 degF**	**Error**
Pressure, psi	GOR, SCF/STB	GOR, SCF/STB	%
3014.696	88.40	78.92	10.72
2014.696	88.40	78.92	10.72
1514.696	88.40	78.92	10.72
1014.696	88.40	78.92	10.72
764.696	88.40	78.92	10.72
514.696	88.40	78.92	10.72
414.696	88.40	78.92	10.72
364.696	88.40	78.92	10.72
14.696	88.40	0.00	100.00

Table 4.10 Density Comparison, Tested vs Simulated

Oil Density	**Tested, 205 degF**	**Simulated, 205 degF**	**Error**
Pressure, psi	Density, g/cc	Density, g/cc	%
3014.696	0.806	0.853	5.854
2014.696	0.800	0.840	5.021
1514.696	0.796	0.832	4.463
1014.696	0.793	0.823	3.808
764.696	0.791	0.818	3.444
514.696	0.789	0.813	3.029
414.696	0.788	0.810	2.874
364.696	0.786	0.802	2.109
14.696	0.811	0.807	0.538

4.3 Minimum Miscibility Pressure

Minimum Miscibility Pressure measurements from the laboratory is absent for the G-Field black oil. The MMP can be observed with the slim-tube test or needle-test, however, in order to find the MMP without laboratory measurements, slim-tube simulation on ECLIPSE300 or some models can be used.

4.3.1 MMP Simulation

Slim-tube simulation is an ECLIPSE300 process where the slim-tube is modeled as 1D grids, with one injector at the beginning and one producer at the end of the grid. The grids initially are filled with the live oil of G-Field modeled in FluidModeler. CO2 is injected at several pressure values, and then the recovery of oil is recorded. The pressure point where the whole pore volume of oil is recovered can be said to be the Minimum Miscibility Pressure of the oil of G-Field.

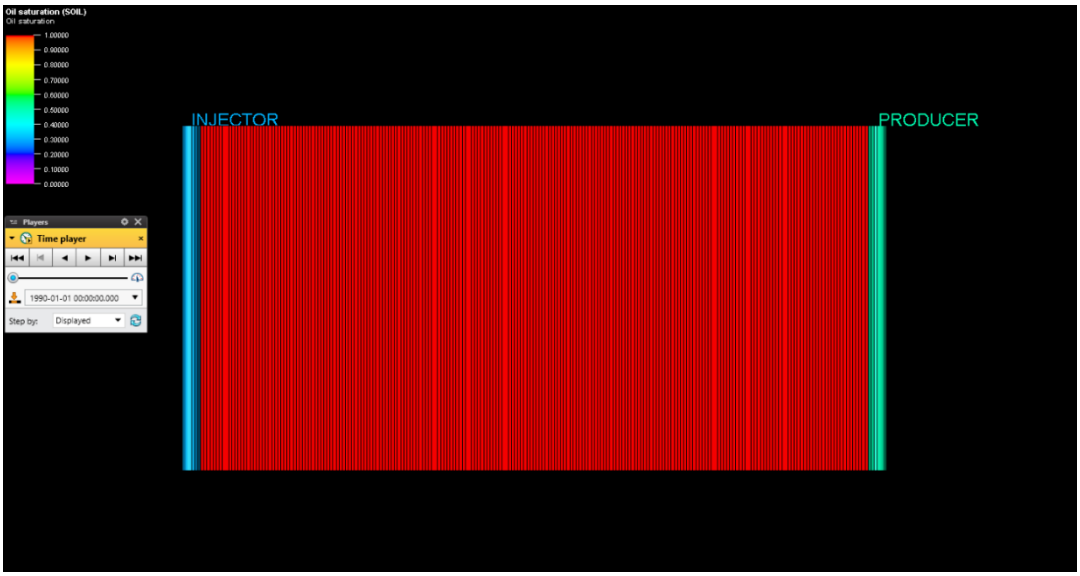

Figure 4.15 Slim-tube experiment simulation grid with oil saturation at time zero

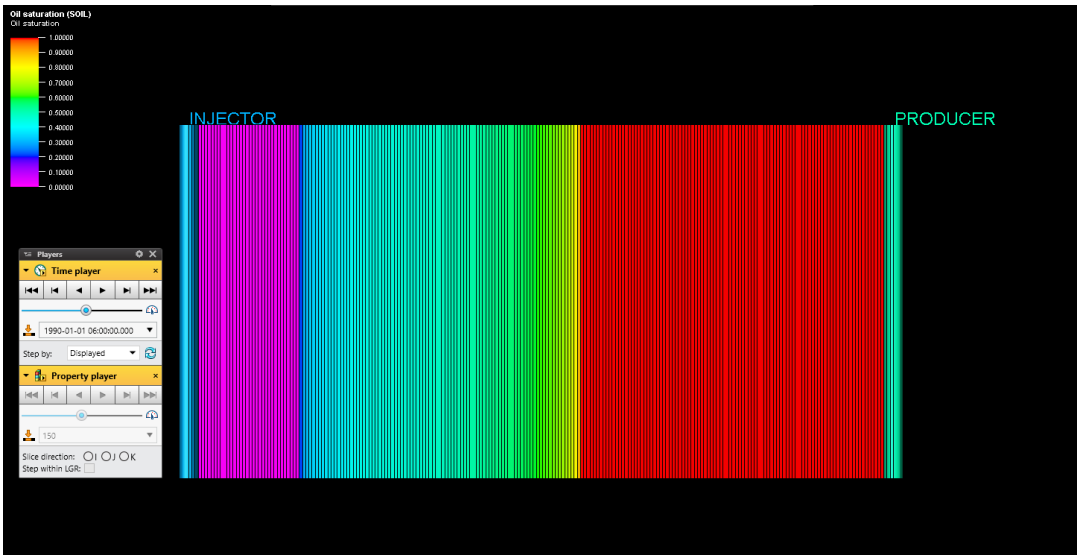

Figure 4.16. Slim-tube experiment simulation grid with oil saturation at time 6 hours with the pressure of 100 atm

The pressure steps are determined as 367.5, 735, 882, 955.5, 1029, 1102,5 1470, 2205, 2940, 3675, 4410 psi. In order to validate the results, H2S is also injected due

to its requirements of low pressure for miscibility with the oil. The MMP value is 2000 psi for the CO2 and 1100 psi for the H2S.

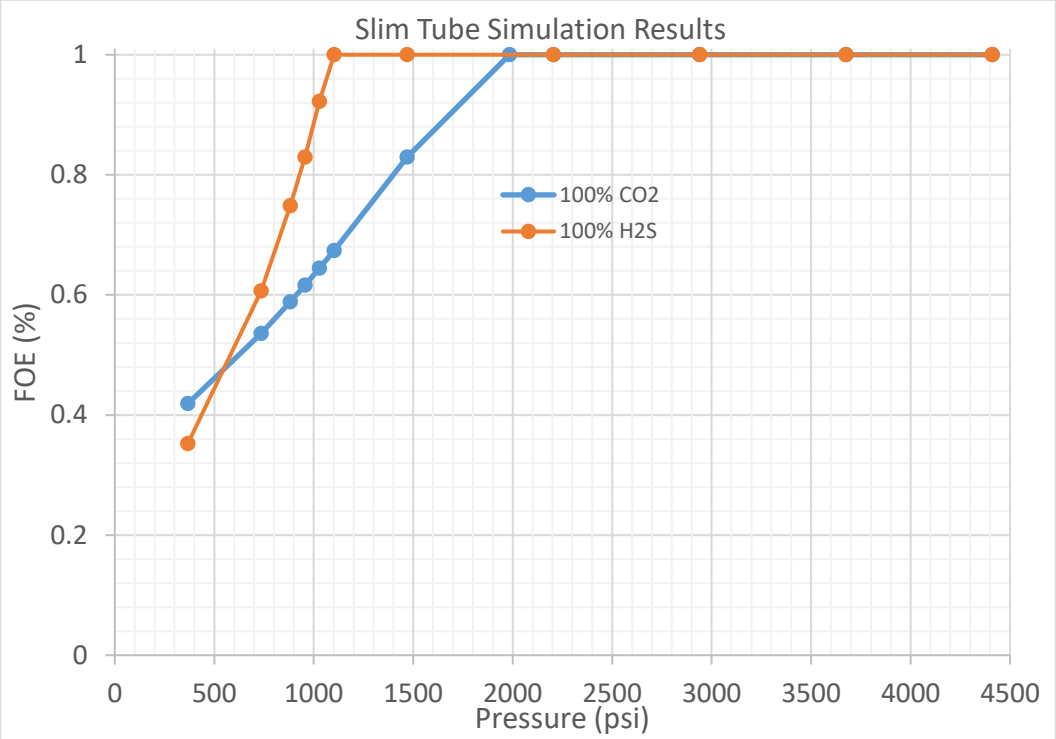

Figure 4.17. Slim-tube experiment simulation results for H_2S and CO_2

4.3.2 MMP Calculation

In the literature, there are several correlations to find the Minimum Miscibility Pressure. In their article, Zhang, Hou, and Li gathered the correlations for calculating the Minimum Miscibility Pressure. They introduced 11 different correlations from different authors. They also emphasized the limitations of those equations. The limitations are based on the reservoir temperature, guessed MMP value, and the molar fraction of some components in the live oil. The G-Field has reservoir temperature of 96 ^{o}C and MMP value coming from the slim-tube simulation in Eclipse300. The component list of the G-Field is as follows;

Table 4.11 Component List of G-Field Oil

Component	Seperator Gas Mol %	Seperator Oil Mol %	Reservoir Oil Mol %	MW (g/mol)
N2	26.59	0	0.59	28.014
CO2	37.09	0	0.83	44.01
C1	15.78	0	0.35	16.043
C2	5.14	0	0.11	30.07
C3	6.54	0.74	0.87	44.097
i-C4	1.38	1.99	1.98	58.124
n-C4	4.03	0	0.09	58.124
i-C5	1.51	0	0.03	72.151
n-C5	1.65	0.18	0.21	72.151
n-C6	0.09	0.71	0.7	86.178
n-C7	0.13	3.3	3.23	96
C8	0.06	14.64	14.32	107
C9	0	11.13	10.88	121
C10	0	13.49	13.19	134
C11	0	7.86	7.68	147
C12	0	8.32	8.14	161
C13	0	5.2	5.09	175
C14	0	6.54	6.39	190
C15+	0	25.89	25.31	310.136

Table 4.12 Expressions for the Literature Equations to Calculate MMP

Component	Percent
M_{C5+}	95.18
M_{C7+}	94.24
x_{vol}	0.94
x_{med}	3.88
x'_{med}	4.82
x_1,°C	96.11
x_2	0.94
x_3	3.88
x_4	95.18
x_{C1+N2}	0.94
x_{C2-C6}	3.99

The mentioned equations use the above expressions derived from the component table of the live oil. Cronquist, Lee, Glaso and Alston equations' limitations are suitable for the G-Field live oil. However, G-Field can not satisfy the limitations of Yelling-Metcalfe, Orr-Jensen, Emera-Sarma, Yuan, Shokir, and Chen equations.

Table 4.13 MMP Results with the Literature Equations

Equation	MMP, psi
Cronquist	1481
Lee	3296
Glaso	5407
Alston	679

Based on the values founded above, no equations in the literature fit with the slim-tube simulation on Eclipse300. The simulation studies will use Eclipse300 result as MMP value.

4.4 Rock Properties

4.4.1 Porosity-Permeability

A core sample is taken from the G-4 well in the K-C formation. The total length of the core was 9 meters; however, the total recovery was 50% so that the 4.5 meters of the formation could be sampled. 7 core plugs taken from the core sample were available for the fundamental and special core analysis.

The plug samples were kept under a vacuum and in alcohol and cleaned of formation water and drilling fluid residues. After the cleaned plug samples were dried in a temperature-controlled oven at 70 ^{o}C, their dimensions and weights were measured and they were made ready for testing.

Porosity and grain volumes were measured with a Vinci helium porosimeter and with the help of "Boyle and Charles Law", and the data obtained from these measurements were used to calculate the grain density values of the samples and reported. Permeability measurements were measured with the Vinci Airperm device using the steady-state method using the Darcy equation for gases.

Table 4.14 Porosity-Permeability Test Results (Ercan, 2022)

Plug #	Depth, m	Grain Density, g/cc	Porosity, %	k_{air}, mD	k_{liq}, mD
189	2418.49	2.70	4.3%	0.54	0.35
190	2418.82	2.70	4.0%	0.06	0.03
191	2419.28	2.71	2.5%	3.64	2.67
192	2419.70	2.70	3.7%	0.37	0.23
193	2420.09	2.70	3.4%	1.01	0.68
194	2420.34	2.71	2.9%	0.09	0.05
195	2420.44	2.70	2.1%	0.06	0.03

Permeability and porosity measurements were carried out automatically with the CMS (CoreLab USA) test system under 500 and 4350 psi net overburden pressure, using the unsteady-state measurement method valid for gases (Helium or Nitrogen).

Table 4.15 Porosity Permeability Results under Overburden

Plug No	NOP, psi	Porosity, %	$k_{AIR,}$ mD	$k_{LIQ,}$ mD
189	500	4.81	4.40E-01	3.85E-01
189	4350	4.12	6.52E-02	4.46E-02
190	500	4.29	2.15E-02	6.54E-03
190	4350	3.66	9.37E-03	2.98E-03
191	500	2.72	3.38E+00	2.61E+00
191	4350	2.23	8.51E-01	7.86E-01
192	500	3.99	2.82E-01	1.60E-01
192	4350	3.50	6.49E-02	2.42E-02
193	500	3.50	4.88E-01	4.14E-01
193	4350	2.94	2.15E-02	4.98E-03
194	500	2.70	1.68E-02	4.73E-03
194	4350	2.22	6.68E-03	1.36E-03
195	500	2.08	1.86E-02	5.43E-03
195	4350	1.62	4.12E-03	6.92E-04

The porosity-permeability graph is created with the limited core plug data. Since there are no heterogeneity observed, the correlation between the porosity and the permeability should be used as an input to the geological model as one rock type. The permeability property of the geological model will be related to the porosity distribution of the model. One basic formula derived from the porosity-permeability graph is enough to characterize the permeability of the matrix since the matrix quality of the G-Field is very low. Porosity-permeability graph is also important to characterize the rock for its incapability to flow. The cut-off value for the flowability

of a matrix will be assumed as 0.25 mD, where the corresponding value of the porosity is 3%.

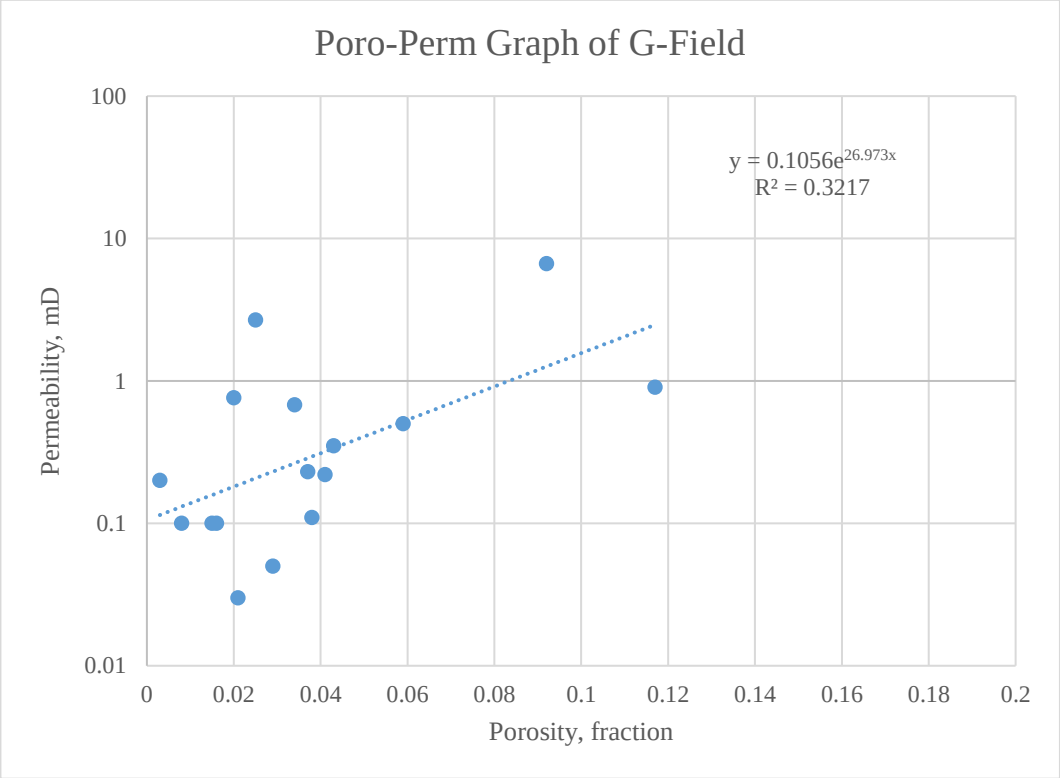

Figure 4.18. Poro-Perm Graph of G-Field

The exponential formula of;

$$Permeability_{matrix} = 0.1056 * e^{(26.973 * Porosity_{matrix})} \qquad (4.2)$$

will be used to characterize the matrix permeability where the porosity is higher than 3%. The grid blocks that have porosity lower than 3% will have a permeability 0.1 due to incapability to flow. These values are special to the k_x and k_y anisotropy, k_z values are assumed to be 10% of the k_x and k_y values.

4.4.2 Capillary Pressure

Special core analysis was done in the laboratory with the Micrometrics Autopore III Porosimeter. There are no relative permeability tests for the mentioned core plugs, however, the Mercury Injection Capillary Pressure test is done for the core plugs. The MICP test gives the capillary pressure for the Mercury-Air interaction. It is possible to convert the values of Mercury-Air Capillary Pressure to the Oil-Water Capillary Pressure with the below formula. It is important to convert the MICP values to the Oil-Water CP since the reservoir fluids in the formation are oil and water.

$$P_{c,\,res} = P_{c,\,lab} * \left(\frac{\gamma * \cos\theta_{oil\text{-}water}}{\gamma * \cos\theta_{mercury\text{-}air}} \right) \qquad (4.1)$$

The interfacial tension and the contact angle between mercury and air has been measured as 480 dynes/cm and 40^{o} for the G-Field, respectively. There are no measurements for the reservoir oil and reservoir water interfacial tension and contact angle specifically for the G Field. The formations composed with the limestone tend to be heavily oil-wet rocks. The contact angle between oil and water depends on the wettability of the reservoir rock. Most of the oil-wet limestones have contact angle higher than 120^{o}. Assuming the G-Field formations is heavily oil-wet based on the capillary pressures also, the contact angle can be assumed to be 165^{o}. The general measurements for the interfacial tension of oil and water is 30 dynes/cm. So, the mercury-air capillary pressure can be converted into the oil-water capillary pressure with the coefficient of 0.078808 for the G-Field.

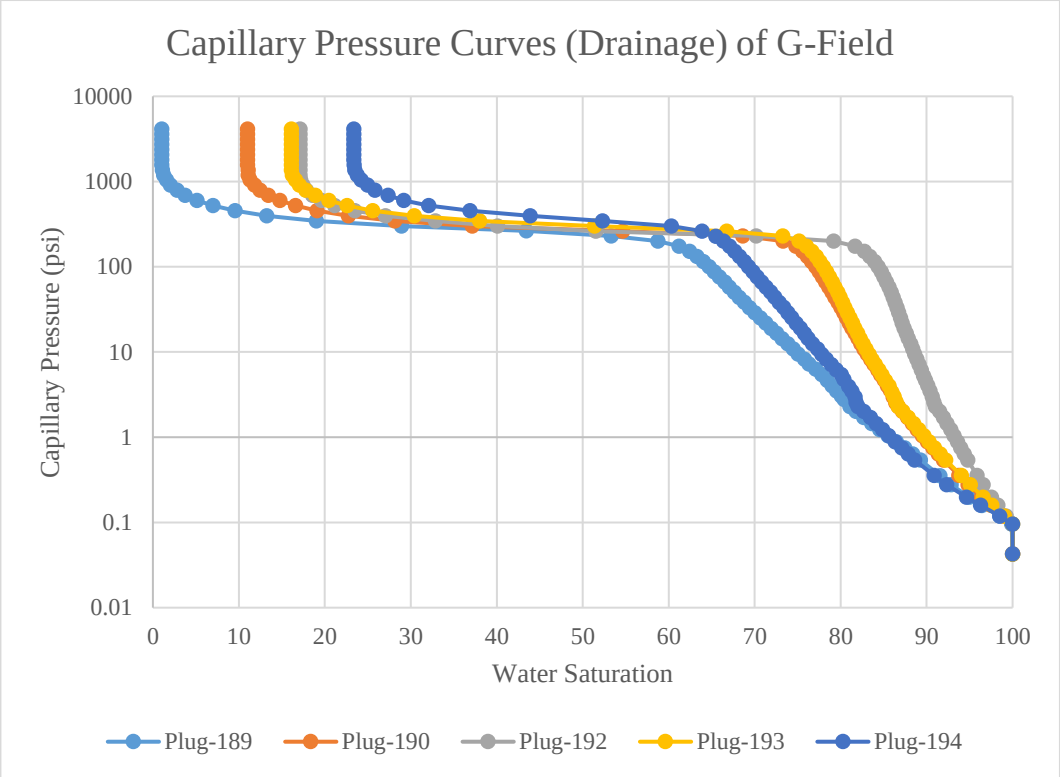

Figure 4.19. Capillary Pressure Drainage Curves of G-Field (Ercan, 2022)

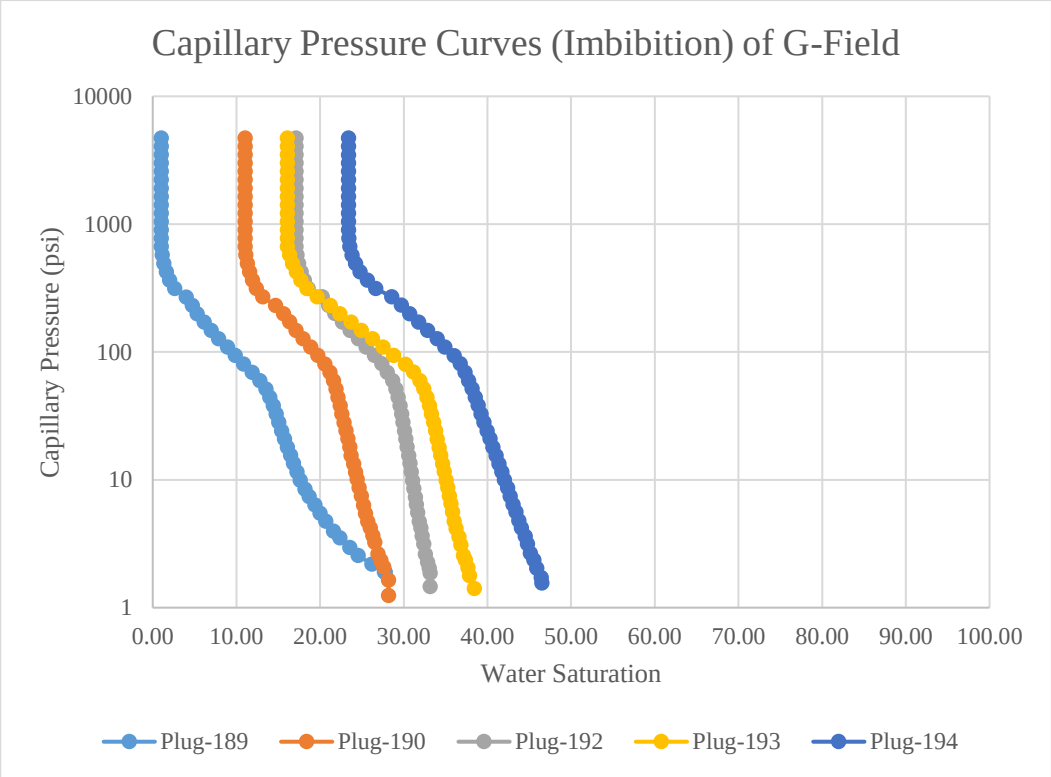

Figure 4.20. Capillary Pressure Imbibition Curves of G-Field (Ercan, 2022)

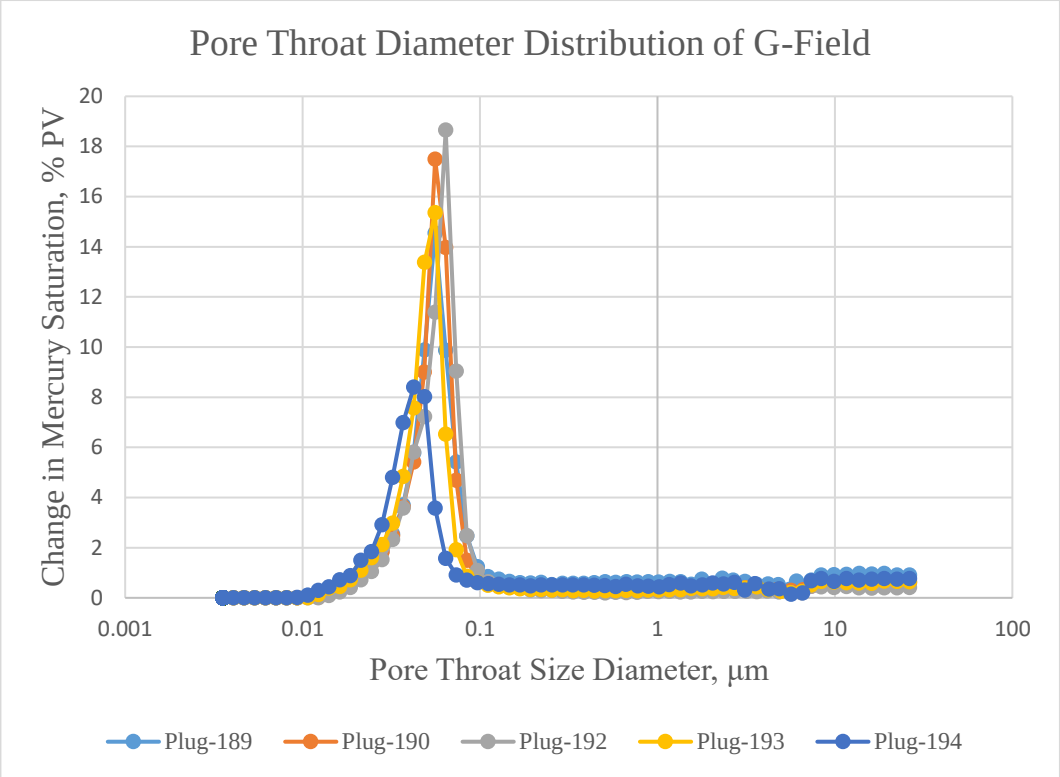

Figure 4.21. Pore Throat Diameter Distribution of G-Field (Ercan, 2022)

All of the plug drainage capillary pressure curves, imbibition capillary pressure curves and pore throat diameter curves shows the same behavior. The rock typing is done by analyzing all the curves above, however, the plugs show no rock typing due to the mentioned reason. The reservoir rock does not show heterogeneity for the matrix, due to result of the special core analysis.

4.4.3 Relative Permeability

4.4.3.1 Brooks-Corey Power Law

There are no laboratory measurements for the relative permeability from a core plug of G-Field. Both oil-water relative permeability and gas-oil relative permeability is unknown. Therefore, in order to create a relative permeability data, Brooks-Corey Relative Permeability Equation is used to characterize matrix two and three phase flow. The power-law relationships between oil, gas and water relative permeabilities are described as the following equations, respectively,

$$k_{ro} = k_{ro,max}\left(\frac{S_o - S_{or}}{1 - S_{or} - S_{wc} - S_{gc}}\right)^{n_o} \quad (4.2)$$

$$k_{rw} = k_{rw,max}\left(\frac{S_w - S_{wc}}{1 - S_{or} - S_{wc} - S_{gc}}\right)^{n_w} \quad (4.3)$$

$$k_{rg} = k_{rg,max}\left(\frac{S_g - S_{gc}}{1 - S_{or} - S_{wc} - S_{gc}}\right)^{n_g} \quad (4.4)$$

Where the exponents of n_o (Corey O/W), n_w (Corey Water), n_g (Corey Gas) exponents range from 1 to 6. For the G-Field, the n_o, n_w, and n_g values used as custom values for a sandstone rock, this is due to no confirmation for limestones.

Table 4.16 Power-Law Relative Permeability Constraints

Variable	Value	Variable	Value	Variable	Value
Sgcr	0.05	Sorw	0.6686427	Swmin	0.17115
Corey Gas	6	Sorg	0.6686427	Swcr	0.21155
Krg,Swmin	0.3	Corey O/W	3	Corey Wat.	4
Krg,Sorg	0.3	Corey O/G	4	Krw,Sorw	0.5
		Kro,Swmax	1	Krw,S=1	1

The oil-water permeability model values can be extracted from the oil-water capillary pressure data, where the laboratory measurements are available. The capillary pressure of oil and water gives the irreducible water and the residual oil saturation.

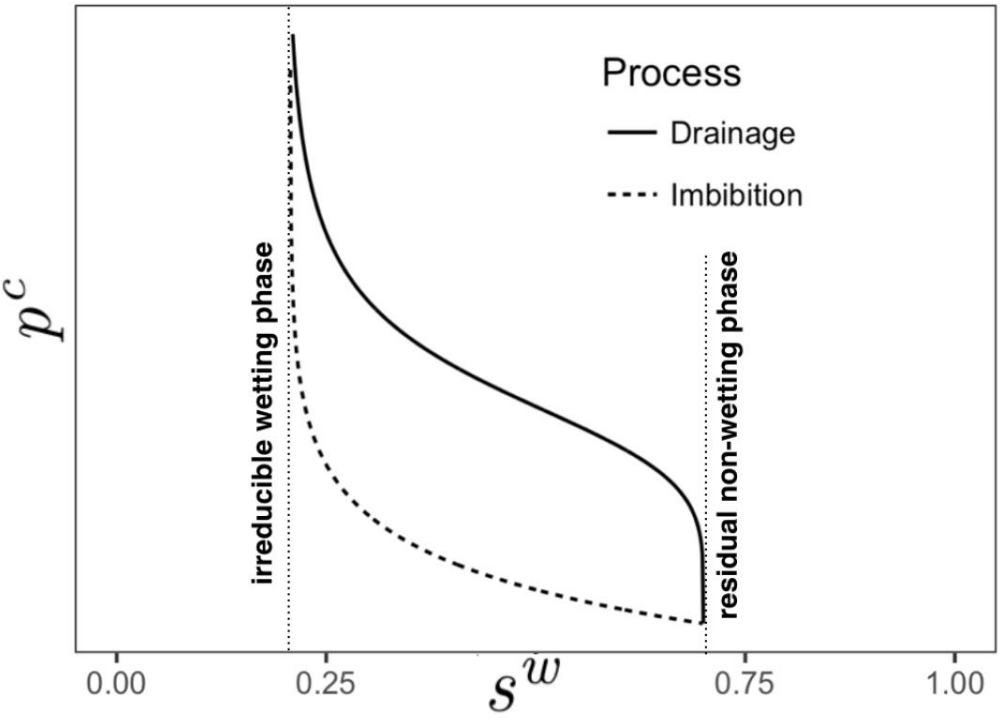

Figure 4.22. Capillary Pressure Drainage and Imbibition Curve (Mcclure et al., 2018)

Based on the capillary pressure data taken from the plug no 192, the irreducible water saturation and residual oil saturation is as follows;

Table 4.17 Residual Oil Saturation and Irreducible Water Saturation

S_{or}	S_{irrw}
0.6686427	0.17115

For the gas-oil relative permeability, there are no data, so the assumptions of critical gas saturation, Corey gas exponent and the gas-oil capillary pressure will be done to create the gas-oil relative permeability.

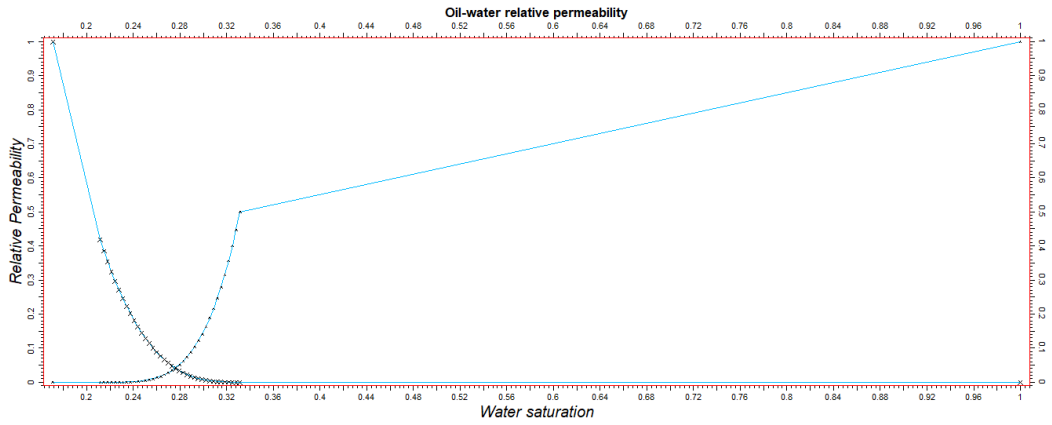

Figure 4.23. Oil-Water Relative Permeability derived from Power Law for Matrix

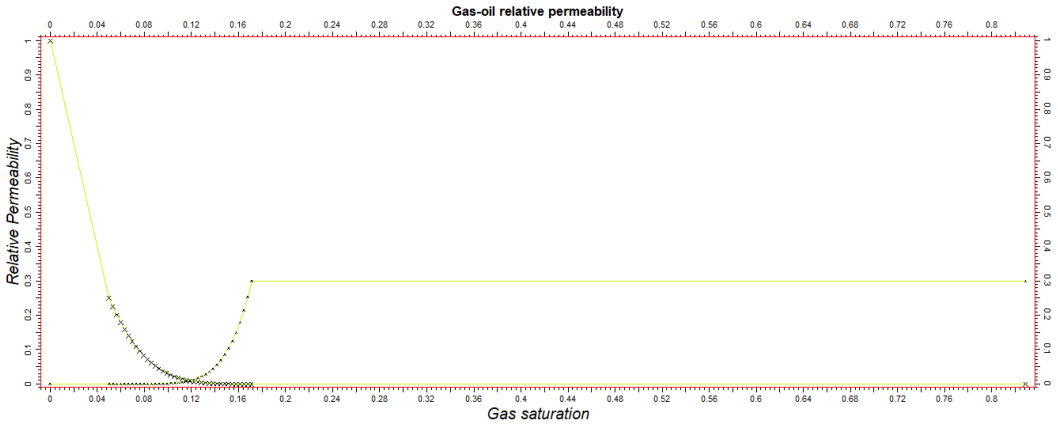

Figure 4.24. Oil-Gas Relative Permeability derived from Power Law for Matrix

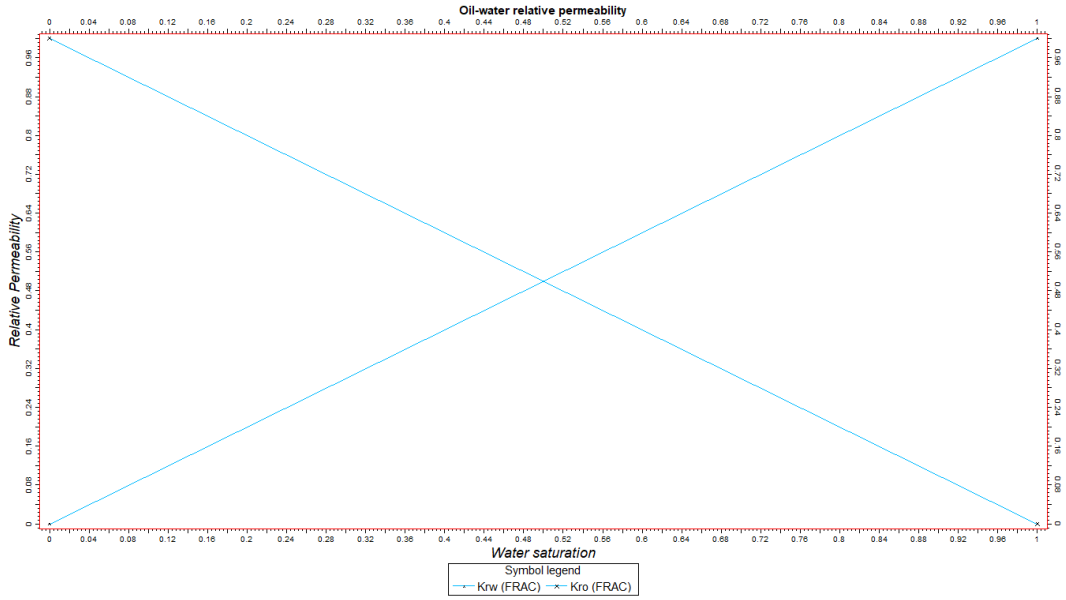

Figure 4.25. Oil-Water Relative Permeability for Fractures

4.4.3.2 Brooks-Corey Relative Permeability Model

Brooks-Corey Relative Permeability model is used to do sensitivity analysis. Brooks-Corey Relative Permeability model depends on the λ term, described as the distribution of pore sizes. The λ term can be found by fitting the actual capillary pressure data with the Brooks-Corey Capillary Pressure Model. The Plug 192 is used to fit the Brooks-Corey Capillary Pressure model.

$$P_c = P_{ent} * \left(\frac{1-S_{wirr}}{S_w - S_{wirr}} \right)^{\frac{1}{\lambda}} \qquad (4.5)$$

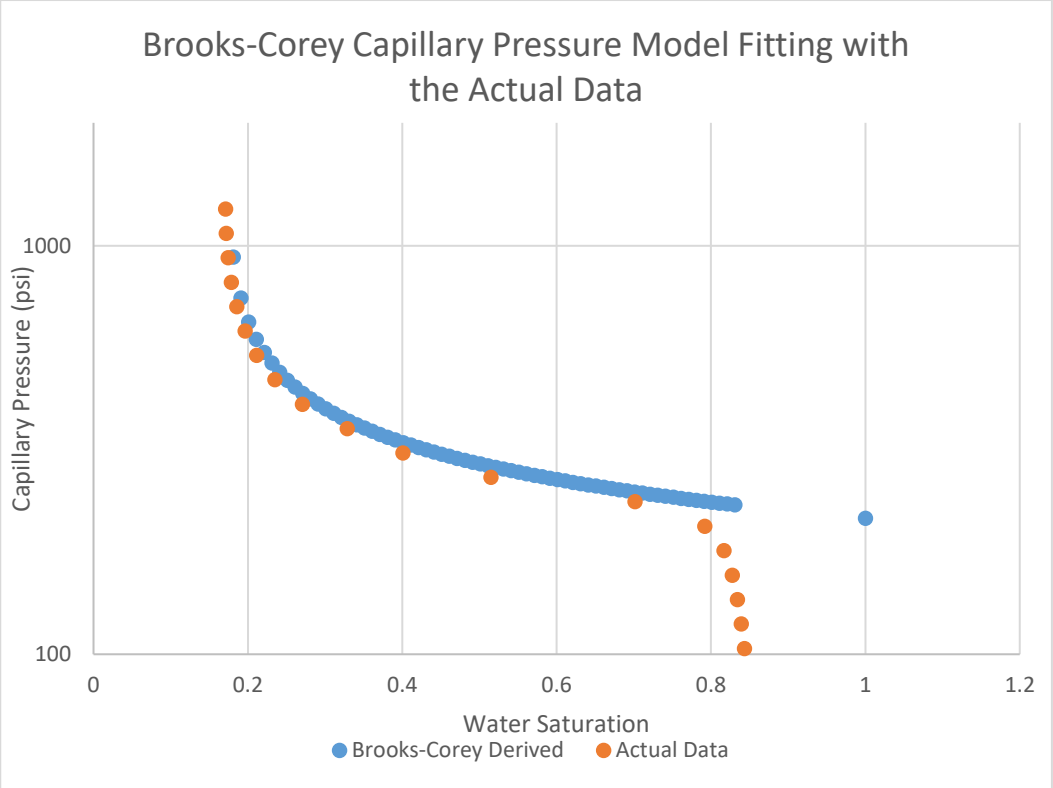

Figure 4.26. Brooks-Corey Capillary Pressure Model Fitting

The entry pressure is 215 psi and the irreducible water saturation is 0.17115. This leads to fitting with the λ value of 3. Brooks-Corey Relative Permeability Model (Brooks & Corey, 1964) can be created with the λ term equals to 3.

$$k_{ro}=\left(\frac{S_o-S_{or}}{1-S_{or}}\right)^{\frac{2+\lambda}{\lambda}} \quad (4.6)$$

$$k_{rw}=\left(\frac{S_w-S_{wirr}}{1-S_{wirr}}\right)^{\frac{2+\lambda}{\lambda}} \quad (4.7)$$

$$k_{rg}=\left(\frac{1-S_g}{1-S_{gc}}\right)^{2} * \left[1-\left(\frac{S_g-S_{gc}}{1-S_{gc}}\right)^{\frac{2+\lambda}{\lambda}}\right] \quad (4.8)$$

The irreducible water saturation, critical gas saturation and residual oil saturation values are taken as 0.17115, 0 and 0.66865, respectively. The irreducible water saturation and residual oil saturation is known from the capillary pressure curve of Plug 192. There is no data for the gas saturation and capillary pressure of gas-oil. Therefore, it is assumed that gas can flow in the matrix at the first time it invades the matrix.

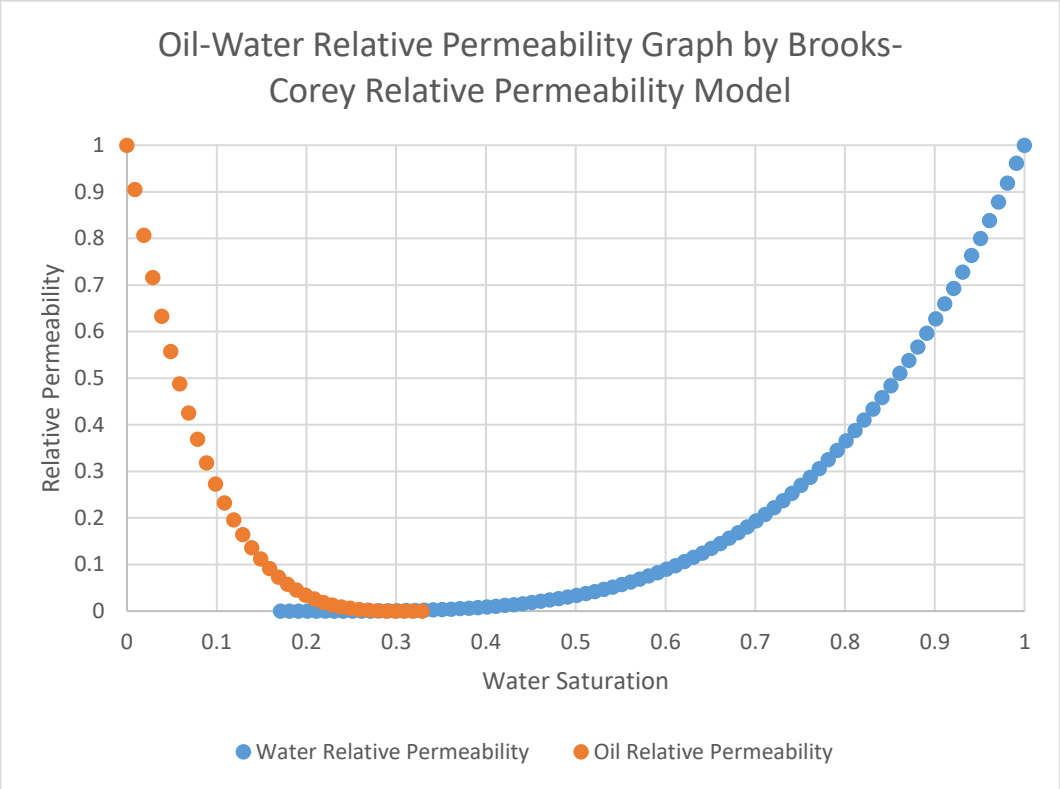

Figure 4.27. Oil-Water Relative Permeability Derived with BC RPM for Matrix

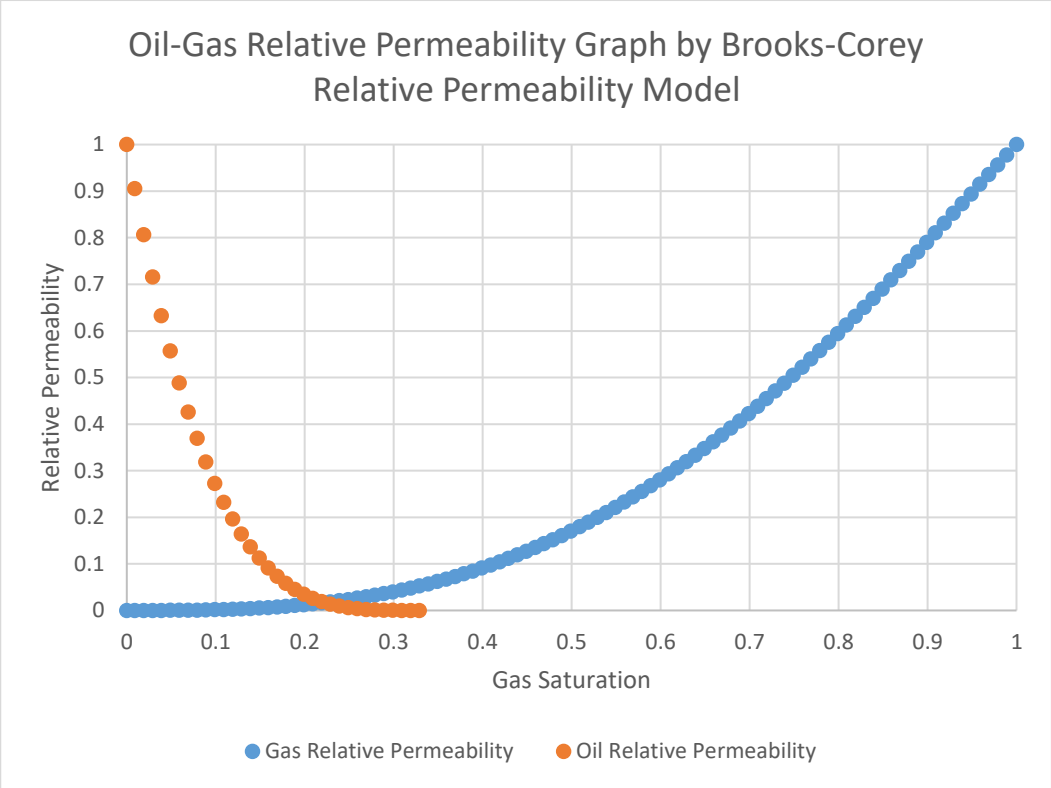

Figure 4.28. Oil-Gas Relative Permeability Derived with BC RPM for Matrix

4.5 Geological Model

The G-Field geological model consists of the data coming from the five wells (one well abandoned due to geological reasons, four production wells) and two 2-D seismic lines. The Adiyaman Fault has been detected with the seismic line, however, the G Fault was thought to be far away than its actual location. The G-2S (abandoned well) has gone through the G Fault at an unexpected level, thus, the boundaries of the field are corrected. All of the production wells that is inside the field has full-set logs containing sonic log, density-neutron log, resistivity log, and borehole image log to detect fractures.

The formation thicknesses and well-tops of the geological model have been created with the well data and the seismic data. Sonic log and density-neutron log

data have been used to create the matrix porosity cube with the geostatistical methods. The porosity of the wells that is calculated from the sonic and density-neutron logs is upscaled to the model grid, then, geostatistically distributed. The log-normal distribution is used to give a value to the grid for the porosity of the matrix.

The water saturation throughout a well is calculated using the resistivity logs. Resistivity logs are used to differentiate the hydrocarbon bearing zones and water bearing zones due to their respond to the electrical waves radiated from the resistivity log tool. Hydrocarbons do not conduct the electricity, thus, creating a high resistive respond to the tool. On the other hand, the water in the formation and in the aquifer, due to their saline environment, conducts electricity, thus respond low resistive values. The salinity values used to calculate water saturation in the matrix are 50,000 ppm and 8,000 ppm for the formation water and the aquifer, respectively. The important point for the water saturation calculation is porosity also. Due to capillarity effects, during the migration era of hydrocarbon, the hydrocarbon can not settle to the low-pore throat environment. Since the oil can not displace the water in the low-pore throat environment, the low porous sections of the matrix have higher water saturation. The irreducible water saturation calculated from the well logs is suitable with the capillary pressure curve of the plug no 192. Thus, the plug no 192 is used to characterize the rock physics.

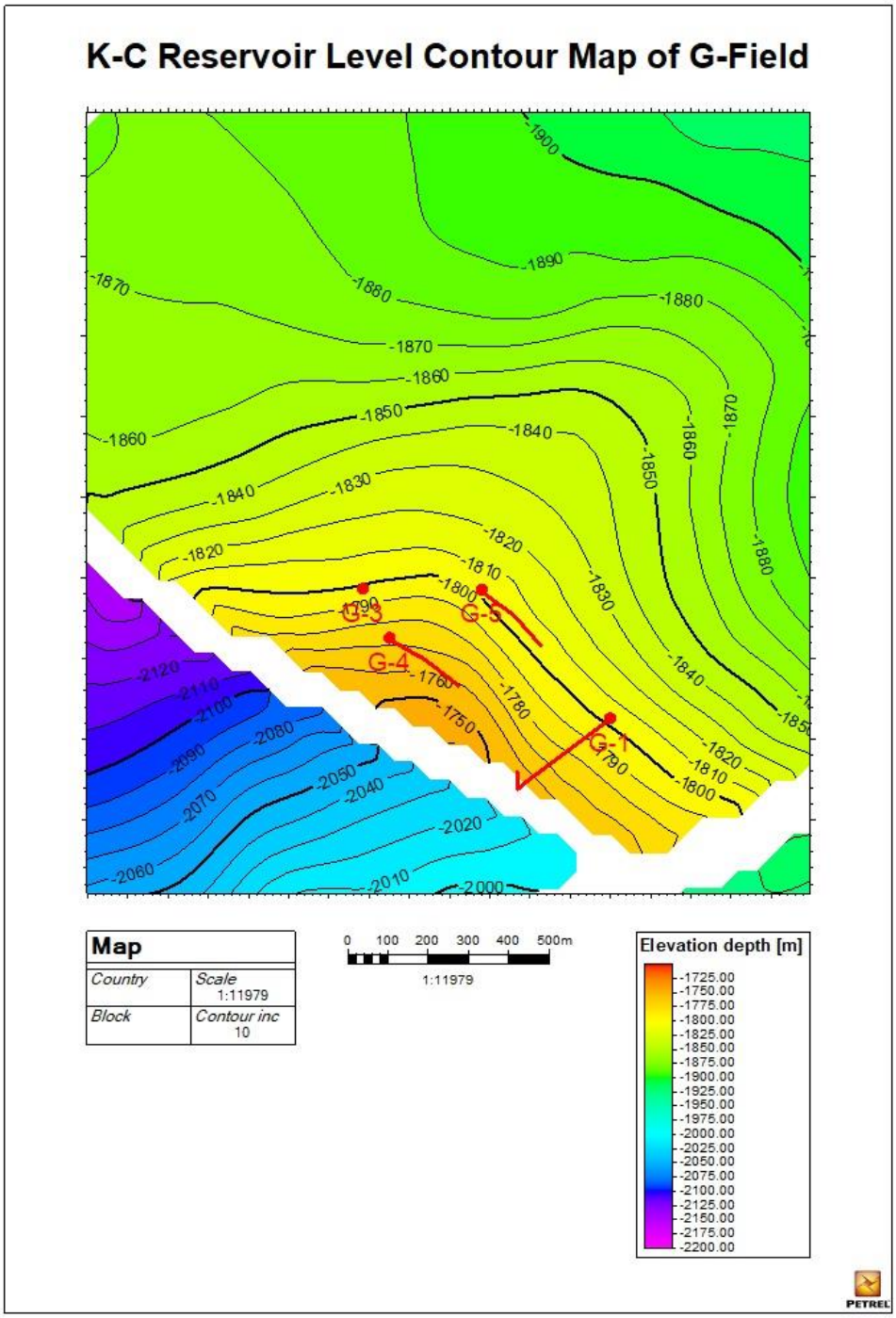

Figure 4.29. K-C Reservoir Level Contour Map of G-Field

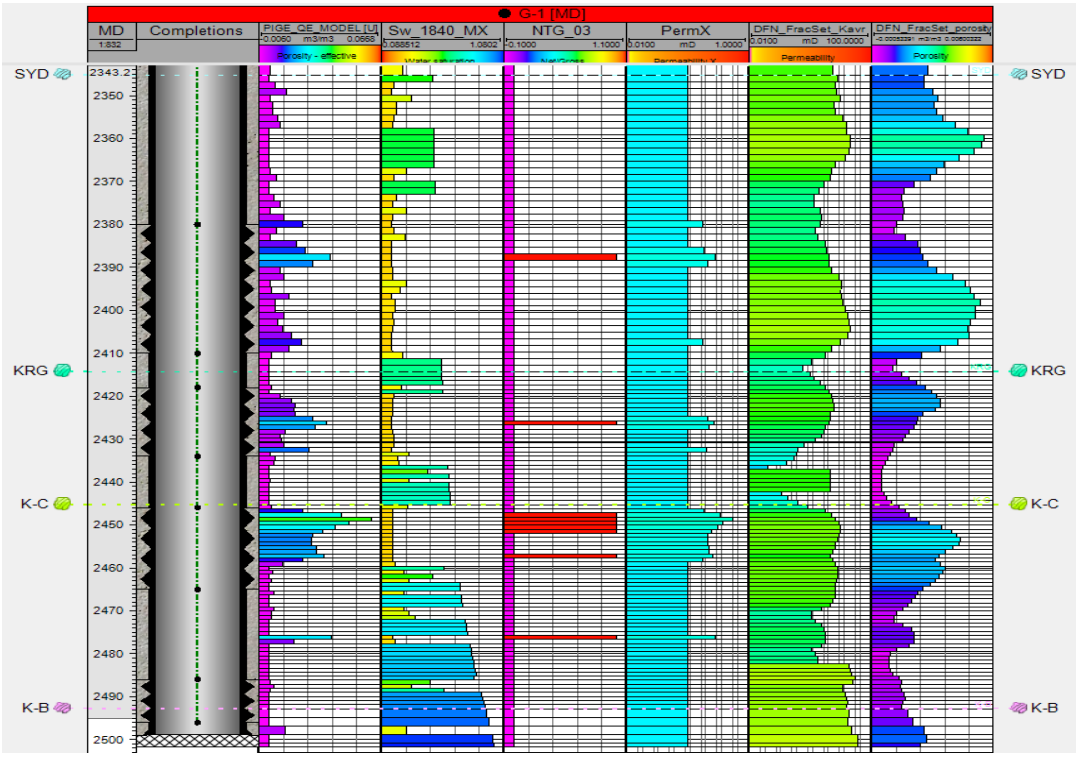

Figure 4.30. Well schematic of G-1 (Güner Çiçek, C., 2022)

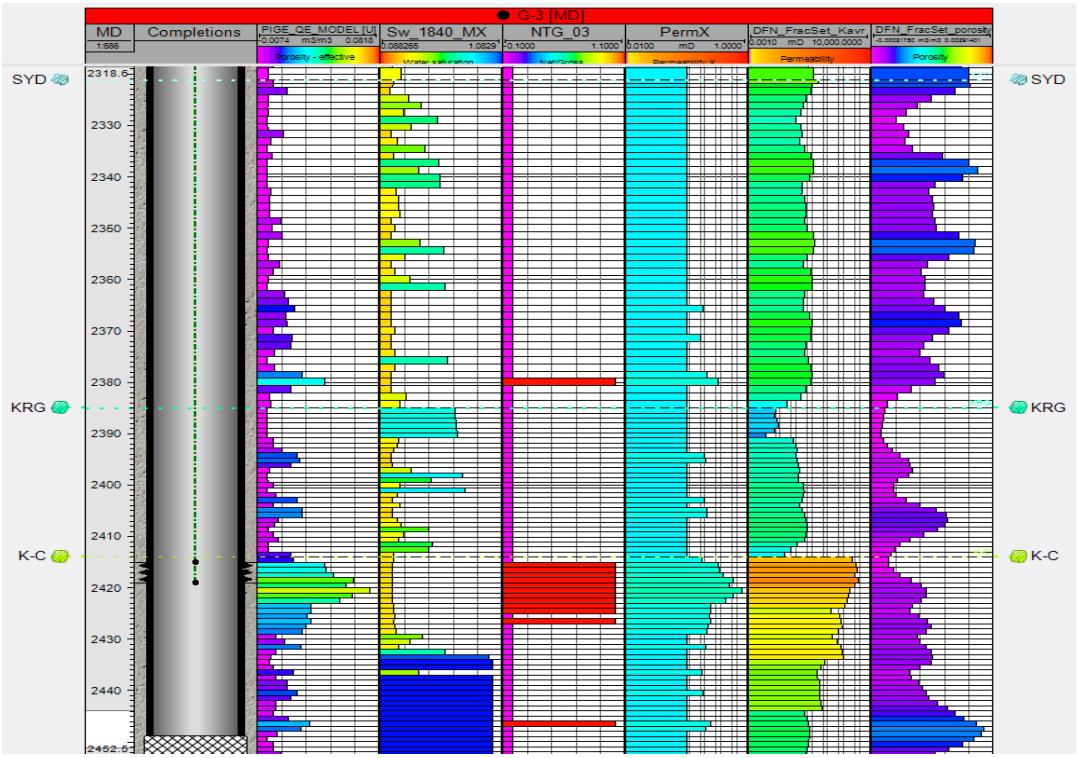

Figure 4.31. Well schematic of G-3 (Güner Çiçek, C., 2022)

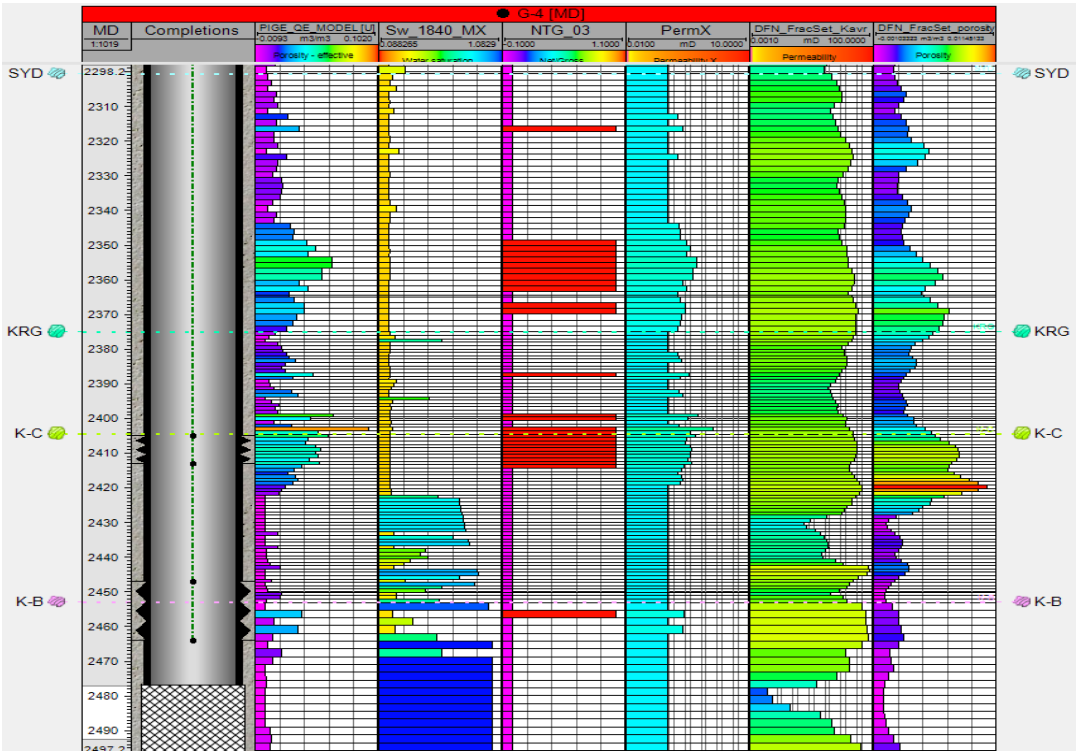

Figure 4.32. Well schematic of G-4 (Güner Çiçek, C., 2022)

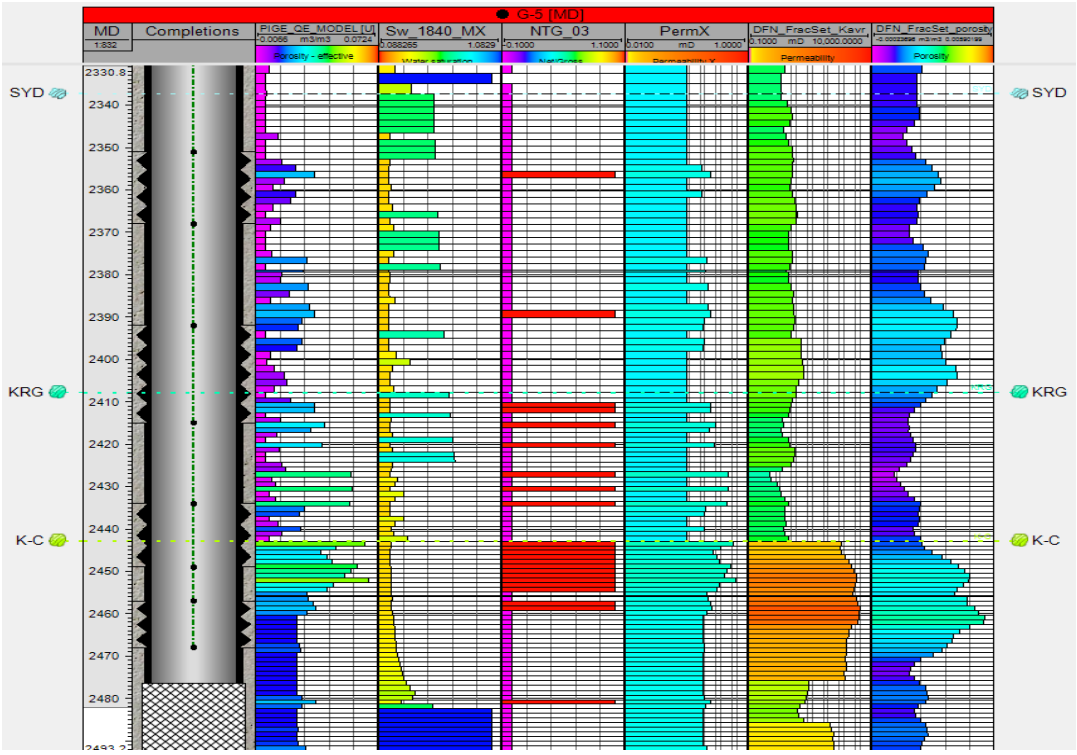

Figure 4.33. Well schematic of G-5 (Güner Çiçek, C., 2022)

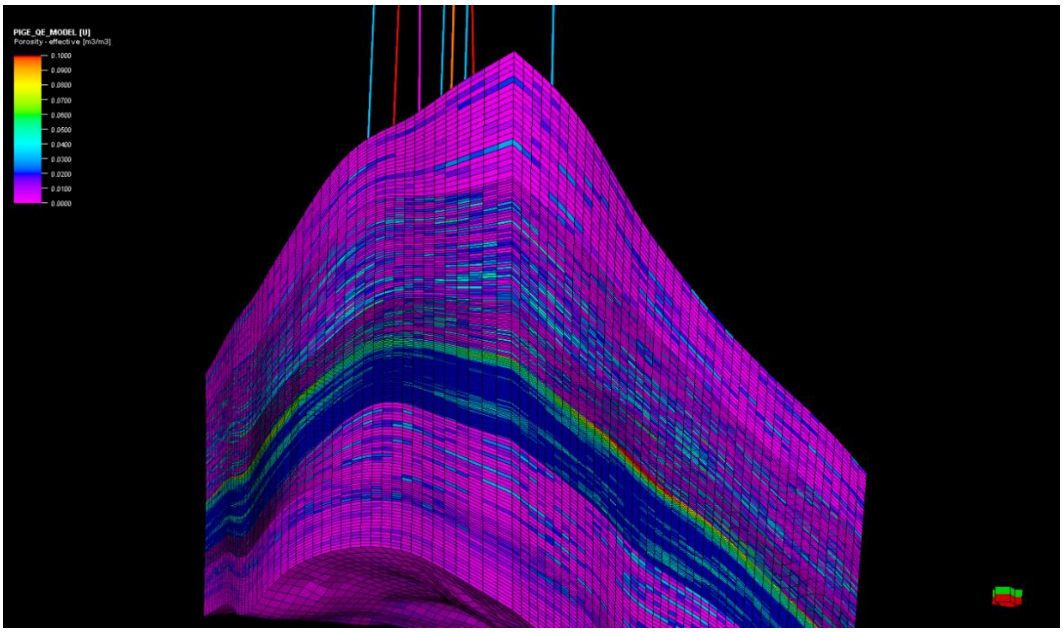

Figure 4.34. Porosity distribution of G-Field in geomodel (Özkaya Türkmen et al. 2022)

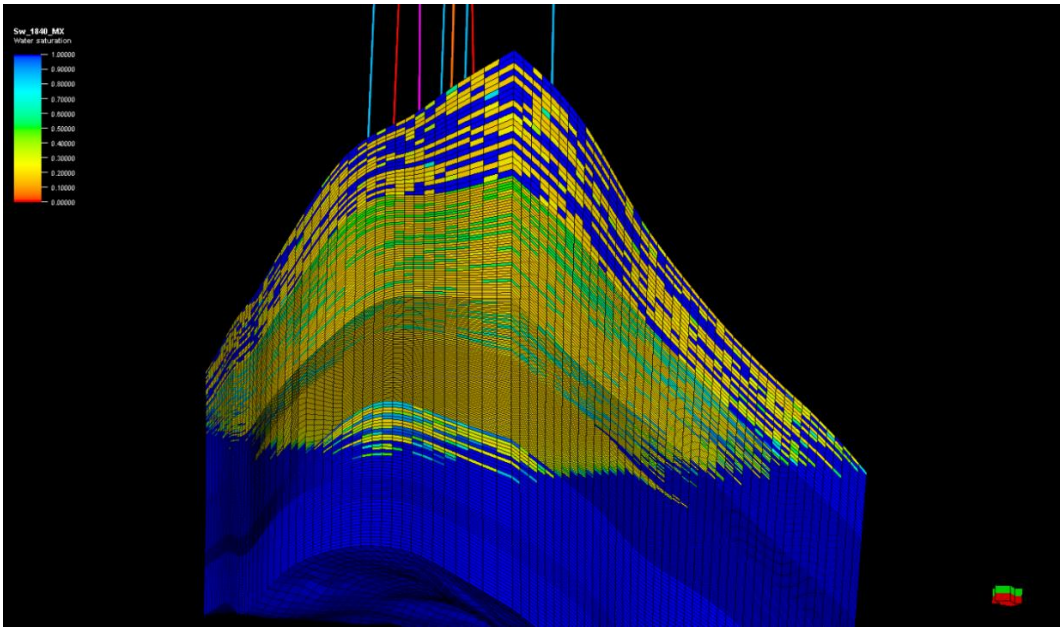

Figure 4.35. Water Saturation distribution of G-Field in geomodel (Özkaya Türkmen et al. 2022)

There are 376,740 grids in the geological model. The x and y direction of each grid is 100 meters; however, z direction differs from zone to zone with the values of 2.5 meters to 10 meters of thickness of a grid. It is useless to put all the geological model to the simulation due to run-time and convergence problems. In order to restrict the grid number, ACTNUM keyword can be used to select the grids that can be put into simulation. In the simulation, the grids that have the grid center lower than -1845 TVDSS do not inserted to the simulation. The reason for the -1845 TVDSS meters is that free water level is properly modeled for the -1840 meters, the extra 5 meters is for the assure the flow of free water level. Another grid elimination method is net-to-gross cut off for the matrix where the grids that have porosity less than three percent can not go into simulation. However, for the fractures, every grid that is not eliminated by the ACTNUM keyword is available for the simulation. Thus, the simulation has 18,885 grid for matrix and 123,550 grid for fracture, making 142,435 grid in total.

4.6 Initial and Boundary Conditions

The original reservoir pressure and temperature of the G-Field is 3030 psi and 205 ^{o}F, respectively. The model is isothermal, which means no temperature changes along the simulation. The bottom of the reservoir contains aquifer which was modeled with Fetkovich Aquifer Model.

Table 4.18 Fetkovich Aquifer Model Values

	Value	Unit
Volume	70,215,202	STB
Total Compressibility	1.00E-06	1/psi
Productivity Index	1	STB/d/psi
Total	24.58	2.78

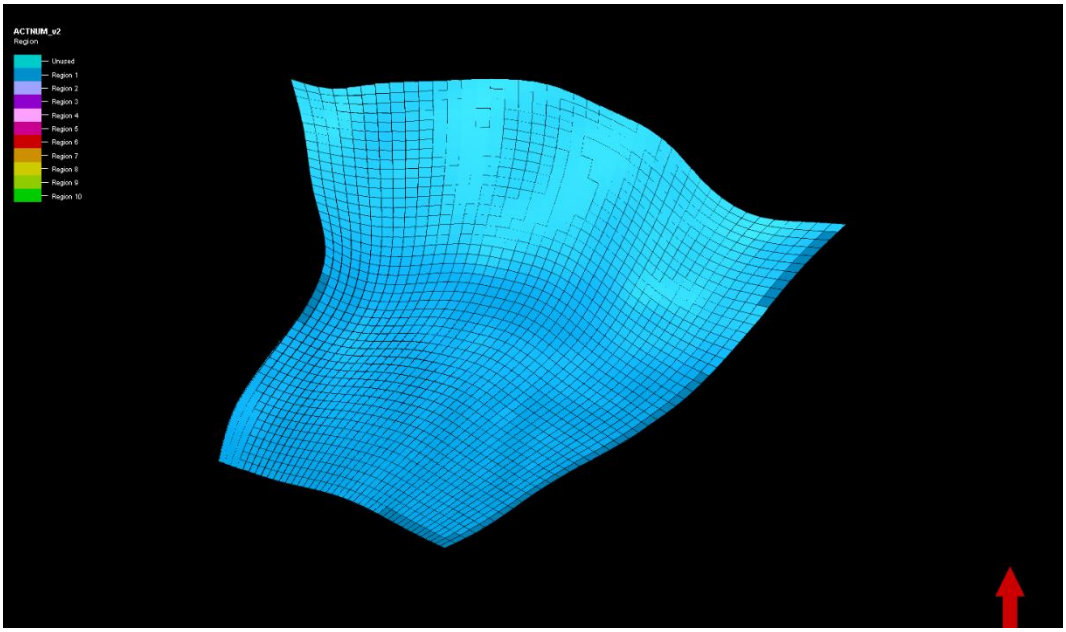

Figure 4.36. Reservoir bottom with the connected aquifer

4.7 Fracture Properties

G-Field fracture properties such as fracture porosity, fracture sigma value and fracture permeability is found by the DFN model of Petrel by Slb. There are DST operations conducted in the wells, however, none of them was analyzable to find the system permeability or fracture properties can be found from pressure transient analysis. However, the properties derived from the DFN model is used to match the production history of the field, thus, confirming the model has low uncertainity with the reality.

The average fracture permeability is 12 mD in the field. This value is low comparing the other fields, thus making the G-Field is a low quality naturally fractured carbonate reservoir.

The fracture model of the G-Field created by the DFN module of Petrel by Slb. The module uses the fracture sets appointed to the well to create the grid properties by upscaling while using corrected Oda Method. The fracture sets are obtained from the well image logs. The corrected Oda Method is a complex way to calculate the permeability tensor of a grid. The upscaled grid property later geostatistically distributed along the field.

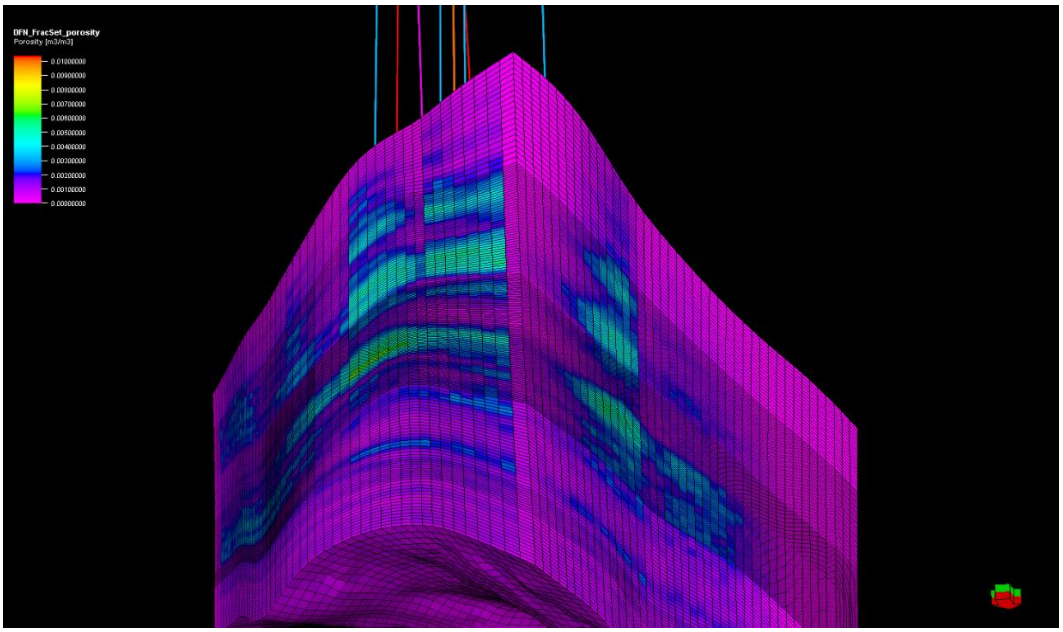

Figure 4.37. Fracture porosity 3D Grid

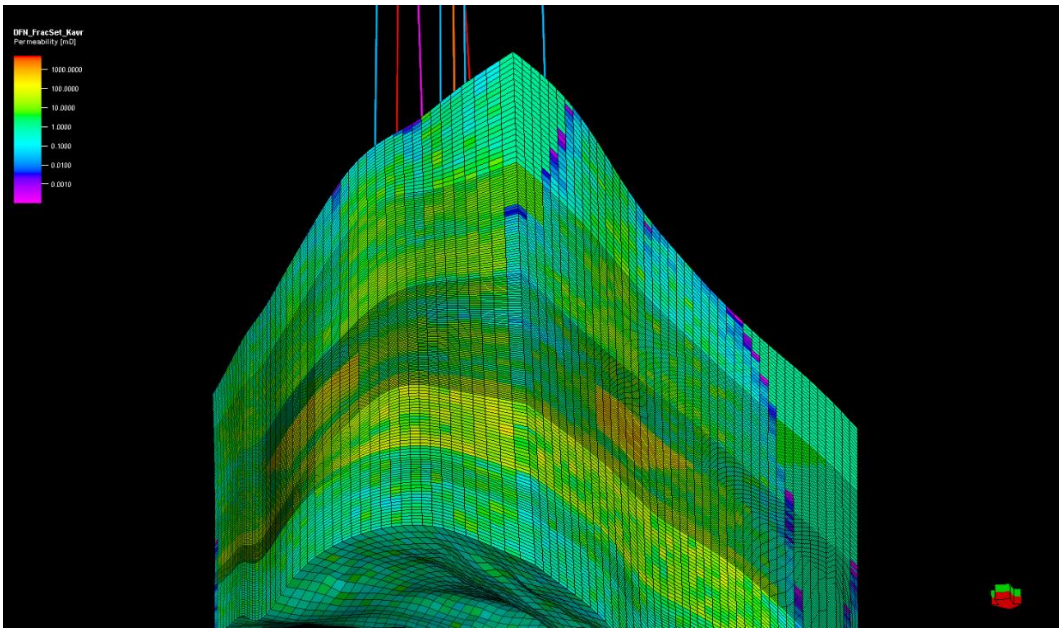

Figure 4.38. Fracture permeability 3D Grid

Table 4.19 Fracture Permeability Statistical Values

	Value
Min	0.0001
Max	5306.9629
Mean	12.9552
Std. Dev.	90.7896
Variance	8242.7564

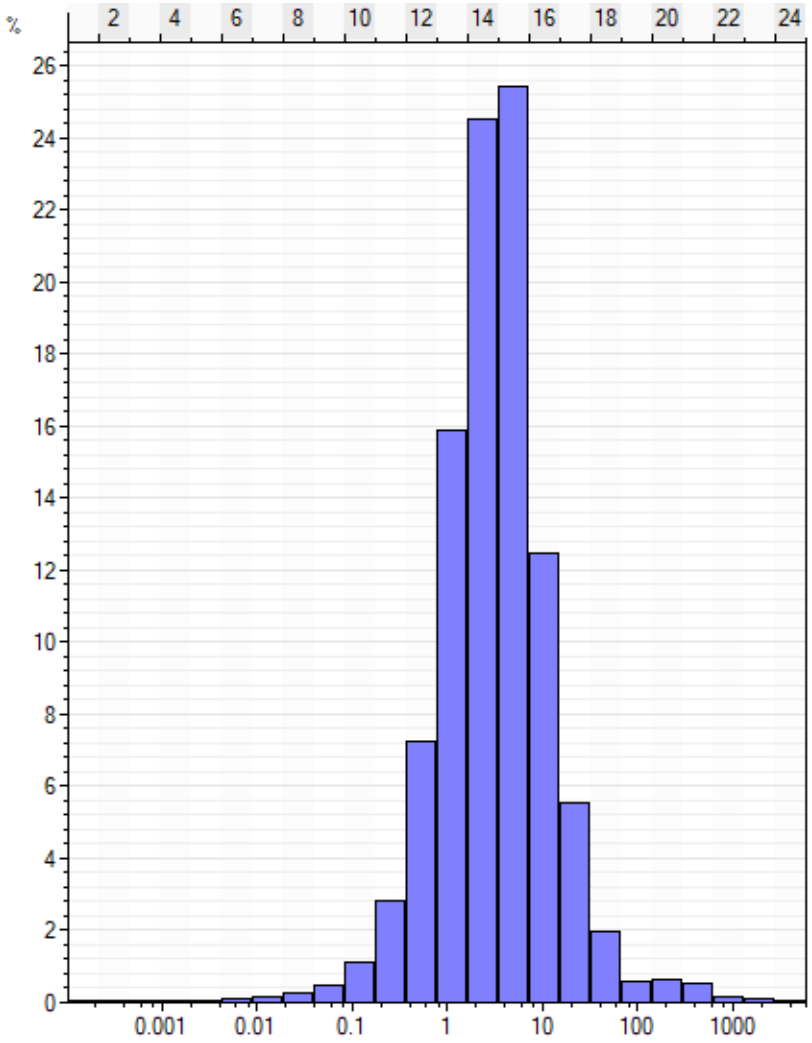

Figure 4.39. Fracture permeability histogram

4.8 Bottom Hole Pressure

In G-Field, to determine the bottom hole pressure of a well is to measure the liquid height in the annulus. Since the true datum depth and liquid height of each well are different, and to analyze the well productivity decently, the bottom hole pressures of each well should be observed in the same datum depth which is -1750 meters TVDSS in the G-Field.

Bottom hole pressure at a certain depth can be observed in the datum depth by the formula;

$$BHP_{Datum\ Depth} = (TVD_{Datum} - TVD_{Observed}) * 0{,}43316 * 3{,}281 * \rho_{fluid} \quad (4.9)$$

However, the problem in this situation is that the fluid density can change throughout the wellbore due to the pressure difference at the observed and datum depths. To solve the problem, a MatLab code that uses the Newton-Raphson iteration method to calculate the density of the fluid at the corresponding pressure is developed. It also considers liquid height loss due the compressibility of the fluid since the liquid loses its volume in the wellbore due to head load even though the fluid considered to be slightly-compressible.

Considering the bottom hole pressures of each well at a certain datum depth can give ideas about the well performance and the reservoir areas that have good system permeability.

The MatLAB Code is in the Appendix-A.

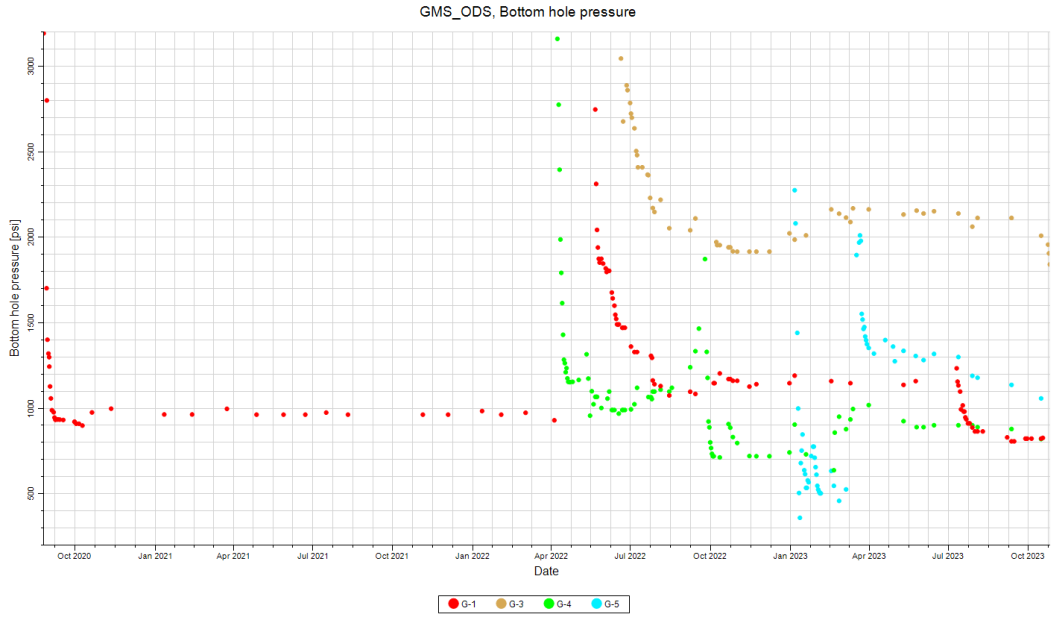

Figure 4.40. Bottom Hole Pressure history at TVDSS -1750 for each well

4.9 History Match

The history match for the G-Field is done with the observed data coming from the well-site measurements. Oil rate, water rate and the liquid height, later turned into the bottom hole pressure with the MatLAB Code, were measured with the appropriate tools. Oil rate is selected for the controlling mechanism of the simulation, means that the simulation software, Intersect, will follow the oil rate appointed to the wells, and outputs the bottom hole pressure and the water rate with the given grid properties. For the sensitivity analysis, two different relative permeability curves derived with the Brooks-Corey Relative Permeability Model and modified Brooks-Corey Relative Permeability Model were used to do history matches. There is no difference observed in the two relative permeability models since the matrix contributiın to the flow is limited in the history match era of the production.

The SYD Formation is modelled as single porosity where the KRG, K-C and K-B Formations are modelled as dual porosity. As mentioned, SYD Formation is the cap

rock of the petroleum system. It lacks matrix properties such as porosity and permeability. However, in the well logs, it is observed that several porosity packs exist at the bottom of the formation. In order to not exaggerate the flow capacity of the SYD Formation, it has modelled as single porosity. However, the other three formations, KRG, K-C and K-B, were modelled as dual porosity due to its matrix and fracture properties coming from the Discrete Fracture Network model.

The observed data set of the G-Field starts from the August 2020, where the first well put on the production, G-1. 74 months of observed data is used to do history match. October 2023 is the final step of the history match. Four wells are historically matched with their unique observed data.

For the upcoming figures, green dots are the observed data of each graph and the red line is the output of the simulation software. The upper left graph shows the bottom hole pressure in psi of a well at the -1750 TVDSS reference depth. The upper right graph shows the cumulative oil production of the well. The bottom left graph shows the oil rate in STB/d and the bottom right graph shows the water cut of the well in fractions.

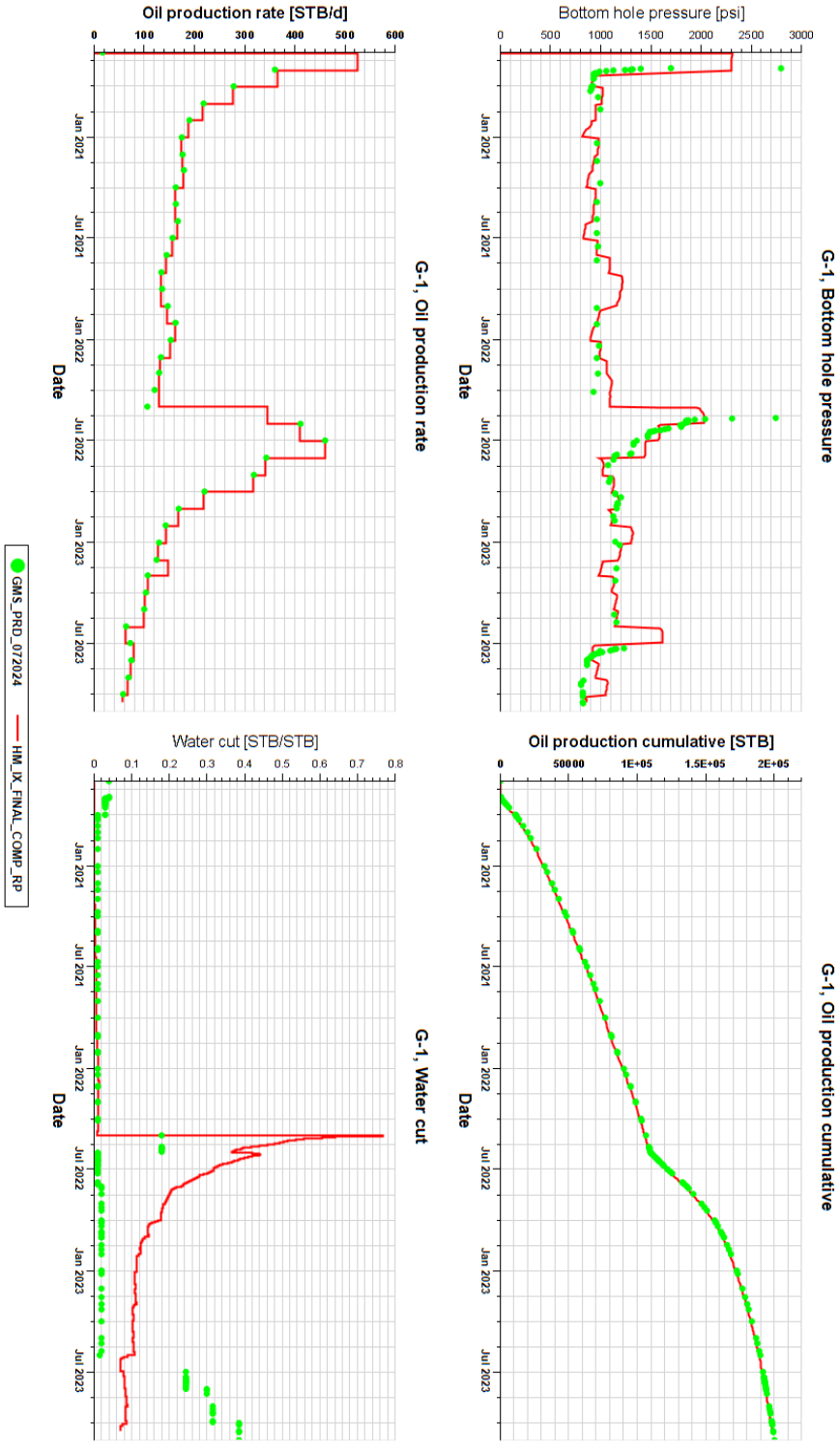

Figure 4.41. History match of G-1

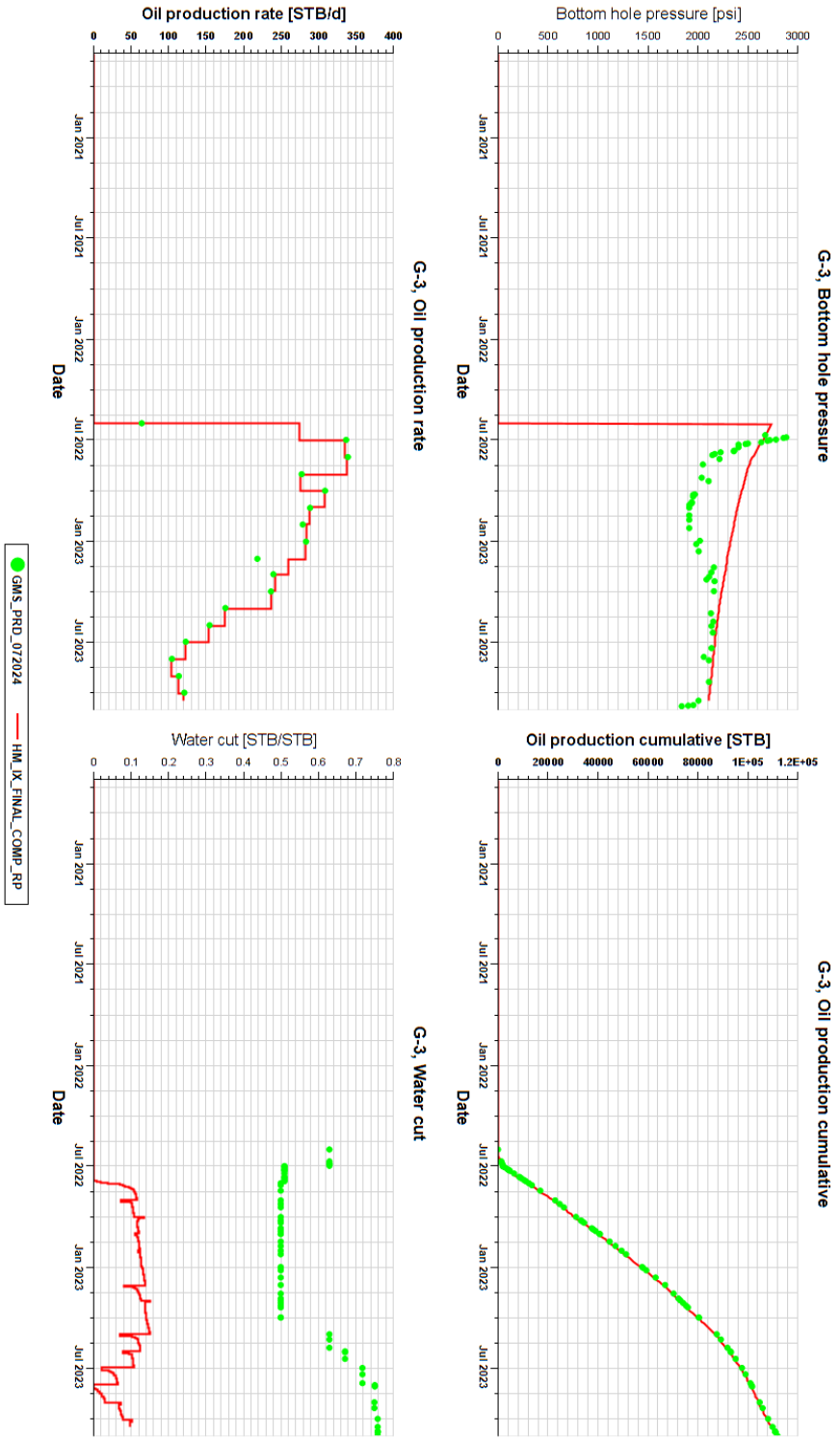

Figure 4.42. History Match of G-3

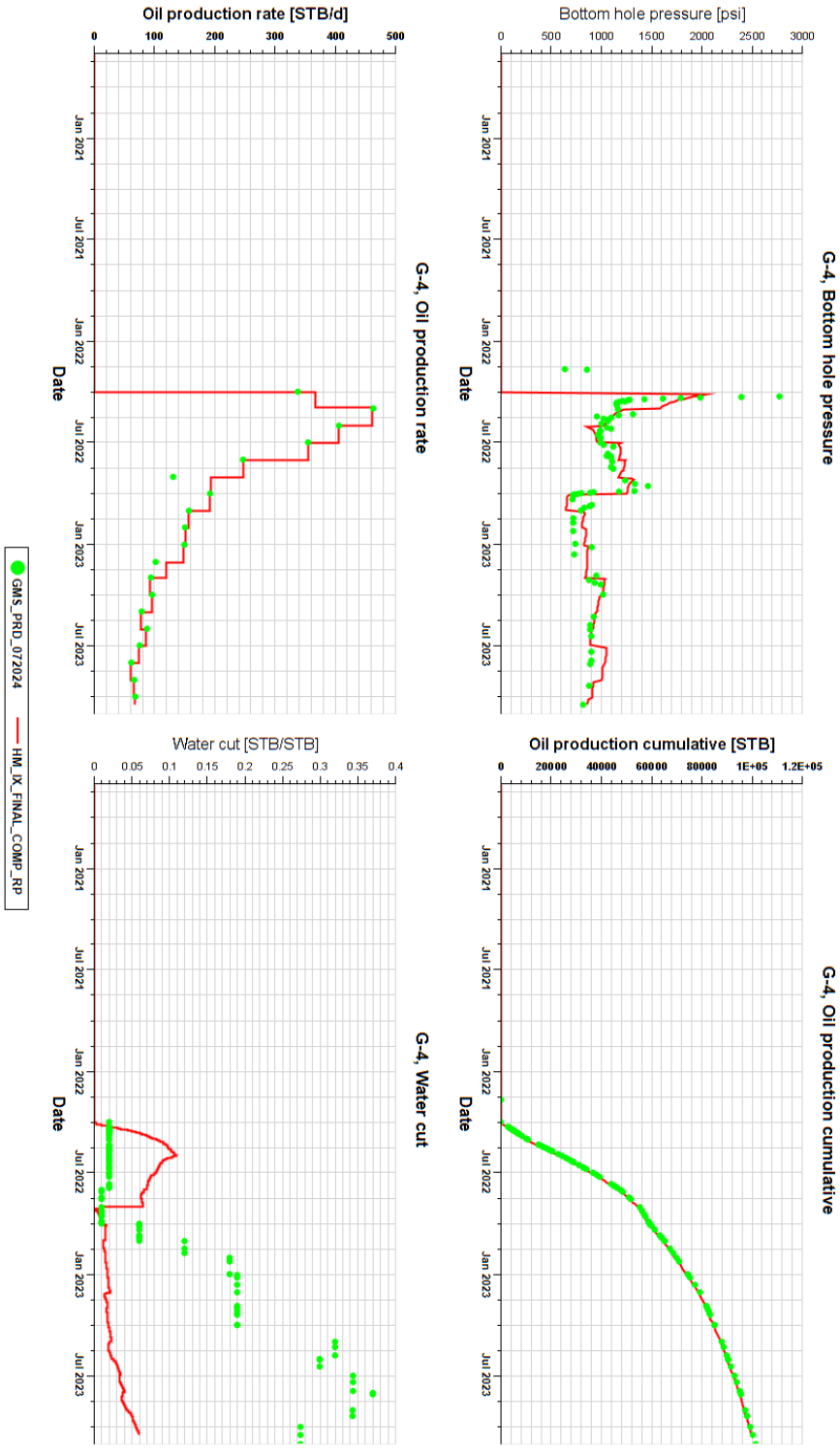

Figure 4.43. History Match of G-4

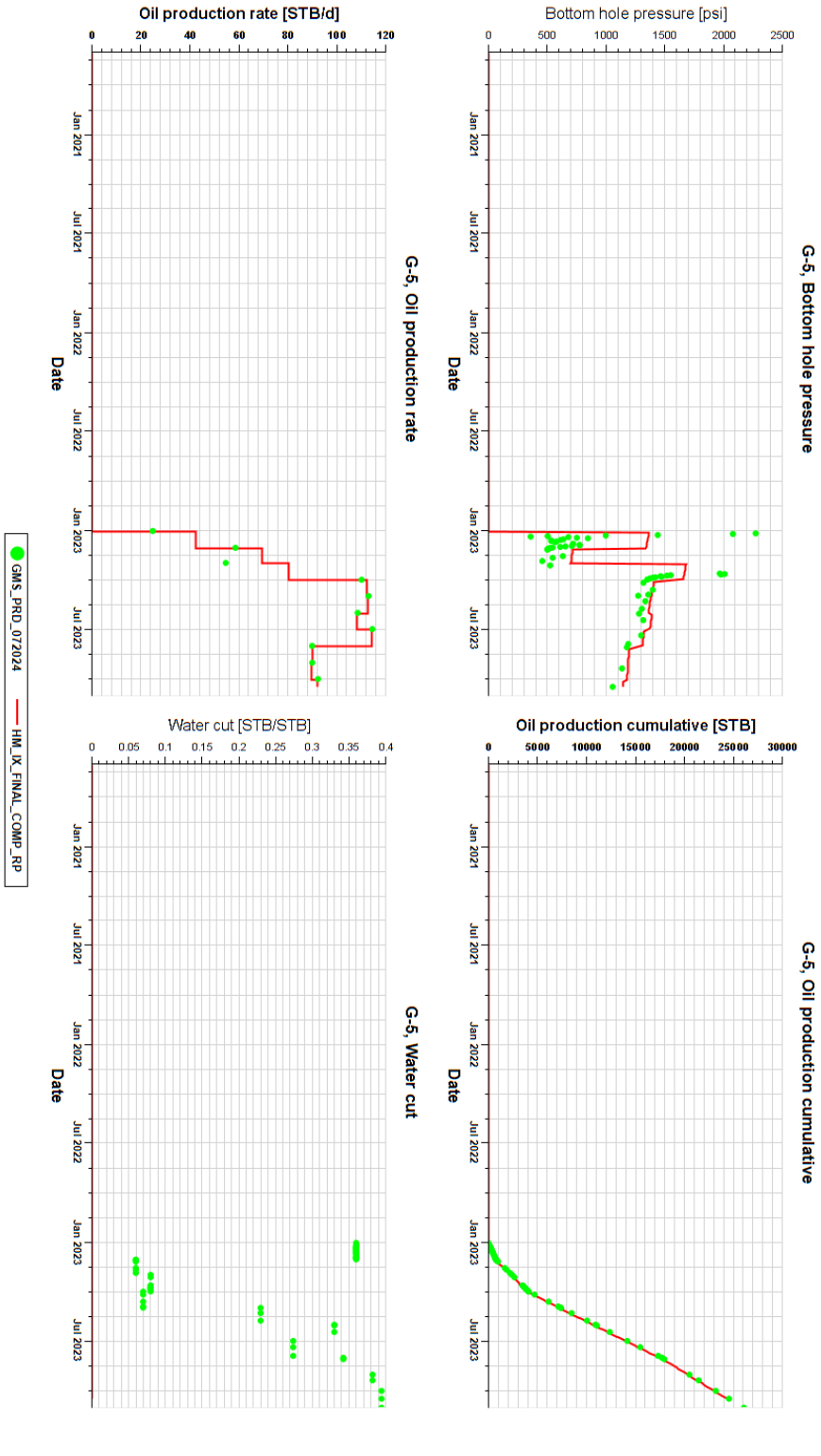

Figure 4.44. History Match of G-5

CHAPTER 5

RESULTS AND DISCUSSION

Simulation results should be investigated with the Oil Initially In Place and with the matrix to fracture flow in cumulative. Oil Initially In Place value is important for the economic value of the prospect. It should be divided into two as the oil initially in matrix and oil initially in fractures. The matrix to fracture flow in cumulative is important to investigate whether the gravity drainage is working for this field or not. It is essential to know that how much oil volume is recovered from the matrix to fractures.

Table 5.1 Oil Inıtially In Place in Matrix and in Fractures for G-Field

Formation	OIIP, STB
SYD	3,757,300
KRG - M	1,195,609
KC - M	2,345,497
KB - M	29,580
KRG - F	393,116
KC- F	506,641
KB - F	56,607
FIELD	8,284,353
FIELD - M	7,327,986
FIELD - F	956,366
F/M	13.1 %

It is observed that the volume of oil in fractures 0.13 times of the volume of oil in matrix. It means that 11 % of the oil volume is in fractures for the whole field.

Table 5.2 Matrix to Fracture Flow of each Formation

From / To	KRG - F	KC - F	KB - F
SYD	17,467	-	-
KRG - M	83,938	-	-
KC - M	-	185,053	-
KB - M	-	-	2,433

Table 5.3 Percentages of Matrix to Fracture Flow of History Match

Formation	OIIP, STB	M TO F (%)
SYD	3,757,300	0.5
KRG - M	1,195,609	7.0
KC - M	2,345,497	7.9
KB - M	29,580	8.2

From SYD formation to KRG formations fractures, there are 17,467 STB of oil transported at the end of the history match. It is 83,938 STB of oil from KRG matrix to KRG fractures, 185,053 STB of oil from K-C matrix to K-C fractures and 2,433 STB of oil from K-B matrix to K-B fractures. Those numbers correspond of 0.5 %, 7 %, 7.9 % and 8.2 % of oil initially in those formations' matrix, respectively, were recovered from matrix up to October 2023. From Table 5.4 to 5.45, the produced volumes, the inter-region flow cumulatives and the percentage of the recovery factor is decribed for the specified cases.

5.1 Case No Further Action

After the history match, no further action case is simulated for 30 years. No further action means there will be no other production well to be drilled or no other perforation in a producing well. This case will be the base case to compare the upcoming results. If the field continues to produce with no intervention, the estimated ultimate recovery will be 1,359,090 STB of oil which equals to the %16.41 of the Initial Oil In Place. In other words, the recovery factor will be %16.41 for the G-Field. This is normal value for an naturally fractured carbonate reservoir with tight matrix and low fracture quality, and also with weak aquifer support.

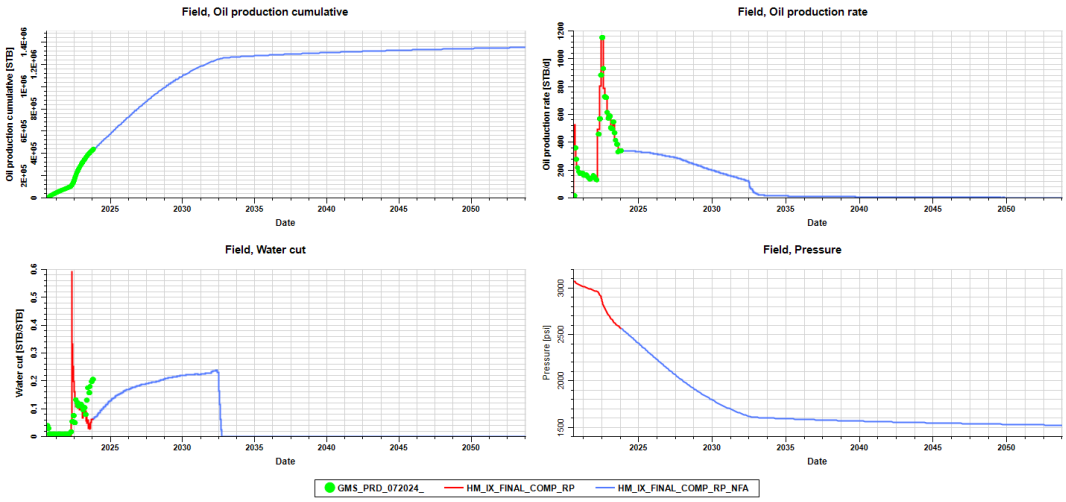

Figure 5.1. No Further Action Results

It has been observed that 42.12 % of the fracture volume is recovered while it is only 13.05 % for the matrix. This numbers show that the field has oil producible in the matrix with the appropriate techniques. It is essential to check the volume that is transferred from matrix to the fracture and the volume difference between the diminishing oil volume from matrix and the total production values if the convergence problems of the simulation affect the results or not.

Table 5.4 NFA Results

Initial State		*Produced*		*Percent*
Formation	Oil, STB	Formation	Oil, STB	%
SYD	3,757,300	SYD	132,744	3.53
KRG - M	1,195,609	KRG - M	253,235	21.18
KC - M	2,345,497	KC - M	563,225	24.01
KB - M	29,580	KB - M	7,107	24.03
KRG - F	393,117	KRG - F	133,824	34.04
KC- F	506,642	KC- F	227,440	44.89
KB - F	56,608	KB - F	41,515	73.34
FIELD	8,284,353	FIELD	1,359,090	16.41
FIELD - M	7,327,987	FIELD - M	956,312	13.05
FIELD - F	956,367	FIELD - F	402,778	42.12
F/M	13.1	F/M	42.1	

Table 5.5 Volume of Oil from Matrix to Fracture Flow of Case NFA

From / To	KRG - F	KC - F	KB - F
SYD	126,938	-	-
KRG - M	253,205	-	-
KC - M	-	562,607	-
KB - M	-	-	7,102

Table 5.6 Percentages of Oil Transported from Matrix to Fractures for Case NFA

FORMATION	OIL IN PLACE, STB	M TO F, STB	M TO F (%)
SYD	3,757,300	126,938	3.3
KRG - M	1,195,609	235,205	19.6
KC - M	2,345,497	562,607	24
KB - M	29,580	7,102	24

There are less than 1 % percent of material balance error due to convergence problems of simulation, so it can be said that results do not change much due to convergence problems.

5.2 Carbon-Dioxide Injection with Power Law Relative Permeability Model

For the matrix recovery purpose, gravity drainage is used where the CO2 injection takes place. The CO2 that fills the fracture changes place with the oil in matrix, thus increase matrix recovery. The main idea in the gravity drainage is to inject the CO2 from the upper part of the naturally fractured reservoir so that CO2 starts to invade the fractures from upper part, therefore no oil by-passed. The injection wells in the field are located as follows;

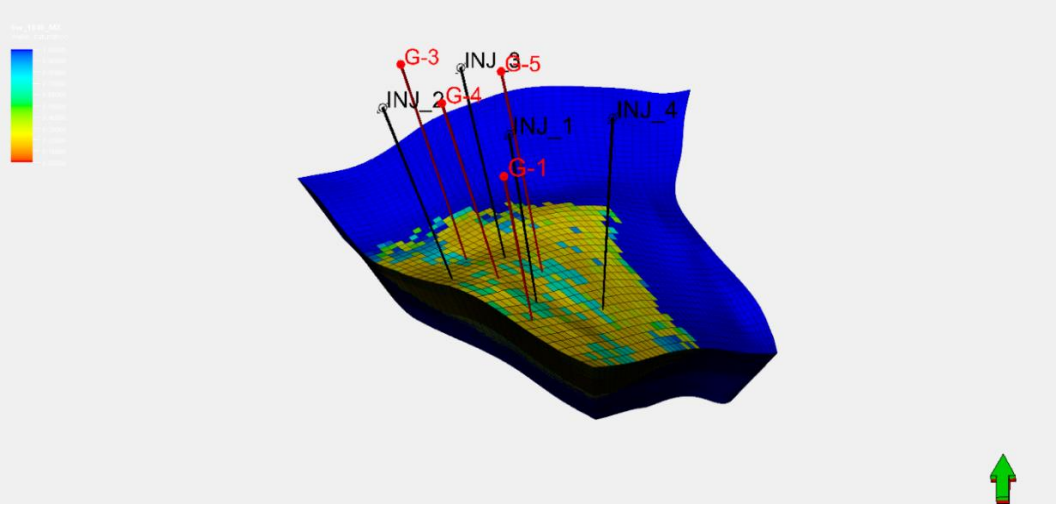

Figure 5.2. Injector Locations for G-Field

CO2 injection starts at the beginning of June 2024 with the four injection wells. The KRG formation is perforated in each well. In order to understand the efficiency of recovery, 4 cases are studied under the minimum miscibility pressure and one case is simulated above the minimum miscibility pressure. The amount of CO2 that is injected each day is 2500 sm^3, 5000 sm^3, 10000 sm^3, 25000 sm^3 and 50000 sm^3 respectively. The carbon-dioxide is in super-critical fluid phase in the reservoir conditions of G-Field and the conditions never drops below the required pressure or temperature to change the carbon-dioxide phase.

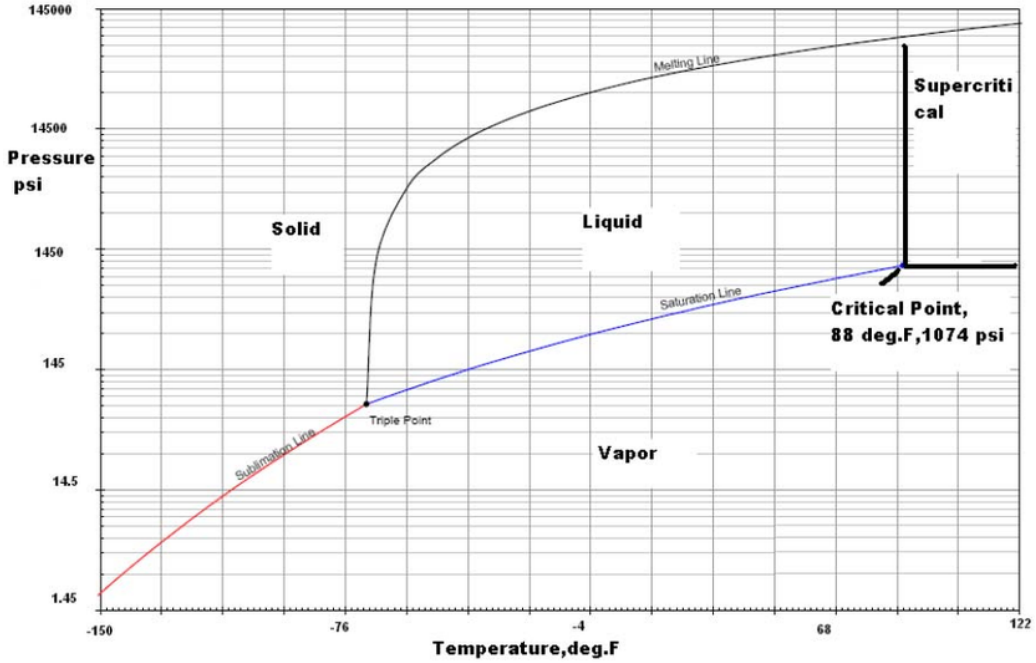

Figure 5.3. Carbon-dioxide phase diagram (El-Hajj et al., 2013)

5.2.1 2500 SM3 CO2 Injection

Table 5.7 2500 SM3 CO2 Injection Results

Initial State		*Produced*		*Percent*
Formation	Oil, STB	Formation	Oil, STB	%
SYD	3,757,300	SYD	141,582	3.77
KRG - M	1,195,609	KRG - M	434,538	36.34
KC - M	2,345,497	KC - M	782,841	33.38
KB - M	29,580	KB - M	7,457	25.21
KRG - F	393,117	KRG - F	286,248	72.82
KC- F	506,642	KC- F	384,702	75.93
KB - F	56,608	KB - F	38,553	68.11
FIELD	8,284,353	FIELD	2,075,922	25.06
FIELD - M	7,327,987	FIELD - M	1,366,418	18.65
FIELD - F	956,367	FIELD - F	709,504	74.19
F/M	13.1	F/M	51.9	

Table 5.8 Volume of Oil from Matrix to Fracture Flow of Case 2500 SM3 CO2 Injection

From / To	KRG - F	KC - F	KB - F
SYD	136,519	-	-
KRG - M	432,857	-	-
KC - M	-	777,419	-
KB - M	-	-	7,473

Table 5.9 Percentages of Oil Transported from Matrix to Fractures for Case 2500 SM3 CO2 Injection

FORMATION	OIL IN PLACE, STB	M TO F, STB	M TO F (%)
SYD	3,757,300	136,519	3.6
KRG - M	1,195,609	432,857	36.2
KC - M	2,345,497	777,419	33.1
KB - M	29,580	7,473	25.3

5.2.2 5000 SM3 CO2 Injection

Table 5.10 5000 SM3 CO2 Injection Results

Initial State		*Produced*		*Percent*
Formation	Oil, STB	Formation	Oil, STB	%
SYD	3,757,300	SYD	142,462	3.79
KRG - M	1,195,609	KRG - M	499,470	41.78
KC - M	2,345,497	KC - M	851,666	36.31
KB - M	29,580	KB - M	7,955	26.89
KRG - F	393,117	KRG - F	291,309	74.10
KC- F	506,642	KC- F	398,811	78.72
KB - F	56,608	KB - F	40,416	71.40
FIELD	8,284,353	FIELD	2,232,090	26.94
FIELD - M	7,327,987	FIELD - M	1,501,554	20.49
FIELD - F	956,367	FIELD - F	730,537	76.39
F/M	13.1	F/M	48.7	

Table 5.11 Volume of Oil from Matrix to Fracture Flow of Case 5000 SM3 CO2 Injection

From / To	KRG - F	KC - F	KB - F
SYD	137,318	-	-
KRG - M	494,497	-	-
KC - M	-	843,804	-
KB - M	-	-	7,940

Table 5.12 Percentages of Oil Transported from Matrix to Fractures for Case 5000 SM3 CO2 Injection

FORMATION	OIL IN PLACE, STB	M TO F, STB	M TO F (%)
SYD	3,757,300	137,318	3.7
KRG - M	1,195,609	494,497	41.4
KC - M	2,345,497	843,804	36.0
KB - M	29,580	7,940	26.8

5.2.3 10000 SM3 CO2 Injection

Table 5.13 10000 SM3 CO2 Injection Results

Initial State		*Produced*		*Percent*
Formation	Oil, STB	Formation	Oil, STB	%
SYD	3,757,300	SYD	142,758	3.80
KRG - M	1,195,609	KRG - M	594,920	49.76
KC - M	2,345,497	KC - M	1,001,840	42.71
KB - M	29,580	KB - M	8,614	29.12
KRG - F	393,117	KRG - F	296,389	75.39
KC- F	506,642	KC- F	411,941	81.31
KB - F	56,608	KB - F	42,334	74.78
FIELD	8,284,353	FIELD	2,498,796	30.16
FIELD - M	7,327,987	FIELD - M	1,748,132	23.86
FIELD - F	956,367	FIELD - F	750,664	78.49
F/M	13.1	F/M	42.9	

Table 5.14 Volume of Oil from Matrix to Fracture Flow of Case 10000 SM3 CO2 Injection

From / To	KRG - F	KC - F	KB - F
SYD	137,620	-	-
KRG - M	589,811	-	-
KC - M	-	992,342	-
KB - M	-	-	8,593

Table 5.15 Percentages of Oil Transported from Matrix to Fractures for Case 10000 SM3 CO2 Injection

FORMATION	OIL IN PLACE, STB	M TO F, STB	M TO F (%)
SYD	3,757,300	137,620	3.7
KRG - M	1,195,609	589,811	49.3
KC - M	2,345,497	992,342	42.3
KB - M	29,580	8,593	29.1

5.2.4 25000 SM3 CO2 Injection

Table 5.16 25000 SM3 CO2 Injection Results

Initial State		*Produced*		*Percent*
Formation	Oil, STB	Formation	Oil, STB	%
SYD	3,757,300	SYD	136,216	3.63
KRG - M	1,195,609	KRG - M	692,056	57.88
KC - M	2,345,497	KC - M	1,310,201	55.86
KB - M	29,580	KB - M	11,783	39.83
KRG - F	393,117	KRG - F	304,020	77.34
KC- F	506,642	KC- F	427,273	84.33
KB - F	56,608	KB - F	45,558	80.48
FIELD	8,284,353	FIELD	2,927,107	35.33
FIELD - M	7,327,987	FIELD - M	2,150,256	29.34
FIELD - F	956,367	FIELD - F	776,851	81.23
F/M	13.1	F/M	36.1	

Table 5.17 Volume of Oil from Matrix to Fracture Flow of Case 25000 SM3 CO2 Injection

From / To	KRG - F	KC - F	KB - F
SYD	136,382	-	-
KRG - M	719,249	-	-
KC - M	-	1,381,460	-
KB - M	-	-	12,760

Table 5.18 Percentages of Oil Transported from Matrix to Fractures for Case 25000 SM3 CO2 Injection

FORMATION	OIL IN PLACE, STB	M TO F, STB	M TO F (%)
SYD	3,757,300	136,382	3.6
KRG - M	1,195,609	719,249	60.2
KC - M	2,345,497	1,381,460	58.9
KB - M	29,580	12,760	43.1

5.2.5 50000 SM3 CO2 Injection, Miscible Injection

Table 5.19 Change in Component Fractions

Component	Initial State, Fraction	Last Step, Fraction	Change in Percent
N2-C1	0.009401	0.003311	64.77
CO2	0.008301	0.600169	7130.2
C2	0.001100	0.000389	64.61
C3	0.008701	0.003090	64.48
C4	0.020702	0.007378	64.36
C5	0.002400	0.000863	64.03
C6	0.007001	0.002545	63.64
C7+	0.942394	0.382255	59.43
Total	1.000000	1.000000	

It can be said that the CO2 successfully mixed with the oil. It heavily decreased the other components mole fraction, especially the heavy components as C7+.

It has been observed that as the injected CO2 volume increases, the recovered oil from both fracture and matrix has increased. However, the matrix volume that is been produced to the fracture is increased more in percent, therefore, the CO2 injection can be said that is improving the oil recovery.

Table 5.20 50000 SM3 CO2 Injection Results

Initial State		*Produced*		*Percent*
Formation	Oil, STB	Formation	Oil, STB	%
SYD	3,757,300	SYD	131,920	3.51
KRG - M	1,195,609	KRG - M	1,068,710	89.39
KC - M	2,345,497	KC - M	2,108,077	89.88
KB - M	29,580	KB - M	21,071	71.24
KRG - F	393,117	KRG - F	300,831	76.52
KC- F	506,642	KC- F	443,662	87.57
KB - F	56,608	KB - F	50,358	88.96
FIELD	8,284,353	FIELD	4,124,629	49.79
FIELD - M	7,327,987	FIELD - M	3,329,778	45.44
FIELD - F	956,367	FIELD - F	794,851	83.11
F/M	13.1	F/M	23.9	

Table 5.21 Volume of Oil from Matrix to Fracture Flow of Case 50000 SM3 CO2 Injection

From / To	KRG - F	KC - F	KB - F
SYD	131,458	-	-
KRG - M	1,068,215	-	-
KC - M	-	2,099,845	-
KB - M	-	-	20,562

Table 5.22 Percentages of Oil Transported from Matrix to Fractures for Case 50000 SM3 CO2 Injection

FORMATION	OIL IN PLACE, STB	M TO F, STB	M TO F (%)
SYD	3,757,300	131,458	3.5
KRG - M	1,195,609	1,068,215	89.3
KC - M	2,345,497	2,099,845	89.5
KB - M	29,580	20,562	69.5

In this case, reservoir pressure never drops below to the minimum miscibility pressure along the reservoir. Therefore the injected carbon-dioxide sweeps the oil in the reservoir by mixing with it. The recovery of the field increased nearly to the half of the initial oil in place volume.

5.3 Carbon-Dioxide Injection with Brooks-Corey Relative Permeability Model

It is essential to do sensitivity analysis based on the relative permeability data since the relative permeability measurements in lab from a core is absent. Two different relative permeability models were mentioned above. Up to now, the Power-Law Relative Permeability Model was used in the simulation. In this part, the Brooks-Corey Relative Permeability Model will be used to determine the oil recovery.

5.3.1 Case No Further Action

Table 5.23 Case NFA Results

Initial State		*Produced*		*Percent*
Formation	Oil, STB	Formation	Oil, STB	%
SYD	3,757,300	SYD	57,635.22	1.53
KRG - M	1,195,609	KRG - M	251,542.90	21.04
KC - M	2,345,497	KC - M	559,174.74	23.84
KB - M	29,580	KB - M	7,031.99	23.77
KRG - F	393,117	KRG - F	135,286.13	34.41
KC- F	506,642	KC- F	223,876.31	44.19
KB - F	56,608	KB - F	41,033.52	72.49
FIELD	8,284,353	FIELD	1,275,280	15.39
FIELD - M	7,327,987	FIELD - M	875,384	11.94
FIELD - F	956,367	FIELD - F	400,196	41.84
F/M	13.1	F/M	46	

Table 5.24 Volume of Oil from Matrix to Fracture Flow of Case NFA

From / To	KRG - F	KC - F	KB - F
SYD	57,143	-	-
KRG - M	251,582	-	-
KC - M	-	558,878	-
KB - M	-	-	7,038

Table 5.25 Percentages of Oil Transported from Matrix to Fractures for Case NFA

FORMATION	OIL IN PLACE, STB	M TO F, STB	M TO F (%)
SYD	3,757,300	57,143	1.59
KRG - M	1,195,609	251,582	21.04
KC - M	2,345,497	558,878	23.82
KB - M	29,580	7,038	23.79

5.3.2 2500 SM3 CO2 Injection

Table 5.26 2500 SM3 CO2 Injection Results

Initial State		*Produced*		*Percent*
Formation	Oil, STB	Formation	Oil, STB	%
SYD	3,757,300	SYD	62,076	1.65
KRG - M	1,195,609	KRG - M	416,159	34.81
KC - M	2,345,497	KC - M	764,568	32.60
KB - M	29,580	KB - M	7,302	24.69
KRG - F	393,117	KRG - F	290,585	73.92
KC- F	506,642	KC- F	389,237	76.83
KB - F	56,608	KB - F	39,767	70.25
FIELD	8,284,353	FIELD	1,969,694	23.78
FIELD - M	7,327,987	FIELD - M	1,250,105	17.06
FIELD - F	956,367	FIELD - F	719,589	75.24
F/M	13.1	F/M	57.6	

Table 5.27 Volume of Oil from Matrix to Fracture Flow of Case 2500 SM3 CO2 Injection

From / To	KRG - F	KC - F	KB - F
SYD	62,480	-	-
KRG - M	412,147	-	-
KC - M	-	757,297	-
KB - M	-	-	7,334

Table 5.28 Percentages of Oil Transported from Matrix to Fractures for Case 2500 SM3 CO2 Injection

FORMATION	OIL IN PLACE, STB	M TO F, STB	M TO F (%)
SYD	3,757,300	62,480	1.7
KRG - M	1,195,609	412,147	34.5
KC - M	2,345,497	757,297	32.3
KB - M	29,580	7,334	24.8

5.3.3 5000 SM3 CO2 Injection

Table 5.29 5000 SM3 CO2 Injection Results

Initial State		*Produced*		*Percent*
Formation	Oil, STB	Formation	Oil, STB	%
SYD	3,757,300	SYD	61,736	1.64
KRG - M	1,195,609	KRG - M	474,423	39.68
KC - M	2,345,497	KC - M	826,732	35.25
KB - M	29,580	KB - M	7,738	26.16
KRG - F	393,117	KRG - F	296,061	75.31
KC- F	506,642	KC- F	404,796	79.90
KB - F	56,608	KB - F	42,084	74.34
FIELD	8,284,353	FIELD	2,113,571	25.51
FIELD - M	7,327,987	FIELD - M	1,370,630	18.70
FIELD - F	956,367	FIELD - F	742,941	77.68
F/M	13.1	F/M	54.2	

Table 5.30 Percentages of Matrix to Fracture Flow of Case 5000 SM3 CO2 Injection

From / To	KRG - F	KC - F	KB - F
SYD	62,188	-	-
KRG - M	467,796	-	-
KC - M	-	816,951	-
KB - M	-	-	7,745

Table 5.31 Percentages of Oil Transported from Matrix to Fractures for Case 5000 SM3 CO2 Injection

FORMATION	OIL IN PLACE, STB	M TO F, STB	M TO F (%)
SYD	3,757,300	62,188	1.7
KRG - M	1,195,609	467,796	39.1
KC - M	2,345,497	816,951	34.8
KB - M	29,580	7,745	26.2

5.3.4 10000 SM3 CO2 Injection

Table 5.32 10000 SM3 CO2 Injection Results

Initial State		*Produced*		*Percent*
Formation	Oil, STB	Formation	Oil, STB	%
SYD	3,757,300	SYD	61,063	1.63
KRG - M	1,195,609	KRG - M	558,024	46.67
KC - M	2,345,497	KC - M	964,395	41.12
KB - M	29,580	KB - M	8,216	27.78
KRG - F	393,117	KRG - F	301,469	76.69
KC- F	506,642	KC- F	419,781	82.86
KB - F	56,608	KB - F	43,802	77.38
FIELD	8,284,353	FIELD	2,356,750	28.45
FIELD - M	7,327,987	FIELD - M	1,591,698	21.72
FIELD - F	956,367	FIELD - F	765,052	80.00
F/M	13.1	F/M	48.1	

Table 5.33 Percentages of Matrix to Fracture Flow of Case 10000 SM3 CO2 Injection

From / To	KRG - F	KC - F	KB - F
SYD	61,575	-	-
KRG - M	549,516	-	-
KC - M	-	950,859	-
KB - M	-	-	8,222

Table 5.34 Percentages of Oil Transported from Matrix to Fractures for Case 10000 SM3 CO2 Injection

FORMATION	OIL IN PLACE, STB	M TO F, STB	M TO F (%)
SYD	3,757,300	61,575	1.6
KRG - M	1,195,609	549,516	46.0
KC - M	2,345,497	950,859	40.5
KB - M	29,580	8,222	27.8

5.3.5 25000 SM3 CO2 Injection

Table 5.35 25000 SM3 CO2 Injection Results

Initial State		*Produced*		*Percent*
Formation	Oil, STB	Formation	Oil, STB	%
SYD	3,757,300	SYD	56,572	1.51
KRG - M	1,195,609	KRG - M	665,105	55.63
KC - M	2,345,497	KC - M	1,277,191	54.45
KB - M	29,580	KB - M	10,999	37.18
KRG - F	393,117	KRG - F	306,424	77.95
KC- F	506,642	KC- F	431,449	85.16
KB - F	56,608	KB - F	46,807	82.69
FIELD	8,284,353	FIELD	2,794,547	33.73
FIELD - M	7,327,987	FIELD - M	2,009,867	27.43
FIELD - F	956,367	FIELD - F	784,680	82.05
F/M	13.1	F/M	39.0	

Table 5.36 Percentages of Matrix to Fracture Flow of Case 25000 SM3 CO2 Injection

From / To	KRG - F	KC - F	KB - F
SYD	59,939	-	-
KRG - M	678,999	-	-
KC - M	-	1,308,515	-
KB - M	-	-	11,694

Table 5.37 Percentages of Oil Transported from Matrix to Fractures for Case 25000 SM3 CO2 Injection

FORMATION	OIL IN PLACE, STB	M TO F, STB	M TO F (%)
SYD	3,757,300	59,939	1.6
KRG - M	1,195,609	678,999	56.8
KC - M	2,345,497	1,308,515	55.8
KB - M	29,580	11,694	39.5

5.4 Difference Between Two Relative Permeability Models

Table 5.38 Volume of Oil produced from the specified formation

CASE	SYD	KRG-M	KC-M	KB-M	KRG-F	KC-F	KB-F
NFA	132,744	253,235	563,225	7,107	133,824	227,440	41,515
BC_NFA	57,635	251,543	559,175	7,032	135,286	223,876	41,034
DIFF.	56.58	0.66	0.72	1.05	1.09	1.56	1.16
2_5K	141,582	434,538	782,841	7,457	286,248	384,702	38,553
BC_2.5K	62,076	416,159	764,568	7,302	290,585	389,237	39,767
DIFF.	56.2	4.2	2.3	2.1	1.5	1.2	3.1
5K	142,462	499,470	851,666	7,955	291,309	398,811	40,416
BC_5K	61,736	474,423	826,732	7,738	296,061	404,796	42,084
DIFF.	56.7	5.0	2.9	2.7	1.6	1.5	4.1
10K	142,758	594,920	1,001,840	8,614	296,389	411,941	42,334
BC_10K	61,063	558,024	964,395	8,216	301,469	419,781	43,802
DIFF.	57.2	6.2	3.7	4.6	1.7	1.9	3.5
25K	136,216	692,056	1,310,201	11,783	304,020	427,273	45,558
BC_25K	56,572	665,105	1,277,191	10,999	306,424	431,449	46,807
DIFF.	58.5	3.9	2.5	6.7	0.8	1.0	2.7

The table describes the volume of oil recovered from the specified formation. Between two relative permeability models, the biggest difference is in the SYD formation where the whole formation is modeled as single-porosity. There is no difference between two relative permeabilities' history match observed.

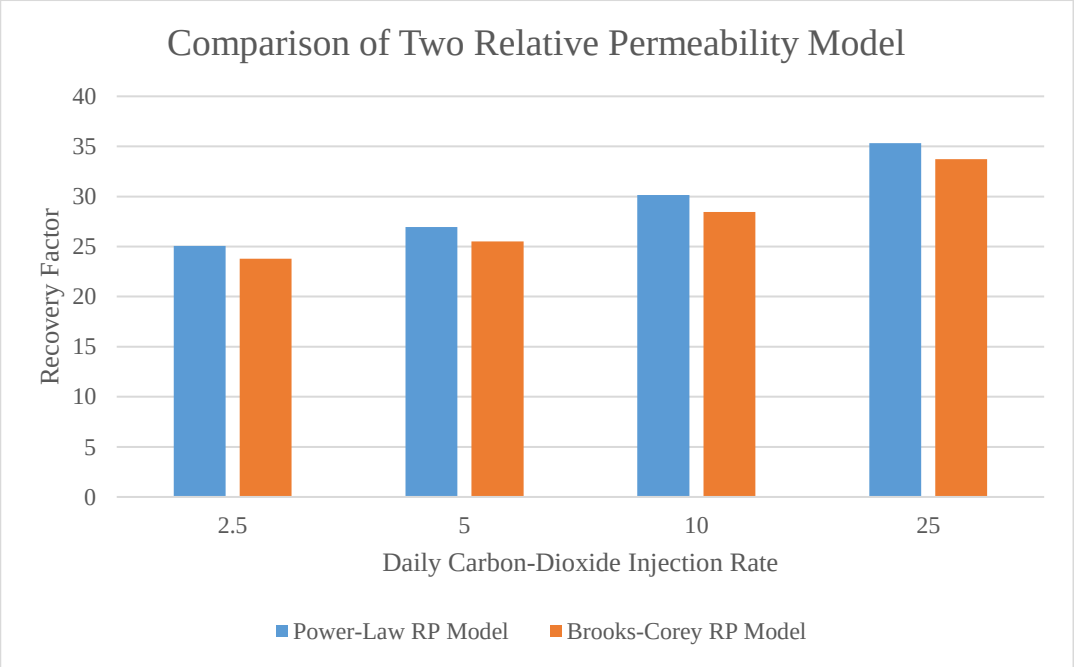

Figure 5.4. Bar chart for the comparison of the recovery factors of two models

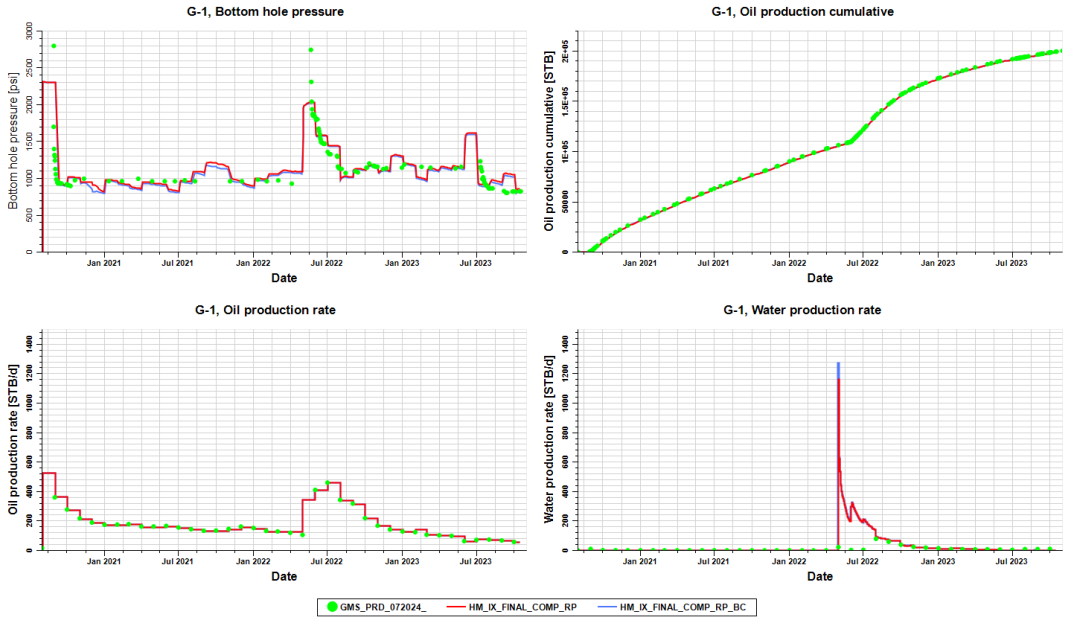

Figure 5.5. Comparison of two relative permeability models history match for G-1 well

5.5 Huff and Puff Method with 5000 SM3 CO2 Injection

In this case, the producer wells produce for three months. After the production period, the producer wells shut for three months. The injection wells continue to inject gas of 5000 SM3 of carbon-dioxide.

Table 5.39 Huff and Puff CO2 Injection Results

Initial State		*Produced*		*Percent*
Formation	Oil, STB	Formation	Oil, STB	%
SYD	3,757,300	SYD	170,038	4.53
KRG - M	1,195,609	KRG - M	603,979	50.52
KC - M	2,345,497	KC - M	1,030,422	43.93
KB - M	29,580	KB - M	8,805	29.77
KRG - F	393,117	KRG - F	307,136	78.13
KC- F	506,642	KC- F	424,349	83.76
KB - F	56,608	KB - F	43,931	77.61
FIELD	8,284,353	FIELD	2,588,658	31.25
FIELD - M	7,327,987	FIELD - M	1,813,243	24.74
FIELD - F	956,367	FIELD - F	775,416	81.08
F/M	13.1	F/M	42.8	

Table 5.40 Percentages of Matrix to Fracture Flow of Case Huff and Puff SM3 CO2 Injection

From / To	KRG - F	KC - F	KB - F
SYD	174,892	-	-
KRG - M	736,584	-	-
KC - M	-	1,328,372	-
KB - M	-	-	14,891

Table 5.41 Percentages of Oil Transported from Matrix to Fractures for Case Huff and Puff CO2 Injection

FORMATION	OIL IN PLACE, STB	M TO F, STB	M TO F (%)
SYD	3,757,300	174,892	4.7
KRG - M	1,195,609	736,584	61.6
KC - M	2,345,497	1,328,373	56.6
KB - M	29,580	14,891	50.3

This case should be compared with the continous 5000 SM3 carbon-dioxide injection and continuous production since the only variable is the production phase.Huff and Puff method let the injected gas imbibe the matrix during the shut-in period. Since the system, especially the fractures, is continously flooded with the gas and there are no output from the system, the carbon-dioxide in the fractures can change sides with the oil in the matrix more easily.

Table 5.42 Comparison of Huff and Puff method and continous 5000 SM3 carbon-dioxide injection

	Field	*Matrix*	*Fracture*	*Rec. Fac.*
Huff&Puff	2,588,658	1,813,243	775,416	31.25%
Continuous 5000	2,232,090	1,501,554	730,537	26.94%
Difference	356,568	311,689	44,879	4.30%

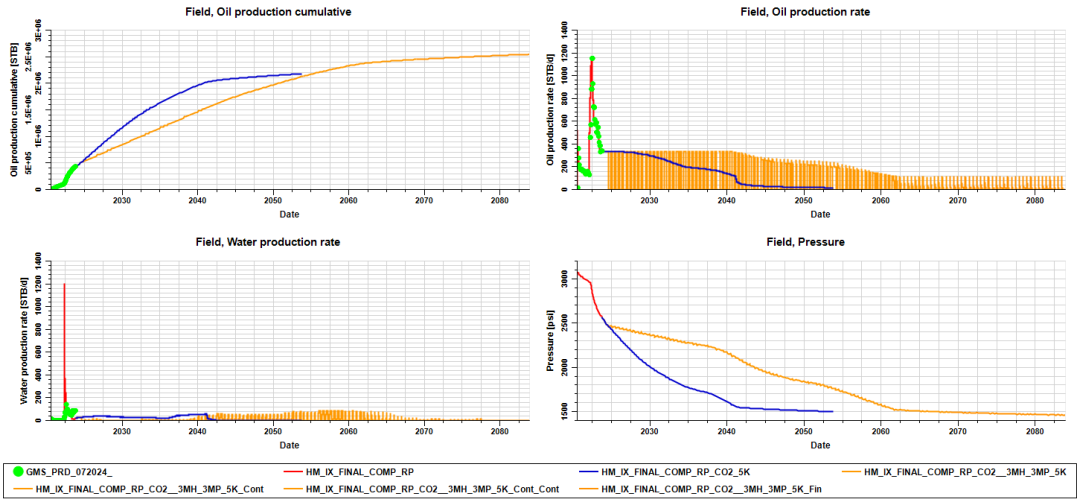

Figure 5.6. Graphical comparison of Huff and Puff method and continous 5000 SM3 carbon-dioxide injection

The reason Huff and Puff method extends to the 2083 is to compare both case correctly. Since the wells do not produce at the half of year, the life time of the Huff and Puff method should be double of the continous inejction and production.

It has been observed that the Huff and Puff method increases the cumulative oil production by 4.3 %. The waiting time for the carbon-dioxide to imbibe the matrix causes this increase.

5.6 Gravity Drainage Effect

In order to show the gravity drainage effect for the carbon-dioxide injection to the tight matrix and low quality fractured reservoir, a simulation that dismiss the gravity drainage effect is run with continuous 5000 SM3 carbon-dioxide injection. Thus, it can be comparable with the continuous 5000 SM3 carbon-dioxide injection case with the gravity drainage effect is open. Both cases uses Power-Law model for the relative permeability.

Table 5.43 5000 SM3 CO2 Injection without Gravity Drainage Results

Initial State		*Produced*		*Percent*
Formation	Oil, STB	Formation	Oil, STB	%
SYD	3,757,300	SYD	137,411	3.66
KRG - M	1,195,609	KRG - M	340,415	28.47
KC - M	2,345,497	KC - M	637,806	27.19
KB - M	29,580	KB - M	7,019	23.73
KRG - F	393,117	KRG - F	239,606	60.95
KC- F	506,642	KC- F	304,096	60.02
KB - F	56,608	KB - F	39,594	69.94
FIELD	8,284,353	FIELD	1,705,948	20.59
FIELD - M	7,327,987	FIELD - M	1,122,651	15.32
FIELD - F	956,367	FIELD - F	583,296	60.99
F/M	13.1	F/M	52.0	

Table 5.44 Percentages of Matrix to Fracture Flow of Case 5000 SM3 CO2 Injection without Gravity Drainage

From / To	KRG - F	KC - F	KB - F
SYD	132,418	-	-
KRG - M	341,439	-	-
KC - M	-	639,372	-
KB - M	-	-	7,032

Table 5.45 Percentages of Oil Transported from Matrix to Fractures for Case 5000 SM3 CO2 Injection without Gravity Drainage

FORMATION	OIL IN PLACE, STB	M TO F, STB	M TO F (%)
SYD	3,757,300	132,418	3.5
KRG - M	1,195,609	341,439	28.6
KC - M	2,345,497	639,372	27.3
KB - M	29,580	7,032	23.8

Table 5.46 Comparison of WoGD and GD 5000 SM3 carbon-dioxide injection

	Field	*Matrix*	*Fracture*	*Rec. Fac.*
WoGD 5K	1,705,948	1,122,651	583,296	20.59%
GD 5K	2,232,090	1,501,554	730,537	26.94%
Difference	526,143	378,902	147,241	-6.35%

Gravity drainage contributes recovery by 6.35 % in the tight matrix and low quality fractured reservoir. The injection of carbon-dioxide is only supports the pressure in the fracture, thus it increases the recovery factor to the 20.59 % where it was 16.41 % in the no further action case.

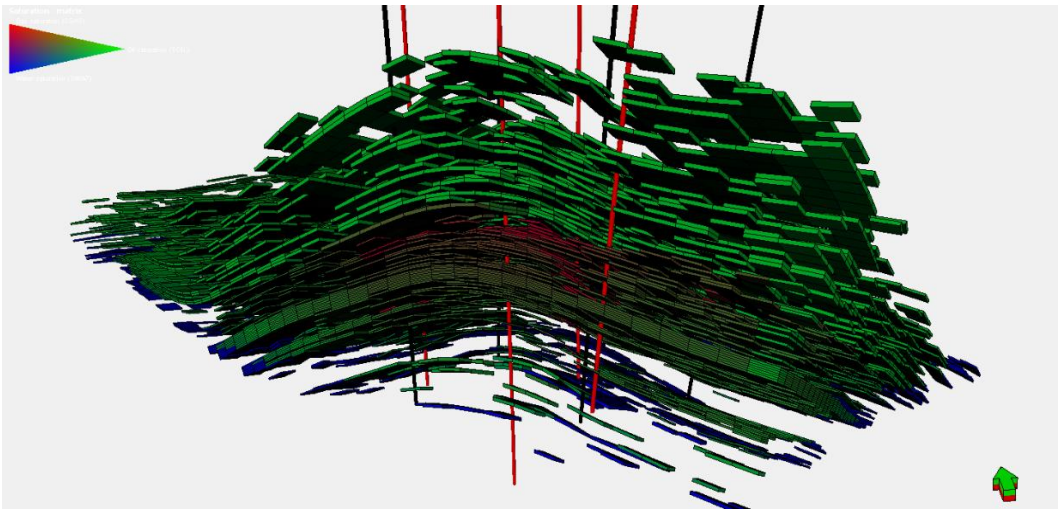

Figure 5.7. The three phase saturation results on the 3D Grid of GD 5000 SM3 Carbon-dioxide injection

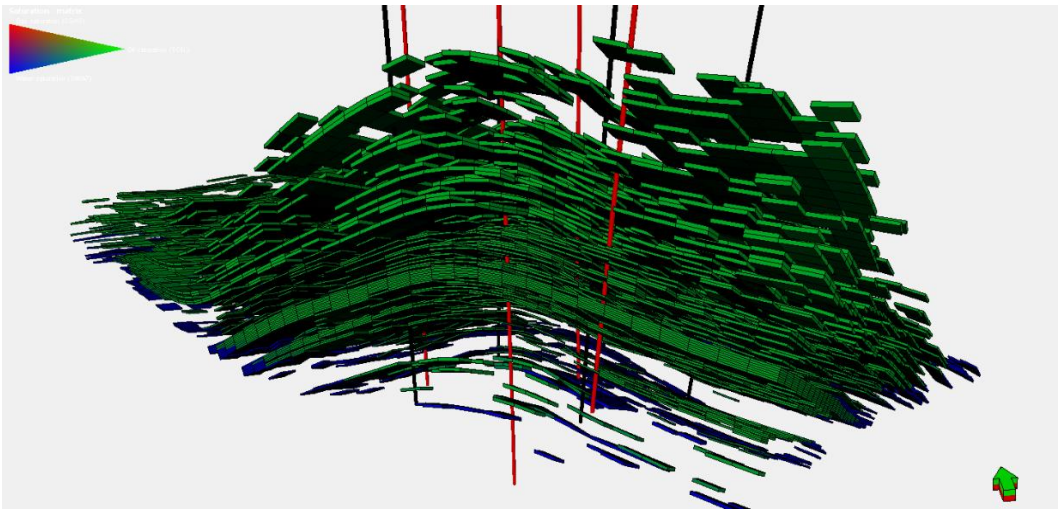

Figure 5.8. The three phase saturation results on the 3D Grid of WoGD 5000 SM3 Carbon-dioxide injection

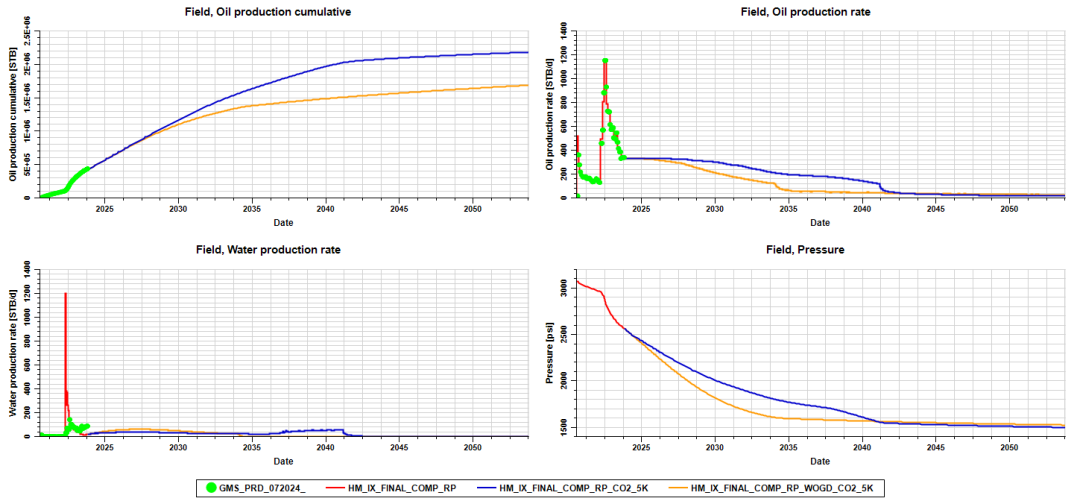

Figure 5.9. Graphical comparison of WoGD and GD 5000 SM3 Carbon-dioxide injection cases

5.7 Discussion

In this thesis, the effect of gravity drainage, miscible injection and relative permeability model is studied with an appropriate simulator. The simulated reservoir was carbonate reservoir with low matrix porosity – permeability and low quality naturally fractured. The imbibition process of the injected gas into the matrix observed with both continuous production and 3 months shut-produce method. Brooks-Corey and Power Law model is used for the relative permeability effect on the gas injection. The results of the immiscible and miscible injection has been shown. In order to maintain miscible injection, 50000 standard cubic meters of carbon-dioxide is injected into the reservoir.

It has been observed that, as the injection rate of carbon-dioxide is increase, the recovery factor increases. However, miscible injection brings more recovery factor.

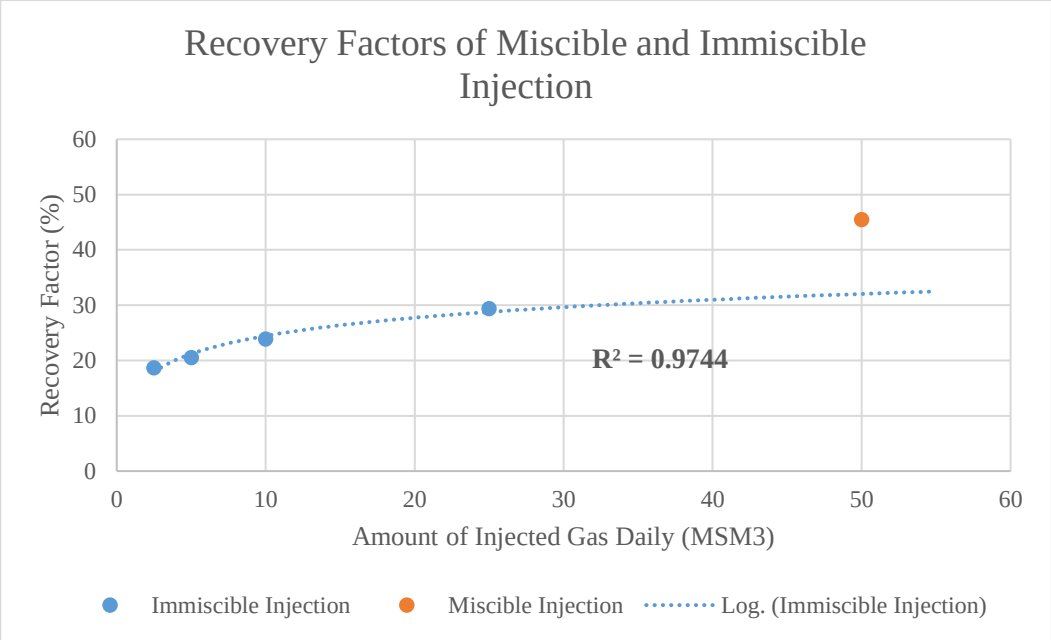

Figure 5.10. Recovery Factors of the Injection Cases

It can be clearly seen that the recovery factors of the immiscible injections increases logaritmically as the injection rate increases, however, the miscible injection recovers more oil than expected.

Table 5.47 Recovery Factors of Two Relative Permeability Models

	Injection Rate (MSM3/day)	Recovery Factor (%)
	2.5	25.06
Power-Law	5	26.94
Relative	10	30.16
Permeability Model	25	35.33
	50	49.79
Corey-Brooks	2.5	23.78
Relative	5	25.51
Permeability Model	10	28.45
	25	33.73

Table 5.48 Recovery Factors of Different Cases with Power-Law RP Model

	Injection Rate (MSM3/day)	Recovery Factor (%)
Continuous Prod.	5	26.9
Huff & Puff	5	31.2
WoGD	5	20.6

CHAPTER 6

CONCLUSION

Eventhough the different relative permeability models used, the flow in the matrix did not changed massively, thus the recovery factor did not affected. It is almost 2% of difference in recovery factors between two district relative permeabilities. This is because of the matrix contribution to the flow, where it is very restricted in the tight matrix and tight fracture. This sensitivity analysis proved that the relative permeability of the matrix in tight matrix reservoirs affects the recovery factor insignificantly. It also did not effect the history match, since the matrix flow is very low in numbers.

The sweep efficiency of the carbon-dioxide injection increases significantly while it is in miscible conditions with oil. The immiscible injection pressurizes the field which is one of the main problems, however, the sweep efficiency of the injection after the gas imbibes matrix is low due to low matrix permeability. On the other hand, miscible injection led oil flow with carbon-dioxide in it and decreases viscosity. Fluid easily flows through the matrix in the miscibile injection. Miscible injection increases the recovery factor up to 50%, however, this number would be 33% if the miscible injection rate can not make the miscibility.

The dual porosity formula, which consists of three terms; viscous displacement, imbibition term, and gravity drainage, is analyzed in the terms of gravity drainage. Gravity drainage term, replacing the gas in the fracture and the oil in the matrix due to density difference, affecting the recovery in the matrix less than viscous displacement term and imbibition term, but the question of how much in tight matrix and tight fracture was unanswered. In the G-Field simulations, the gravity drainage term effect measured as 6.3% by neglecting the gravity drainage term in the

simulation. However, it can be further increased by letting the gas soak in to the matrix by stopping the production while the injection continues. Three months of production and three months of shut-in scenario increased the recovery factor by 4.3%. This number can be named as the gravity drainage effect also, thus, the gravity drainage effect can be increased. In the huff&puff scenario, the gravity drainage effect can be said to be 10.6%.

REFERENCES

Hashemi, S. M. H., Monfaredi, K., & Sedaee, B. (2020). An inclusive consistency check procedure for quality control methods of the black oil laboratory data. Journal of Petroleum Exploration and Production Technology, 10(5), 2153–2173. https://doi.org/10.1007/s13202-020-00869-6

Hoffman A, Crump J, Hocott C (1953) Equilibrium constants for a gas-condensate system. J Petrol Technol 5(01):1–10

Li, H., Qin, J., & Yang, D. (2012b). An improved CO2–Oil minimum miscibility pressure correlation for live and dead crude oils. Industrial & Engineering Chemistry Research, 51(8), 3516–3523. https://doi.org/10.1021/ie202339g

Ameri, M., Fard, M. S., Akbari, Zamanzadeh, S., & Nasiri, E. (2013). A comparison of accuracy and computational time for common and artificial methods in predicting minimum miscibility pressure. Energy Exploration & Exploitation, 31(2), 221–236. https://doi.org/10.1260/0144-5987.31.2.221

Zhang, H., Hou, D., & Li, K. (2015). An improved CO2-crude oil minimum miscibility pressure correlation. Journal of Chemistry, 2015, 1–10. https://doi.org/10.1155/2015/175940

Cronquist, C. (1977). Carbon dioxide dynamic miscibility with light reservoir oils. in Proceedings of the 4th Annual U.S. DOE Symposium, Tulsa, Okla, USA

Lee, J. I. (1979). Effectiveness of carbon dioxide displacement under miscible and immiscible conditions. Report RR-40, Petroleum Recovery Institute, Calgary, Canada

Yellig, W. F. & Metcalfe, R. S. (1980). Determination and prediction of CO2 minimum miscibility pressures. Journal of Petroleum Technology, vol. 32, no. 1, pp. 160–168

Orr, F. M. Jr. & Jensen, C. M. (1984). Interpretation of pressure-composition phase diagrams for CO2 / crude oil systems. Society of Petroleum Engineers Journal, vol. 24, no. 5, pp. 485-497

Alston, R. B., Kokolis, G. P. & James, C. F. (1985). CO2 minimum miscibility pressure: a correlation for impure CO2 streams and live oil systems. Society of Petroleum Engineers Journal, vol. 25, no. 2, pp. 268–274

Emera, M. K. & Sarma, H. K. (2005). Use of genetic algorithm to estimate CO2-oil minimum miscibility pressure—a key parameter indesign of CO2 miscible flood. Journal of Petroleum Science and Engineering, vol. 46, no. 1-2, pp. 37–52

Chen, B. L., Huang H. D., Zhang, Y.. (2013). An improved predicting model for minimum miscibility pressure (MMP) of CO2 and crude oil. Journal of Oil and Gas Technology, vol. 35, no. 2, pp. 126–130

Nelson, R.A. (2001). Geologic Analysis of Naturally Fractured Reservoirs. 2nd ed. GulfProfessional Publishing.

Brooks, R.H. & Corey, A.T. (1964). Hydraulic Properties of Porous Media. Hydrology Papers, No. 3, Colorado State U., Fort Collins, Colorado.

Mcclure, J., Armstrong, R., Berrill, M., Schlüter, S., Berg, S., Gray, W., Miller, C. (2018). Geometric state function for two-fluid flow in porous media. Physical Review Fluids. https://doi.org/3. 10.1103/PhysRevFluids.3.084306.

Corey, A.T. (1954). The interrelation between gas and oil relative permeabilities. Producers Monthly 19 (November): 38–41.

Ahmed, T. H. (2019). Reservoir Engineering Handbook. In *Elsevier eBooks*. https://doi.org/10.1016/b978-0-7506-7972-5.x5000-5

Zobeidi, K., & Fassihi. (2018). Block to block interactions and their effects on miscibility gravity drainage in fractured carbonate reservoirs, experimental and analytical results. Journal of Petroleum Science and Engineering, 164, 696–708. https://doi.org/10.1016/j.petrol.2018.01.015

Abdullah, N., & Hasan, N. (2021). Effects of miscible CO2 injection on production recovery. Journal of Petroleum Exploration and Production Technology, 11(9), 3543–3557. https://doi.org/10.1007/s13202-021-01223-0

Cooney, G., Littlefield, J., Marriott, J., Skone, TJ. (2018). Evaluating the climate benefits of CO2- enhanced oil recovery using life cycle analysis. Environ Sci Technol 49(12):7491–7500

Steinsbo, M., Brattekas, B., Ferno, MA., Graue, A. (2014). Supercritical CO2 injection for enhanced oil recovery in fractured chalk. In: International symposium of the society of core analysts, at Avignon, France

Tadesse. NS, (2018). Simulation of CO2 injection in a reservoir with an underlying paleo residual oil zone, Thesis, NTNU

Whittaker, S., Perkins, E. (2013). Technical aspects of CO2 enhanced oil recovery and associated carbon storage. Global CCS Institute, Docklands

Kalra, S., Tian, W., Wu, X. (2017). A numerical simulation study of CO2 injection for enhancing hydrocarbon recovery and sequestration in liquid-rich shales. Pet Sci 15:103–115

Al-netaifi, AS. (2008). Experimental Investigation of CO2— miscible oil recovery at different conditions, A Thesis Submitted in Partial Fulfillment of the Requirement of the Degree of Master of Science in the Department of Petroleum and Natural Gas Engineering, King Saud University, KSA

Liu, R. (2013). A miscible CO2 injection project and evaluation in Daqing, China. Pet Technol Altern Fuels 4(6):113–118

Rezaei, M., Eftekhari, M., Schaffie, M., Ranjbar, M. (2013). A CO2- oil minimum miscibility pressure model based on multi-gene genetic programming. Energy Explor Exploit 31(4):607–622

Ansarizadeh, M., Dodds, K., Gurpinar, O., Pekot, LJ., Kalfa, O., Sahin, S., Uysal, S., Ramakrishnan, TS., Sacuta, N., Whittajer, S. (2015). Carbon dioxide—challenges and opportunities. Oilfield Rev 27(2):1–15

Aroher, B., Archer, R. (2010). Enhanced natural gas recovery by carbon dioxide injection for storage. In: 17th Australia fluid mechanics, 5–9 December, Auckland, New Zealand

Meyer, JP. (2007). Summary of carbon dioxide enhanced oil recovery (CO2 EOR) injection well technology, Prepared for the American Petroleum Institute

Bergmo, P., Anthonsen, KL. (2014). Overview of available data on candidate oil fields for CO2 EOR. SINTEF Petroleum, pp 1–20

Cook, BR. (2012). Wyoming's miscible CO2 enhanced oil recovery potential from main pay zones: an economic scoping study, University of Wyoming, USA

US Chambers C. (2021). C02 enhanced oil recovery, Technological Breakthrough Allows for Greater Domestic Oil Production

Tian, S., Zhao, G. (2008). Monitoring and predicting CO flooding using material balance equation. In: Petroleum Society of Canada, 8–10 June, Calgary, Alberta, Petroleum Society of Canada, p 47

Sonier, F., Souillard, P., & Blaskovich, F. T. (1988). Numerical simulation of naturally fractured reservoirs. SPE Reservoir Engineering, 3(04), 1114–1122. https://doi.org/10.2118/15627-pa

Thomas, L. K., Dixon, T. N., & Pierson, R. G. (1983). Fractured reservoir simulation. Society of Petroleum Engineers Journal, 23(01), 42–54. https://doi.org/10.2118/9305-pa

El-Hajj, H., Odi, U., & Gupta, A. (2013). Carbonate reservoir interaction with supercritical carbon dioxide. *All Days*. https://doi.org/10.2523/iptc-16561-abstract

Ercan, C., 2022, "Conventional and Special Core Analysis Report of Well G-4", TPAO, Research Center, Reservoir Technologies Center

Güner Çiçek, C., 2022 "Log Process of G-Field Wells", TPAO, Production Department, Reservoir Management, 2022.

Türkmenoğlu, A. & Arslan, E., 2020, “PVT Analysis Report of G-1 Reservoir Oil”, Report No 4567, TPAO, Research Center, Reservoir Management

Özkaya Türkmen, M., Yürüker, O., & Güner Çiçek, C., 2022 “Reservoir Model of G-Field”, TPAO, Production Department, Reservoir Management, 2022.

Alvarado, V., & Manrique, E. (2010). Enhanced Oil Recovery: An Overview. Energy & Fuels, 24(1), 1-24. https://doi.org/10.1021/ef900713h

Liu, Q., Zhang, Z., & Zhang, Z. (2018). Multiple-contact miscibility of CO_2 with crude oil: Laboratory tests and implications for CO_2 EOR. Journal of Petroleum Science and Engineering, 165, 248-257. https://doi.org/10.1016/j.petrol.2018.02.056

Rojas, J., Martinez, A., & Giner, J. (2015). Analysis of multiple-contact miscibility in CO_2-EOR processes. International Journal of Greenhouse Gas Control, 37, 114-125. https://doi.org/10.1016/j.ijggc.2015.03.020

Srivastava, R., Sahni, M., & Kumari, S. (2017). Experimental and theoretical studies on CO_2-oil miscibility: Implications for enhanced oil recovery. Fuel, 194, 341-353. https://doi.org/10.1016/j.fuel.2017.01.077

Adams, F. R., & Green, N. C. (2010). Impact of gravity drainage on oil recovery in dual porosity reservoirs: A comparative study. Journal of Energy Resources Technology, 132(4), 042903.

Hartman, T. N., & Stevens, L. B. (1995). Numerical simulation of gravity drainage in dual porosity reservoirs. Society of Petroleum Engineers Journal, 15(2), 123-134.

Ho, R. C. A., & Haaland, S. B. (1985). Modeling of gravity drainage in fractured reservoirs. SPE Reservoir Evaluation & Engineering, 1(1), 45-55.

Liu, Z. H., & Zhang, W. L. (2000). Experimental study on gravity drainage in fractured reservoirs. Journal of Petroleum Science and Engineering, 26(1-4), 165-175.

McLennan, J. H., & Fancher, G. H. (1980). Gravity drainage in dual-porosity reservoirs. Journal of Petroleum Technology, 32(10), 2075-2086.

Smith, M. J., & Johnson, P. L. (2005). Gravity assisted oil recovery in dual-porosity reservoirs. Energy & Fuels, 19(3), 887-898.

Watson, K. M., & McLaughlin, J. P. (1990). Gravity drainage in matrix-fracture systems: A review. Petroleum Science and Engineering, 5(2), 123-136.

Alvarado, V., & Manrique, E. (2002). Enhanced oil recovery: An update review. Energy Sources, 24(9), 741-750.

Doughty, C., & Hsu, H. (1990). Experimental investigation of CO_2-oil miscibility and phase behavior. Journal of Petroleum Science and Engineering, 5(2), 85-96.

Hsu, H., & Morrison, R. (1974). The miscibility of carbon dioxide with oil: Fundamental principles and models. Journal of Petroleum Technology, 26(5), 531-541.

Johnson, B., & Tham, S. (2001). Modeling of CO_2-oil miscibility and its effect on enhanced oil recovery. SPE Reservoir Evaluation & Engineering, 4(4), 287-298.

Zhang, Y., & Wichterle, I. (1995). Experimental validation of CO_2-oil miscibility models: Pressure and temperature effects. Energy & Fuels, 9(3), 421-430.

Brooks, R. H., & Corey, A. T. (1980). Properties of porous media affecting fluid flow. Journal of Soil Science, 31(1), 96-109.

Corey, A. T. (1977). The relative permeability of petroleum reservoir rocks. Society of Petroleum Engineers.

Morrow, N. R., & Buckley, J. S. (2006). Improved relative permeability models for oil and gas reservoirs. Journal of Petroleum Science and Engineering, 51(1-2), 18-30.

Stone, L. S. (1979). Models for the relative permeability of multi-phase flow in porous media. Society of Petroleum Engineers Journal, 19(1), 13-22.

Van Genuchten, M. T. (1991). A closed-form equation for predicting the relative permeability of unsaturated soils. Soil Science Society of America Journal, 55(3), 572-582.

Zhang, Y., Li, Q., & Wang, J. (2012). Unified models for relative permeability in oil and gas reservoirs. Energy & Fuels, 26(8), 4595-4608.

Lie, K. (2019). An introduction to reservoir simulation using MATLAB/GNU Octave. Cambridge University Press. https://doi.org/10.1017/9781108591416

APPENDICES

A. Bottom Hole Pressure MatLAB Code

```
obs_data = load('obs_data.txt');

Density_vs_Pressure = load('dens.txt');

Comp_vs_Pressure = load('comp.txt');


Flow_Rate = obs_data(:, 1);         %bbl/day

Water_Saturation = obs_data(:, 2);  %percent

Liquid_Level = obs_data(:, 3);      %meters

Salinity_ppm = obs_data(:, 4);      %ppm

Annulus_Pressure = obs_data(:, 5);  %psi


Perforation_Depth = input('Enter the depth in meters: ');   %meters

Perforation_Depth_ft = Perforation_Depth / 0.3048;          %feet

Liquid_Level_ft = Liquid_Level / 0.3048;                    %feet


[numRows, numCols] = size(Liquid_Level);

Bottom_Hole_History = zeros(numRows,1);


for row = 1:numRows

Density_Surface = 0.84;   %g/cc
```

```
rho0 = 62.368;  %lb/ft^3

a0 = 0.438603;

a1 = 0.00160074;


Salinity = Salinity_ppm(row,:) / 10000;  %psu


Water_Density = ( rho0 + (a0 * Salinity) + (a1 * Salinity^2) ) * 0.01602;   %g/cc

Water_Saturation_Frac = Water_Saturation(row,:) / 100;  %fraction


Density_Guess = Density_Surface;



Oil_Pressure = (Perforation_Depth_ft - Liquid_Level_ft(row,:)) * Density_Guess *
0.43316 * (1-Water_Saturation_Frac);  %psi

Water_Pressure = (Perforation_Depth_ft - Liquid_Level_ft(row,:)) * Water_Density
* 0.43316 * Water_Saturation_Frac;    %psi



Pressure_Guess = Oil_Pressure + Water_Pressure;   %psi


Density_Current = Density_Guess;
```

```
Tolerance_dens = 0.0001;

Max_Iterations_dens = 1000;

Iterations_dens = 0;

Error_dens = inf;

Tolerance_comp = 0.0001;

Max_Iterations_comp = 1000;

Iterations_comp = 0;

Error_comp = inf;


while Error_comp > Tolerance_comp && Iterations_comp < Max_Iterations_comp

while Error_dens > Tolerance_dens && Iterations_dens < Max_Iterations_dens

   Dens_Pres = [ Pressure_Guess Density_Current ];


   Density_Current = interp1(Density_vs_Pressure(:,1), Density_vs_Pressure(:,2), Pressure_Guess);  %g/cc


   Oil_Pressure = ( Perforation_Depth_ft - Liquid_Level_ft(row,:) ) * Density_Current * 0.43316 * (1-Water_Saturation_Frac);  %psi

   Water_Pressure = ( Perforation_Depth_ft - Liquid_Level_ft(row,:) ) * Water_Density * 0.43316 * Water_Saturation_Frac;      %psi


   Pressure_Guess = Oil_Pressure + Water_Pressure + Annulus_Pressure(row,:); %psi
```

```
    Comp_Current = interp1(Comp_vs_Pressure(:,1), Comp_vs_Pressure(:,2),
Pressure_Guess);


    Error_dens = abs(Pressure_Guess - Dens_Pres(end, 1));
    Iterations_dens = Iterations_dens + 1;
end
    Comp_Pres = [ Pressure_Guess Comp_Current ];
    num_points = Perforation_Depth - Liquid_Level(row,:);
    pressure = zeros(1, num_points); % psi
    pressure(1) = Pressure_Guess; % psi
for a = 2:num_points
    density = interp1(Density_vs_Pressure(:,1), Density_vs_Pressure(:,2), pressure(a-
1));   %g/cc
    pressure(a) = (pressure(a-1) + 14.7/num_points) - density * 0.43316 * 3.28 ;
% psia
end


liquid_level_lost = zeros(1, num_points);


for b = 1:num_points-1
    density = interp1(Density_vs_Pressure(:,1), Density_vs_Pressure(:,2),
pressure(b));
```

```
    compressibility = interp1(Comp_vs_Pressure(:,1), Comp_vs_Pressure(:,2),
pressure(b));

    delta_liquid_level = compressibility * (Pressure_Guess - pressure(b+1)); % m

    liquid_level_lost(b) = delta_liquid_level;
end

total_liquid_level_lost = sum(liquid_level_lost) / 0.3048;

    Oil_Pressure = ( Perforation_Depth_ft - Liquid_Level_ft(row,:) +
total_liquid_level_lost ) * Density_Current * 0.43316 * (1-Water_Saturation_Frac);
    Water_Pressure = ( Perforation_Depth_ft - Liquid_Level_ft(row,:) +
total_liquid_level_lost ) * Water_Density * 0.43316 * Water_Saturation_Frac;

    Pressure_Guess = Oil_Pressure + Water_Pressure + Annulus_Pressure(row,:);
    Density_Current = interp1(Density_vs_Pressure(:,1), Density_vs_Pressure(:,2),
Pressure_Guess);  %g/cc

    Error_comp = abs(Pressure_Guess - Comp_Pres(end, 1));
    Iterations_comp = Iterations_comp + 1;
end
```

```
Bottom_Hole_Pressure  = Pressure_Guess;


Bottom_Hole_History (row,1) = Bottom_Hole_Pressure;
end


Bottom_Hole_History = round(Bottom_Hole_History, 0);
```